The Dissertation Committee for Jason Michael TenBarge
certifies that this is the approved version of the following dissertation:

Fluid Description of Relativistic, Magnetized Plasmas with Anisotropy and Heat Flow: Model Construction and Applications

Committee:

Richard Hazeltine, Supervisor

Roger Bengston

Wendell Horton

Philip Morrison

Pawan Kumar

Fluid Description of Relativistic, Magnetized Plasmas with Anisotropy and Heat Flow: Model Construction and Applications

by

Jason Michael TenBarge, B.S.

DISSERTATION

Presented to the Faculty of the Graduate School of

The University of Texas at Austin

in Partial Fulfillment

of the Requirements

for the Degree of

DOCTOR OF PHILOSOPHY

THE UNIVERSITY OF TEXAS AT AUSTIN

August 2009

Acknowledgments

The six years I have spent at the University of Texas has been an exciting and intellectually transformative experience. I arrived at the University unsure of what I wanted to do and have emerged with a level confidence and clarity I had not expected.

Many people have had a significant influence on me and my ideas. A few of the most influential were: Dr. Wendell Horton, Dr. Philip Morrison, Dr. Roger Bengston, Dr. Todd Tinsley, and Ms. Brandy Guntel. I would especially like to thank Dr. Horton for introducing me to space and computational physics.

For the last few years, Jesse Pino has been a great friend, travelling partner, and my sounding board for physical ideas. He has always made time when I've needed help, and I learned a great deal from our discussions.

Swadesh Mahajan has been as a second adviser for me. He has been a never ending source of ideas and alternate views of problems. His straightforward approach to physics has been refreshing and rewarding.

I would like to especially thank my adviser, Richard Hazeltine, for his unwavering support and physical insight and the kind and collaborative atmosphere he exudes. I first approached him having little formal knowledge of plasma physics, and he graciously accepted me as his student. He provided

me with a problem that blossomed into a much larger and stimulating project than either of us anticipated.

Fluid Description of Relativistic, Magnetized Plasmas with Anisotropy and Heat Flow: Model Construction and Applications

Publication No. _____

Jason Michael TenBarge, Ph.D.
The University of Texas at Austin, 2009

Supervisor: Richard Hazeltine

Many astrophysical plasmas and some laboratory plasmas are relativistic: either the thermal speed or the local bulk flow in some frame approaches the speed of light. Often, such plasmas are magnetized in the sense that the Larmor radius is smaller than any gradient scale length of interest. Conventionally, relativistic MHD is employed to treat relativistic, magnetized plasmas; however, MHD requires the collision time to be shorter than any other time scale in the system. Thus, MHD employs the thermodynamic equilibrium form of the stress tensor, neglecting pressure anisotropy and heat flow parallel to the magnetic field. We re-examine the closure question and find a more complete theory, which yields a more physical and self-consistent closure. Beginning with exact moments of the kinetic equation, we derive a closed set of Lorentz-covariant fluid equations for a magnetized plasma allowing for pressure and heat flow anisotropy. Basic predictions of the model, including

its thermodynamics and the dispersion relation's dependence upon relativistic temperature, are examined. Further, the model is applied to two extant astrophysical problems.

Table of Contents

List of Figures

Chapter 1

Introduction

1.1 Relativistic Plasmas

A plasma is relativistic if either the thermal speed—the rms speed of the individual particles—measured in the fluid rest-frame, or the local bulk flow measured in some relevant frame approaches the speed of light. Such plasmas are ubiquitous in astrophysical phenomena (eg, pulsars and magnetar magnetospheres [4], galactic and extra-galactic jets [29], accretion discs of active galactic nuclei [55], and electron-positron-ion plasmas in the early universe [7], [77]) and in some laboratory fusion experiments.

Aside from obvious relativistic effects due to a bulk relativistic speed, a plasma's behaviour is strongly modified by relativistic thermal energy. As the thermal energy approaches the rest mass energy, the inertia of the plasma is augmented by the thermal energy. Thus, both effects must be included in any reasonable relativistic fluid closure.

Often (e.g., [2], [15], [51], [72]), relativistic plasmas of interest are magnetized —meaning the dynamics are dominated by the magnetic field. The dynamics of such plasmas are typically described with magnetohydrodynamics (MHD), which captures the large-scale electromagnetic features of a magne-

tized plasma (e.g., $\boldsymbol{E} \times \boldsymbol{B}$ drifts). As an extension to conventional MHD, Lichnerowicz [47] presented a relativistic MHD closure. Despite MHD's success at capturing some of the large scale physics, MHD plasmas are based on the use of a stress tensor whose origin is based on thermodynamic considerations (thermal equilibrium) rather than electrodynamics, in which electromagnetic forces dominate.

1.2 Beyond MHD

The difficulty with any fluid system is closure. Each moment of the kinetic equation is coupled to the next higher moment: density depends upon bulk flow, bulk flow depends upon pressure, and so forth. Two methods are typically employed to achieve closure in fluid systems: truncation and asymptotic expansion in terms of a small parameter. Chapman-Enskog theory of a gas dominated by collisions, in which the mean-free-path provides the expansion parameter, is a standard asymptotic approach [16]. As an example of this approach, de Groot et al. [24] present a Chapmen-Enskog closure for relativistic plasmas. Truncation schemes either set higher moments to zero or prescribe them in terms of lower moments. Fluid MHD is a truncation approach in which moments higher than the pressure are assumed to vanish based upon the assumption of thermal equilibrium. Of the two closure schemes, asymptotic is the more rigorous; however, asymptotic schemes are more difficult computationally and require kinetic computations. Furthermore, the required small parameter is not always available.

Chew, Goldberger, and Low [17] (CGL) present an early departure from the conventional MHD treatment of the stress tensor by allowing gyrotropic pressure: the CGL tensor differentiates between pressures parallel and perpendicular to the magnetic field. However, to close the system CGL neglects heat flow parallel to the magnetic field, which can be rapid in low collisionality plasmas. Partly for this reason, the double adiabatic assumption used by CGL to achieve closure is not valid in many physical situations.

Cissoko [19] presents the first description of an anisotropic relativistic plasma. Tsikarishvili et al. [71] present a double-polytropic closure for an anisotropic relativistic plasma. Their closure consists of having separate equations of state for the parallel and perpendicular pressures with adjustable polytropic indices and reduces to CGL in the non-relativistic limit and with appropriate index choice. The adjustability of the indices allows them to consider any thermally relativistic regime; however, the choice of indicies is ad hoc and not self-consistent. Also, the indicies do not provide a smooth connection between temperature regimes. However the double-polytropic closure does have the advantage of being able to easily explore non-adiabatic processes. Further, one expects heat flow for a relativistic plasma to be very large since even in the simple heat flux limit it scales like $p\boldsymbol{V}$, which is of the order of the thermal energy.

Hazeltine and Mahajan [35] (hereafter referred to as HM) attempted a more physical relativistic closure with gyrotropic pressure and parallel heat flow. However, close scrutiny of the Hazeltine-Mahajan model revealed fun-

damental deficiencies. The details of the deficiencies are covered in chapter 3. The closure method employed in HM uses the stress tensor as the constitutive relation for the fluid closure. The form of the stress tensor is derived from exact fluid equations together with orderings characterizing a magnetized plasma. Predictably, such an approach does not provide a closed system. Closure is achieved through a representative distribution function, consistent with relativity, magnetization, pressure anisotropy, and heat flow.

To achieve our closure, we take an approach parallel to HM; we use HM as a guide in the search for a more physical and self-consistent relativistic, magnetized fluid closure. After developing the closure, we apply it to two outstanding astrophysical problems.

Chapter 2

Relativistic Theory

Before embarking on our development of a novel relativistic fluid closure, we review some basic concepts from relativity theory and introduce the parameters and identities that allow simpler expressions later in our analysis. If the reader desires a more thorough introduction to the material, Jackson [39] provides an excellent introduction to relativity and relativistic electrodynamics, Lichnerowicz [47] and Anile [3] provide introductions to relativistic MHD, and de Groot et al. [24] is a good source for relativistic kinetic theory.

We use the Einstein summation convention throughout, with Greek indices running from 0 to 3 and Roman indices from 1 to 3. Boldface type typically represents the 3-vector portion of a 4-vector, for instance an arbitrary 4-vector C^μ may be written as $C^\mu = (C^0, \mathbf{C})$. All speeds are normalized to the speed of light, so that $c = 1$. We use $\eta^{\mu\nu} = diag\{-1, 1, 1, 1\}$ as the signature for the Minkowski tensor and η is the specific metric for Cartesian spatial coordinates. $g^{\mu\nu}$ will be used to represent an arbitrary metric in flat space-time geometry. ∇_μ will be used to represent the covariant derivative; whereas $\partial_\mu = \frac{\partial}{\partial x^\mu}$ will be used to represent the partial derivative in a particular coordinate system. The derivatives are related through the Christoffel symbol,

$\Gamma^{\nu}_{\alpha\beta} = \frac{g^{\nu\gamma}}{2}(\partial_\alpha g_{\gamma\beta} + \partial_\beta g_{\alpha\gamma} - \partial_\gamma g_{\alpha\beta})$. For instance, $\nabla_\mu C^\nu = \partial_\mu C^\nu + \Gamma^\nu_{\mu\gamma} C^\gamma$. Further properties of the covariant derivative are given in appendix 0.1. Unless otherwise stated, coordinates are assumed to be Cartesian.

2.1 Kinematics

2.1.1 Instantaneous Rest Frame

The following material is sourced from Jackson [39].

We observe a particle in the lab frame with coordinates $(t, \mathbf{x})$ and moving with a velocity $\mathbf{v}(t)$. We can choose a time $\tilde{t}$ at which a frame moving with velocity $\tilde{\mathbf{v}} = \mathbf{v}(\tilde{t})$ will be co-moving with the particle. In this frame, the particle will be observed to be instantaneously at rest –we call this frame the instantaneous rest frame (IRF). Since the IRF's velocity is fixed, it will not move with the particle and the particle is observed to be at rest for only an infinitesimal time. However, the IRF is an inertial frame to which we can apply Lorentz transformations. Also, the IRF provides a convenient reference frame in which to define fluid moments of the plasma.

A Lorentz transformation combines a rotation in coordinate space with a "boost" in velocity space –the boost only transforms coordinates and has no effect on the physical velocity of the system. A boost by velocity $\mathbf{v}$ between two reference frames is obtained by applying the matrix $\Lambda(\mathbf{v})$ n times to a rank n tensor. For instance, a 4-vector transforms according to

$$A'^\mu = \Lambda(\mathbf{v})^\mu_\nu A^\nu,$$

where

$$\begin{aligned}
\Lambda^0_0 &= \gamma \\
\Lambda^0_j &= \gamma v_j \\
\Lambda^i_0 &= \gamma v_i \\
\Lambda^i_j &= \delta^i_j + \hat{v}_i \hat{v}_j (\gamma - 1),
\end{aligned} \tag{2.1}$$

$\hat{\mathbf{v}} = \mathbf{v}/v$, and $\gamma = 1/\sqrt{1 - v^2}$. Explicitly,

$$\begin{aligned}
A'^0 &= \gamma \left(A^0 + \mathbf{v} \cdot \mathbf{A} \right) \\
\mathbf{A}' &= \mathbf{A} + \gamma \mathbf{v} A^0 + (\gamma - 1) \frac{\mathbf{v} \cdot \mathbf{A}}{v^2} \mathbf{v}.
\end{aligned} \tag{2.2}$$

A tensor is a Lorentz tensor if it obeys Lorentz covariance, $A'^{(r)}(x', p') = (\Lambda)^r A(x, p)$ where r is the rank of the tensor. A scalar function is Lorentz invariant if $F(x', p') = F(x, p)$, i.e., the functional form is preserved by the transformation.

If we now denote the coordinates of the IRF by $(t', \boldsymbol{x}')$, the coordinates in the lab frame boosted by a velocity $\tilde{\boldsymbol{v}}$ are given by $x^\mu = \Lambda^\mu_\nu(\tilde{\boldsymbol{v}}) x'^\nu$. The interval between two arbitrarily close space-time points in the IRF can be expressed as $\Delta x'^\mu = (\Delta t', 0)$. We define this time interval in the IRF to be the proper time, $\Delta\tau = \Delta t'$. Equation (2.2) implies $\Delta x^\mu = \Delta\tau u^\mu$, where $u^\mu = \gamma(1, \boldsymbol{v})$ is the 4-velocity. The time intervals of the lab and rest frame are related by $\Delta t = \gamma \Delta\tau$.

2.1.2 Mass Shell

The 4-momentum of a particle is expressed by $p^\mu = mu^\mu$, where m is the rest mass. The momentum is constrained to the mass shell by enforcing

$$p^\mu p_\mu = (p^0)^2 - \mathbf{p}^2 = -m^2. \tag{2.3}$$

Under this condition, we denote p^0 by

$$E(\mathbf{p}) = \sqrt{m^2 + \mathbf{p^2}} = \gamma m.$$

We constrain a function of momentum to the mass shell by [24]

$$g(p^\mu) = \frac{\delta(p^0 - E)}{E} f(\mathbf{p}). \tag{2.4}$$

2.2 Dynamics

2.2.1 Electrodynamics

The material for this section follows from Lichnerowicz [47].

The Faraday tensor is defined by

$$F^{\mu\nu} = \nabla^\mu A^\nu - \nabla^\nu A^\mu,$$

where $A^\mu = (\phi, \mathbf{A})$ is the 4-vector potential. Explicitly

$$F^{\mu\nu} = \begin{vmatrix} 0 & E_x & E_y & E_z \\ -E_x & 0 & B_z & -B_y \\ -E_y & -B_z & 0 & B_x \\ -E_z & B_y & -B_x & 0 \end{vmatrix}. \tag{2.5}$$

The tensor is antisymmetric, and the covariant form of the Faraday tensor varies only in the sign of $\boldsymbol{E}$.

The action of the Faraday tensor on a 4-vector is given by

$$F^{\mu\nu}V_\nu = (\boldsymbol{E}\cdot\mathbf{V}, -\boldsymbol{E}V_0 + \mathbf{V}\times\boldsymbol{B}). \tag{2.6}$$

For the special case of F on the momentum, we recover the familiar Lorentz electromagnetic force

$$F^\mu = qF^{\mu\nu}p_\nu = mq\gamma(\boldsymbol{E}\cdot\mathbf{v}, \boldsymbol{E} + \mathbf{v}\times\boldsymbol{B}), \tag{2.7}$$

where q is the charge and the 0-term corresponds to work done by the field. Note that the antisymmetry of F ensures the electromagnetic force vanish.

Since electromagnetic fields are expressed via the Faraday tensor, the fields transform with the tensor which requires two applications of Λ due to its rank. As such, E and B transform as

$$\begin{aligned}
\boldsymbol{E} &= \gamma(\boldsymbol{E}' + \boldsymbol{v}\times\boldsymbol{B}') - \frac{\gamma^2}{\gamma+1}\boldsymbol{v}(\boldsymbol{v}\cdot\boldsymbol{E}') \\
\boldsymbol{B} &= \gamma(\boldsymbol{B}' - \boldsymbol{v}\times\boldsymbol{E}') - \frac{\gamma^2}{\gamma+1}\boldsymbol{v}(\boldsymbol{v}\cdot\boldsymbol{B}') \\
\boldsymbol{E}' &= \gamma(\boldsymbol{E} - \boldsymbol{v}\times\boldsymbol{B}) - \frac{\gamma^2}{\gamma+1}\boldsymbol{v}(\boldsymbol{v}\cdot\boldsymbol{E}) \\
\boldsymbol{B}' &= \gamma(\boldsymbol{B} + \boldsymbol{v}\times\boldsymbol{E}) - \frac{\gamma^2}{\gamma+1}\boldsymbol{v}(\boldsymbol{v}\cdot\boldsymbol{B}),
\end{aligned} \tag{2.8}$$

where primed quantities are measured in a frame moving at velocity $\boldsymbol{v}$ relative to the unprimed quantities.

The Faraday tensor also has a dual given by

$$\mathcal{F}^{\mu\nu} = \frac{1}{2}\epsilon^{\mu\nu\alpha\beta}F_{\alpha\beta} = \begin{vmatrix} 0 & B_x & B_y & B_z \\ -B_x & 0 & -E_z & E_y \\ -B_y & E_z & 0 & -E_x \\ -B_z & -E_y & E_x & 0 \end{vmatrix}, \tag{2.9}$$

where $\epsilon^{\mu\nu\alpha\beta}$ is the fully antisymmetric Levi-Cevita tensor.

The Faraday tensor and its dual provide two important Lorentz invariant scalars describing the field strength:

$$\mathcal{F}^{\mu\lambda}F_{\lambda\nu} = g^{\mu}_{\nu}\boldsymbol{E}\cdot\boldsymbol{B} \tag{2.10}$$

and

$$F_{\mu\nu}F^{\nu\mu} = 2(B^2 - E^2). \tag{2.11}$$

These scalars will be used often, so we introduce the following notation:

$$h^2 = B^2 - E^2 \tag{2.12}$$

and

$$\lambda = \boldsymbol{E}\cdot\boldsymbol{B}/h^2. \tag{2.13}$$

λ provides the Lorentz invariant description of the magnetized limit, i.e., when $\lambda \to 0$, and expresses the strength of the electric field parallel to the magnetic field.

Having constructed the Faraday tensor, we can now express Maxwell's equations in covariant form:

$$\nabla_{\nu}F^{\mu\nu} = J^{\mu} \tag{2.14}$$

$$\nabla_\alpha F_{\beta\gamma} + \nabla_\gamma F_{\alpha\beta} + \nabla_\beta F_{\gamma\alpha} = 0, \tag{2.15}$$

where $J^\mu = (\rho, \mathbf{J})$ is the 4-vector current density. The current density serves as the source term for Maxwell's equations and requires another expression to close the system.

The homogeneous set of Maxwell equations can be more compactly expressed in terms of the dual Faraday tensor due to their relationship (2.9) and the permutation symmetry of the Levi-Cevita tensor:

$$\nabla_\nu \mathcal{F}^{\mu\nu} = \frac{1}{2}\epsilon^{\mu\nu\alpha\beta}\nabla_\nu F_{\alpha\beta} = \frac{1}{6}\epsilon^{\mu\nu\alpha\beta}\left(\nabla_\alpha F_{\beta\gamma} + \nabla_\gamma F_{\alpha\beta} + \nabla_\beta F_{\gamma\alpha}\right) = 0. \tag{2.16}$$

The Maxwell stress-energy tensor is given by:

$$T^{\mu\nu}_{EM} = F^\mu_\kappa F^{\kappa\nu} - \frac{1}{4} g^{\mu\nu} F_{\kappa\lambda} F^{\kappa\lambda}. \tag{2.17}$$

Explicitly, the components of the Maxwell stress tensor are:

$$\begin{aligned} T^{00}_{EM} &= \frac{1}{2}(E^2 + B^2) \\ T^{0i}_{EM} &= T^{i0} = (\boldsymbol{E} \times \boldsymbol{B})_i \\ T^{ij}_{EM} &= \frac{1}{2}(E^2 + B^2)\delta^{ij} - (E_i E_j + B_i B_j). \end{aligned} \tag{2.18}$$

Maxwell's equations, (2.14) and (2.15) can alternately be expressed in a single equation via the Maxwell stress tensor:

$$\nabla_\nu T^{\mu\nu}_{EM} = -F^{\mu\kappa} J_\kappa. \tag{2.19}$$

2.2.2 Thermodynamic Equilibrium Stress-Energy Tensor

In the rest frame of a fluid, the thermodynamic equilibrium stress-energy tensor of the fluid must have the simple diagonal form

$$T_R^{\mu\nu} = \begin{vmatrix} u & 0 & 0 & 0 \\ 0 & p & 0 & 0 \\ 0 & 0 & p & 0 \\ 0 & 0 & 0 & p \end{vmatrix}, \tag{2.20}$$

where u is the internal energy density and p is the scalar pressure [75]. If we perform a Lorentz boost on the fluid moving with velocity $\boldsymbol{V}$ into the lab frame by applying equation (2.1) twice, we obtain

$$\begin{aligned} T^{00} &= \gamma^2(u + pV^2) \\ T^{0i} &= \gamma^2 V_i(u + p) \\ T^{ij} &= \delta_{ij}p + \gamma^2(u + p)V_iV_j. \end{aligned} \tag{2.21}$$

Therefore,

$$T^{\mu\nu} = p\eta^{\mu\nu} + (u + p)U^\mu U^\nu = p\eta^{\mu\nu} + hU^\mu U^\nu, \tag{2.22}$$

where $h = u + p$ is the enthalpy density of the fluid.

2.3 Kinetic Theory

2.3.1 Tensor Moments

Moments of the distribution can be expressed equivalently in terms of either f, the distribution function of three-vector momenta or g, the distribution of four-vector momenta, as

$$\begin{aligned} M^{\alpha\beta\ldots\omega} &= \int \frac{d^3p}{E} p^\alpha p^\beta \ldots p^\omega f(t, \boldsymbol{x}, \mathbf{p}) \\ &= \int d^4p p^\alpha p^\beta \ldots p^\omega g(x, p), \end{aligned} \tag{2.23}$$

where f and g are Lorentz scalars and interchanged via mass-shell constraint (2.4) [24].

Our analysis involves moments up to and including the fourth rank. We express each moment below:

$$\rho = m^2 \int \frac{d^3p}{E} f, \tag{2.24}$$

$$\Gamma^\alpha = \int \frac{d^3p}{E} f p^\alpha, \tag{2.25}$$

$$T^{\alpha\beta} = \int \frac{d^3p}{E} f p^\alpha p^\beta, \tag{2.26}$$

$$M^{\alpha\beta\gamma} = \int \frac{d^3p}{E} f p^\alpha p^\beta p^\gamma, \tag{2.27}$$

$$R^{\alpha\beta\gamma\delta} = \int \frac{d^3p}{E} f p^\alpha p^\beta p^\gamma p^\delta, \tag{2.28}$$

where ρ is the scalar mass density, Γ^α is the 4-vector fluid particle-flux density, $T^{\alpha\beta}$ is the stress-energy tensor, $M^{\alpha\beta\gamma}$ is typically referred to as the stress flow tensor, and $R^{\alpha\beta\gamma\delta}$ will be referred to as the energy-weighted stress tensor.

The fluid rest frame corresponds to the frame in which Γ has only a temporal component:

$$\Gamma^{\mu}_{R} = n_R(1, 0).$$

The rest frame expression for the flow density provides a convenient definition for the fluid bulk velocity

$$U^{\mu} = \Gamma^{\mu}/n_R = \gamma(\boldsymbol{V})(1, \boldsymbol{V}).$$

This definition of the fluid four-velocity coincides with the Eckart [27] definition. An alternate definition for the four-velocity by Landau and Lifshitz [45] relates the four-velocity to the flow of energy.

2.3.2 Kinetic Equation

In general, the ensemble averaged relativistic kinetic equation may be expressed as

$$\frac{p^{\mu}}{m}\frac{\partial}{\partial x^{\mu}}g(x,p) + \frac{\partial}{\partial p^{\mu}}\left[F^{\mu}(x,p)g(x,p)\right] = C(x,p),$$

where $F^{\mu}(x,p)$ is any externally applied four-force and $C(x,p)$ is a collision operator [24]. For the special case in which the four-force conserves phase space ($\partial F^{\mu}/\partial p^{\mu} = 0$), as is the case for the Lorentz force expressed in equation (2.7), we have

$$\frac{p^{\mu}}{m}\frac{\partial}{\partial x^{\mu}}g(x,p) + F^{\mu}(x,p)\frac{\partial}{\partial p^{\mu}}g(x,p) = C(x,p).$$

Finally, if we recall p^0 is dependent upon $\boldsymbol{p}$ due to the mass shell constraint found in equation (2.3), we can express the relativistic kinetic equation as

$$\frac{p^{\mu}}{m}\frac{\partial}{\partial x^{\mu}}f(x,p) + \mathbf{F}(x,p)\cdot\frac{\partial}{\partial \boldsymbol{p}}f(x,p) = C(x,p) \tag{2.29}$$

2.3.3 Moments of the Kinetic Equation

We now operate on equation (2.29) with $\int \frac{d^3p}{E} p^\alpha \cdots p^\omega$ to obtain evolution equations for the tensor moments. The moment of the first term in equation (2.29) is

$$\int \frac{d^3p}{E} p^\alpha \cdots p^\omega \frac{p^\mu}{m} \frac{\partial f}{\partial x^\mu} = \frac{1}{m} \frac{\partial M^{\mu\alpha\cdots\omega}}{\partial x^\mu}, \tag{2.30}$$

where the equality simply follows from pulling the spatial derivative through the integral because momentum is independent of position.

To obtain the moment of the second term in equation (2.29), we begin by integrating by parts and specialize to the Lorentz force

$$\begin{aligned} \int \frac{d^3p}{E} p^\alpha \cdots p^\omega F^\mu \frac{\partial f}{\partial p^\mu} &= -\int \frac{d^3p}{E} f F^\mu \frac{\partial}{\partial p^\mu} \left(p^\alpha \cdots p^\omega\right) \\ &= -\frac{q}{m} F^{\mu\nu} \int \frac{d^3p}{E} f p_\nu \frac{\partial}{\partial p_\mu} \left(p^\alpha \cdots p^\omega\right) \\ &= -\frac{q}{m} F^{(\alpha\nu} M_\nu^{\beta\cdots\omega)}, \end{aligned} \tag{2.31}$$

where the superscript parentheses indicate unnormalized symmetrization over non-summed indicies:

$$F^{(\alpha\nu} M_\nu^{\beta\gamma)} = F^{\alpha\nu} M_\nu^{\beta\gamma} + F^{\beta\nu} M_\nu^{\alpha\gamma} + F^{\gamma\nu} M_\nu^{\alpha\beta}.$$

Moments of the collision operator are expressed as

$$C^{\alpha\cdots\omega} = m \int \frac{d^3p}{E} p^\alpha \cdots p^\omega f C.$$

Thus, the moment equation for an arbitrary moment can be written

$$\frac{\partial M^{\mu\alpha\cdots\omega}}{\partial x^\mu} = q F^{\{\alpha\nu} M_\nu^{\beta\cdots\omega\}} + C^{\alpha\cdots\omega}. \tag{2.32}$$

2.3.4 Maxwellian Moments

A rest frame Maxwellian distribution can be written as

$$f_{MR}(x,p) = N_M e^{-H(\boldsymbol{x},\boldsymbol{v})/T}, \tag{2.33}$$

where $H(\boldsymbol{x},\boldsymbol{v}) = p^0 + qA^0 = P^0$ is the Hamiltonian and $P^\mu = p^\mu + qA^\mu$ is the canonical momentum, T is related to the temperature, and N_M is a normalization factor related to density [24]. In an arbitrary frame,

$$f_M(x,p) = N_M e^{U_\mu P^\mu/T}. \tag{2.34}$$

This relativistic form of the Maxwellian distribution is also referred to as a Jüttner distribution.

Using equation (2.23) we present the first few moments to introduce the relativistic formalism of taking moments:

$$\begin{aligned} M_R^{(r)\alpha\beta\ldots\omega} &= \int \frac{d^3p}{E} p^\alpha p^\beta \ldots p^\omega f_{MR}(t,\boldsymbol{x},\mathbf{p}) \\ &= N_M m^{r+2} e^{-\Phi/T} \int \frac{d^3s}{\sqrt{1+s^2}} s^\alpha \ldots s^\omega e^{-\zeta\sqrt{1+s^2}}, \end{aligned}$$

where r is the tensor rank, $s^\alpha = p^\alpha/m$, and $\zeta = m/T$.

1. In the rest frame, $\Gamma_R^\mu = M_{MR}^{(1)\mu}$ has only one non-zero component

$$\begin{aligned} \Gamma_R^0 = n_R &= N_M m^3 e^{-\Phi/T} \int d^3s e^{-\zeta\sqrt{1+s^2}} \\ &= 4\pi N_M m^3 e^{-\Phi/T} \int ds s^2 e^{-\zeta\sqrt{1+s^2}} \end{aligned} \tag{2.35}$$

The stress tensor will have two non-zero components in the rest frame:

2.

$$\begin{aligned} T_R^{00} = u &= N_M m^4 e^{-\Phi/T} \int \frac{d^3s}{\sqrt{1+s^2}}(1+s^2)e^{-\zeta\sqrt{1+s^2}} \\ &= 4\pi N_M m^4 e^{-\Phi/T} \int \frac{ds}{\sqrt{1+s^2}}(1+s^2)s^2 e^{-\zeta\sqrt{1+s^2}} \end{aligned} \tag{2.36}$$

and

3.

$$\begin{aligned} T_R^{ij} = p\delta_{ij} &= N_M m^4 e^{-\Phi/T} \int \frac{d^3s}{\sqrt{1+s^2}} s^i s^j e^{-\zeta\sqrt{1+s^2}} \\ &= 4\pi N_M m^4 e^{-\Phi/T} \int \frac{ds}{\sqrt{1+s^2}} s^i s^j s^2 e^{-\zeta\sqrt{1+s^2}}. \end{aligned} \tag{2.37}$$

All of the moments involve integrals of the form

$$\int_0^\infty \frac{ds}{\sqrt{1+s^2}} s^{2n} e^{-\zeta\sqrt{1+s^2}} = \frac{\Gamma(n+1/2)}{\sqrt{\pi}} \left(\frac{2}{\zeta}\right)^n K_n(\zeta) = \frac{1\cdot 3\cdots(2n-1)K_n(\zeta)}{\zeta^n}, \tag{2.38}$$

where K_n is the n^{th} MacDonald function and Γ is the Gamma function.

More generally, the integrals also involve powers of $s^0 = \sqrt{1+s^2}$, which can be obtained via ζ derivatives of the integrals since all of the ζ dependence is in the exponent of the Maxwellian with products of s^0. Therefore,

$$\int_0^\infty ds(1+s^2)^{k/2} s^{2n} e^{-\zeta\sqrt{1+s^2}} = 1\cdot 3\cdots(2n-1)\left(\frac{-\partial}{\partial\zeta}\right)^{k+1}\left(\frac{K_n(\zeta)}{\zeta^n}\right), \tag{2.39}$$

where derivatives and other properties of the MacDonald functions are given in Appendix 0.2.

Using the above identities, the integrated moments are

$$\begin{aligned} n_R &= 4\pi N_M m^2 e^{-\Phi/T} \frac{K_2}{\zeta} \\ u &= 4\pi N_M m^4 e^{-\Phi/T} \left(\frac{K_1}{\zeta} + \frac{3K_2}{\zeta^2} \right) \\ p &= 4\pi N_M m^4 e^{-\Phi/T} \frac{K_2}{\zeta^2}. \end{aligned} \tag{2.40}$$

We can now express N_M in terms of the density

$$N_M = \frac{n_R e^{\Phi/T}}{4\pi m^2 T K_2(\zeta)}, \tag{2.41}$$

which leads to the expression for the Maxwellian in terms of the rest frame density:

$$f_M = \frac{n_R}{4\pi m^2 T K_2(\zeta)} e^{-p^0/T}. \tag{2.42}$$

Expressing our moments in terms of the density, we have:

$$\begin{aligned} u &= m n_R \left(\frac{K_1}{K_2} + \frac{3}{\zeta} \right), \\ p &= n_R T, \end{aligned} \tag{2.43}$$

which implies $\zeta = m/T = m n_R/p$.

2.3.5 Connections Between Moments

Due to the mass shell constraint, equation (2.3), contracting pairs of indices of a tensor moment will be proportional to a tensor two ranks lower

$$M_\alpha^{(r)\alpha\beta\cdots\omega} = -m^2 M^{(r-2)\beta\cdots\omega}. \tag{2.44}$$

This contraction property can be repeated until pairs of indices are exhausted.

The zero component of a rank (r) tensor moment is related to a rank (r-1) Maxwellian moment via a ζ derivative:

$$\begin{aligned}\frac{\partial}{\partial\zeta}M_R^{(r-1)\alpha\cdots\omega} &= \frac{\partial N_m}{\partial\zeta}m^{r+1}e^{-\Phi/T}\int\frac{d^3s}{s^0}s^\alpha...s^\omega e^{-\zeta s^0} \\ &- N_m m^{r+1}e^{-\Phi/T}\int d^3s s^\alpha...s^\omega e^{-\zeta s^0} \\ &= \frac{\partial N_m}{\partial\zeta}m^{r+1}e^{-\Phi/T}\int\frac{d^3s}{s^0}s^\alpha...s^\omega e^{-\zeta s^0} - \frac{1}{m}M_R^{(r)0\alpha\cdots\omega}.\end{aligned} \tag{2.45}$$

2.4 Magnetized Plasma

Two conditions must be satisfied for our relativistic plasma to be considered magnetized [47]:

1. The two electromagnetic field invariants must satisfy

$$h^2 > 0, \tag{2.46}$$

$$\lambda \ll 1. \tag{2.47}$$

2. The thermal gyroradius, $V_T/\Omega_B = V_T eB/\gamma m$, must be small compared to any gradient scale length:

$$\delta \ll 1, \tag{2.48}$$

where δ is the ratio of the thermal gyroradius of any plasma species to any gradient scale length.

We assume the (gyro)ordering $\lambda \sim \delta$ for convenience. We will implicitly use this definition of a magnetized plasma throughout.

2.4.1 Quasi-Projectors

As is typical in a magnetized plasma, notions of parallel and perpendicular to the field play important roles. Thus, we need a covariant meaning for parallel and perpendicular. Such a meaning is provided by:

$$e^{\nu}_{\mu} \equiv -F_{\mu\kappa}F^{\kappa\nu}/h^2 \tag{2.49}$$

and

$$b^{\nu}_{\mu} \equiv g^{\nu}_{\mu} - e^{\nu}_{\mu}. \tag{2.50}$$

e and b become approximate perpendicular and parallel projection operators in the magnetized limit. Explicitly, the components of the projectors are

$$\begin{aligned}
e^0_0 &= -E^2/h^2 \\
e^0_i &= -e^i_0 = (\boldsymbol{E}\times\boldsymbol{B})_i/h^2 \\
e^j_i &= (B^2\delta^j_i - B_iB_j - E_iE_j)/h^2 \\
b^0_0 &= B^2/h^2 \\
b^0_i &= -b^i_0 = -(\boldsymbol{E}\times\boldsymbol{B})_i/h^2 \\
b^j_i &= (-E^2\delta^j_i + B_iB_j + E_iE_j)/h^2.
\end{aligned}$$

In a frame in which the transverse electric field vanishes (the reduced frame, a subset of the IRF), the action of e and b on an arbitrary 4-vector $C_\mu = (C_0, \mathbf{C})$ is given by

$$b^{\mu\kappa}C_\kappa|_R = (C^0, \mathbf{C}_\parallel), \tag{2.51}$$

$$e^{\mu\kappa}C_\kappa|_R = (0, \mathbf{C}_\perp). \tag{2.52}$$

$\parallel$ and $\perp$ have the typical three-dimensional meaning: $\mathbf{C}_\parallel = \boldsymbol{BB}\cdot\mathbf{C}/B^2 = \boldsymbol{bb}\cdot\mathbf{C}$, $\mathbf{C}_\perp = \mathbf{C} - \mathbf{C}_\parallel$, where $\boldsymbol{b}$ is the standard abbreviation $\boldsymbol{b} \equiv \boldsymbol{B}/B$.

Gradients of the projection operators will be used implicitly later in our analysis. Thus, we present their forms. To do so, we begin by expressing the projection operators in terms of the Maxwell stress tensor (2.17) and observe

$$e^{\alpha\beta} = \frac{g^{\alpha\beta}}{2} + \frac{T^{\alpha\beta}_{EM}}{h^2},$$

$$b^{\alpha\beta} = \frac{g^{\alpha\beta}}{2} - \frac{T^{\alpha\beta}_{EM}}{h^2}.$$

Thus, it is straightforward to show

$$\nabla_\nu b^\nu_\mu = \frac{F_{\mu\nu}}{h^2}J^\nu + \left(\frac{1}{2}g^\nu_\mu - b^\nu_\mu\right)\nabla_\nu \log h^2, \tag{2.53}$$

$$\nabla_\nu e^\nu_\mu = -\frac{F_{\mu\nu}}{h^2}J^\nu + \left(\frac{1}{2}g^\nu_\mu - e^\nu_\mu\right)\nabla_\nu \log h^2. \tag{2.54}$$

2.4.2 Reduced Frame

Provided $h^2 > 0$, as required in the magnetized limit, a Lorentz frame can be found in which $\boldsymbol{E}_\perp = 0$. Further, a rotation can be performed in the boosted frame so that the magnetic field lies along the z-axis. In this frame, the Faraday tensor has the reduced form

$$F^{\mu\nu} = \begin{vmatrix} 0 & 0 & 0 & E \\ 0 & 0 & B & 0 \\ 0 & -B & 0 & 0 \\ -E & 0 & 0 & 0 \end{vmatrix}, \tag{2.55}$$

where the surviving component of the electric field must be parallel to the magnetic field. Thus, the magnetized limit of the reduced Faraday tensor can be obtained by setting $E \propto \lambda \simeq 0$.

2.4.3 Field Strength Tensors

Since equation (2.55) represents a rank 2 matrix in the magnetized limit, the Faraday tensor has a two dimensional null space. The first 4-vector in the span of the null space can be found by examining the electromagnetic force on a moving, charged fluid, $qF^{\mu\nu}\Gamma_\nu = qn_R F^{\mu\nu}U_\nu$. Considering force-free flows in the magnetized limit and equation (2.6) implies

$$F^{\mu\nu}U_\nu = \gamma\left(\boldsymbol{E}\cdot\boldsymbol{V}, \boldsymbol{E} + \boldsymbol{V}\times\boldsymbol{B}\right) = \mathcal{O}(\lambda).$$

The above expression implies

$$\boldsymbol{V} = V_\parallel \boldsymbol{b} + \frac{\boldsymbol{E}\times\boldsymbol{B}}{B^2} = V_\parallel \boldsymbol{b} + \boldsymbol{V}_E. \tag{2.56}$$

Thus, we can conclude

$$E^\mu \equiv F^{\mu\nu}U_\nu = \gamma E_\parallel(V_\parallel, \boldsymbol{b}) \tag{2.57}$$

is a 4-vector description of the parallel electric field strength in the magnetized limit [47]. Also, equation (2.56) implies

$$U^\mu U_\mu = -1,$$

as it must to satisfy the mass shell condition for the fluid momentum.

The second vector in the null space must be linearly independent to U^μ, so we can choose it to be an orthogonal vector to U^μ. Equation (2.10) implies any h^μ satisfying $h^\mu \propto \mathcal{F}^{\mu\nu}C_\nu$ for arbitrary C_ν will be in the null space in the magnetized limit. We choose $C^\mu = U^\mu$ to complete our null space. Under this assumption

$$h^\mu = \mathcal{F}^{\mu\nu}U_\nu = (\gamma \boldsymbol{V}\cdot\boldsymbol{B}, \frac{\boldsymbol{B}}{\gamma} + \gamma(\boldsymbol{V}\cdot\boldsymbol{B})\boldsymbol{V}), \tag{2.58}$$

provides a 4-vector description of the magnetic field strength [47].

h^μ satisfies

$$h^\mu h_\mu = B^2(1 - V_E^2) = B^2 - E^2 = h^2.$$

As such, we can also consider the normalized magnetic field strength 4-vector, $k^\mu = h^\mu/h$. Also, h^μ satisfies the following identities:

$$\mathcal{F}^{\mu\nu}h_\nu = h^2 U^\mu$$

and

$$F^{\mu\nu}h_\nu = E_\parallel B U^\mu.$$

2.4.4 Derivatives

The two vectors in the null space of the Faraday tensor provide useful scalar derivatives. As in nonrelativistic theory, the MHD flow provides the

convective time derivative

$$U^\mu \partial_\mu = \gamma d/dt = d/d\tau. \tag{2.59}$$

k^μ generates a directional derivative

$$k^\mu \partial_\mu = d/ds = \frac{B}{h}\left(v_\parallel \frac{d}{d\tau} + \frac{1}{\gamma}\nabla_\parallel\right), \tag{2.60}$$

where $\nabla_\parallel = \boldsymbol{b}\cdot\nabla$ is the directional derivative along the field. $k^\mu\partial_\mu$ reduces to the directional derivative along the magnetic field in the rest frame.

2.4.5 Alternate Expression of Faraday Tensor

We construct a representation of the Faraday tensor and its dual using three basic 4-vectors appearing in our theory: E^μ, h^μ, and U^μ. In the reduced frame, these 4-vectors reduce to

$$E^\mu = (0, 0, 0, E_\parallel),$$

$$h^\mu = (0, 0, 0, B),$$

$$U^\mu = (1, 0, 0, 0).$$

We can construct the reduced Faraday tensor's electric field dependence by inspection from the simple combination $U^\mu E^\nu - U^\nu E^\mu$. The Faraday tensor's magnetic field dependence can be expressed as $\epsilon^{\mu\nu\alpha\beta}U_\alpha h_\beta$. Thus, we can write the Faraday tensor as

$$F^{\mu\nu} = U^\mu E^\nu - U^\nu E^\mu - \epsilon^{\mu\nu\alpha\beta}U_\alpha h_\beta, \tag{2.61}$$

which must hold in any reference frame. Similarly, we obtain the following for the Faraday tensor dual

$$\mathcal{F}^{\mu\nu} = U^{\mu}h^{\nu} - U^{\nu}h^{\mu} + \epsilon^{\mu\nu\alpha\beta}U_{\alpha}E_{\beta}. \tag{2.62}$$

Lichnerowicz [47] presents the same expressions for the Faraday tensors; however, he employs an alternate derivation.

We now use (2.62) and the homogeneous Maxwell equations to construct two useful identities involving U^{μ} and k^{μ}. The first identity follows from

$$U_{\nu}\partial_{\mu}\mathcal{F}^{\mu\nu} = hU_{\nu}U^{\mu}\partial_{\mu}k^{\nu} + k^{\mu}\partial_{\mu}h + h\partial_{\mu}k^{\mu} = 0. \tag{2.63}$$

Re-arranging terms, we obtain

$$\partial_{\mu}k^{\mu} = \gamma\mathbf{k}\cdot\frac{d\boldsymbol{V}}{d\tau} - \frac{d\log h}{ds}. \tag{2.64}$$

In the non-relativistic limit, this identity reduces to: $\nabla\cdot\boldsymbol{b} = -\nabla_{\parallel}\log B$, i.e., $\nabla\cdot\boldsymbol{B} = 0$.

The second identity follows from

$$k_{\nu}\partial_{\mu}\mathcal{F}^{\mu\nu} = U^{\mu}\partial_{\mu}h + h\partial_{\mu}U^{\mu} - hk_{\nu}k^{\mu}\partial_{\mu}U^{\nu} = 0, \tag{2.65}$$

which simplifies to

$$k_{\nu}k^{\mu}\partial_{\mu}U^{\nu} = \gamma\mathbf{k}\cdot\frac{d\boldsymbol{V}}{ds} = \frac{d}{d\tau}\log\left(\frac{h}{n_R}\right). \tag{2.66}$$

In the non-relativistic limit, this identity reduces to: $\boldsymbol{b}\cdot\nabla_{\parallel}\boldsymbol{V} = \frac{d}{dt}\log\left(\frac{B}{n_R}\right)$.

2.4.6 Reduced Projectors

In the magnetized limit of the reduced frame, the parallel projection operator has the simple form

$$b^{\mu\nu} = diag\left\{-1, 0, 0, 1\right\}. \tag{2.67}$$

Also, in the reduced frame,

$$k^{\mu} = (0, 0, 0, 1) \tag{2.68}$$

and

$$U^{\mu} = (1, 0, 0, 0). \tag{2.69}$$

Therefore, we obtain the following alternate expression for the parallel projection operator:

$$b^{\mu\nu} = k^{\mu}k^{\nu} - U^{\mu}U^{\nu}, \tag{2.70}$$

which must hold in any frame related by a proper Lorentz transformation. Similarly,

$$e^{\mu\nu} = g^{\mu\nu} + U^{\mu}U^{\nu} - k^{\mu}k^{\nu}. \tag{2.71}$$

2.4.7 Useful Tensor Products

Below is a summary of useful products involving the basic tensors employed throughout:

$$
\begin{aligned}
e \cdot F = F \cdot e &= F - \lambda \mathcal{F} \\
e \cdot \mathcal{F} = \mathcal{F} \cdot e &= -\lambda F \\
b \cdot F = F \cdot b &= \lambda \mathcal{F} \\
b \cdot \mathcal{F} = \mathcal{F} \cdot b &= \mathcal{F} + \lambda F \\
e \cdot e &= e + \lambda^2 I \\
b \cdot b &= b + \lambda^2 I \\
e \cdot b = b \cdot e &= -\lambda^2 I \\
F \cdot U = F \cdot h &= 0 \\
\mathcal{F} \cdot U = -U \cdot \mathcal{F} &= h \\
\mathcal{F} \cdot h = -h \cdot \mathcal{F} &= h^2 U \\
b \cdot h &= h \\
b \cdot U &= U \\
e \cdot h = e \cdot U &= 0,
\end{aligned}
\tag{2.72}
$$

where dot represents the inner product of the tensors, $I^{\mu}_{\nu} = \delta^{\mu}_{\nu}$ is the unit matrix, and identities involving U and h suppress $\mathcal{O}(\lambda)$ terms as they will not be important for the forthcoming analysis.

Chapter 3

A Critique of Hazeltine Mahajan

We begin our analysis by discussing the covariant fluid closure of Hazeltine and Mahajan [35] (HM) on which our closure is based. Our study of the closure yielded several major shortcomings of the original model. We present the original closure with corrections, then explore the deficiencies of the HM model in detail.

3.1 Closure Summary with Corrections

We briefly review the relativistic fluid closure of HM. However, the form of the relativistic heat flux evolution equation provided in HM omits relevant terms from the gyroscale dependent portion due to an ordering error. Also, the non-relativistic form of the closure presented in Hazeltine and Mahajan (2002b/c) contains algebraic errors which, when combined with the omission noted above, lead to an incorrect evolution equation for the parallel heat flux. These errors are corrected below.

The corrected HM fluid equations in covariant form are:

$$\partial_\nu \Gamma^\nu = 0, \tag{3.1}$$

$$\mathcal{F}_{\mu\kappa}\partial_\nu T^{\kappa\nu} = eE_\parallel \frac{B}{h}\Gamma_\mu, \tag{3.2}$$

$$F^\mu_\kappa \partial_\nu \mathcal{T}^{\kappa\nu} = -h^2 e^{\mu\nu} J_\nu, \tag{3.3}$$

$$e_{\alpha\beta}\partial_\kappa M^{\kappa\alpha\beta} = 0, \tag{3.4}$$

$$\left(U_\alpha k_\beta + U_\beta k_\alpha\right)\partial_\kappa M^{\kappa\alpha\beta} = -2e\frac{B}{h}\left(u + p_\parallel\right)E_\parallel. \tag{3.5}$$

The non-relativistic (NR) limit is found by letting $\zeta = \frac{m}{T} \gg 1$ and $V \to 0$. Formally, we take $V \sim \zeta^{-1/2}$ and $Q_\parallel \sim pV \sim \zeta^{-3/2}$ to obtain:

$$\frac{dn}{dt} + n\nabla\cdot\boldsymbol{V} = 0, \tag{3.6}$$

$$mn\mathbf{b}\cdot\frac{d\mathbf{V}}{dt} + \nabla_\parallel p_\parallel + \left(p_\perp - p_\parallel\right)\nabla_\parallel \log B = enE_\parallel, \tag{3.7}$$

$$B^2\mathbf{J}_\perp = \boldsymbol{B}\times\left(\mathcal{M}n\frac{d\boldsymbol{V}}{dt} + \nabla\mathcal{P}_\perp + \Delta\mathcal{P}\nabla\log B\right), \tag{3.8}$$

$$p_\parallel\frac{d}{dt}\log\left(\frac{p_\parallel B^2}{n^3}\right) + \frac{6}{5}\nabla_\parallel Q_\parallel - \frac{2}{5}Q_\parallel\nabla_\parallel\log B = 0, \tag{3.9}$$

$$p_\perp\frac{d}{dt}\log\left(\frac{p_\perp}{Bn}\right) + \frac{2}{5}\nabla_\parallel Q_\parallel - \frac{4}{5}Q_\parallel\nabla_\parallel\log B = 0, \tag{3.10}$$

$$\frac{dQ_\parallel}{dt} - \frac{16}{5}Q_\parallel \frac{d\log n}{dt} + \frac{9}{5}Q_\parallel \frac{d\log B}{dt} + \frac{p_\parallel}{m}\nabla_\parallel \frac{\frac{3}{2}p_\parallel + p_\perp}{n} - \frac{\Delta p}{mn}\left(2p_\parallel - p_\perp\right)\nabla_\parallel \log B = 0, \tag{3.11}$$

where calligraphic letters indicate summing over species and species indicies have been omitted elsewhere.

The closure is achieved through the use of a model distribution:

$$f\left(x,p\right) = f_M\left[1 + \hat{\Delta} + \Delta p_\alpha e^{\alpha\beta} p_\beta + Q_\alpha b^{\alpha\beta} p_\beta \left(1 + \hat{Q}U^\alpha p_\alpha\right)\right], \tag{3.12}$$

where f_M is the relativistic Maxwellian introduced in §2.3.4. The hatted quantities are chosen to ensure the rest-frame density coincides with that of a Maxwellian and the rest-frame flow vanishes.

$$f_R = f_{MR}\left[1 + \Delta\left(\frac{\mathbf{p}^2 - p_3^2}{m^2} - \frac{2K_3}{\zeta K_2}\right) + \frac{Q_3 p_3}{m}\left(1 - \frac{K_2}{K_3}\frac{p^0}{m}\right)\right], \tag{3.13}$$

where the K_n are MacDonald functions of $\zeta = \frac{m}{T}$, Δ is a function of Δp, and Q_3 is a function of $Q_\parallel$.

3.2 Poor Coupling

The most pertinent deficiency of the HM model is apparent from the linearized, NR equations of motion. Linearizing the NR equations (3.6 - 3.11) about an isotropic equilibrium with no equilibrium heat flow or flow velocity, Fourier transforming the linearized equations using $A = A_0 + \delta A e^{i\mathbf{k}\cdot\mathbf{x} - \omega t}$, and simplifying yields

$$\frac{\delta\Delta p_\alpha}{p_0} = -\frac{\frac{5}{2}v_\parallel^2 - \frac{25}{6}c_{\alpha s}^2}{\frac{5}{6}v_\parallel^2 - \frac{11}{6}c_{\alpha s}^2}\frac{\delta B}{B_0} + \frac{\frac{5}{3}v_\parallel^2 - \frac{5}{3}c_{\alpha s}^2}{\frac{5}{6}v_\parallel^2 - \frac{11}{6}c_{\alpha s}^2}\frac{\delta n}{n_0}, \tag{3.14}$$

where α is a species subscript, $c_{\alpha s}^2 = \frac{p_0}{m_\alpha n}$ is the species sound speed, and $v_\parallel = \omega/k_\parallel$ is the parallel phase velocity. In the $m_e \to 0$ limit, equation (3.14) reduces to

$$\frac{\delta\Delta p_e}{p_0} = -\frac{25}{11}\frac{\delta B}{B_0} + \frac{10}{11}\frac{\delta n}{n_0}. \tag{3.15}$$

If we perform a similar analysis for the set of equations presented by Ramos [58] for a non-relativistic two temperature bi-Maxwellian MHD closure retaining gyroviscous effects, which corresponds to the non-relativistic limit of our model presented in chapter 4, we obtain

$$\frac{\delta\Delta p_\alpha}{p_0} = -\frac{v_\parallel^2\left(3v_\parallel^2 - 4c_{\alpha s}^2\right)}{v_\parallel^4 - 4v_\parallel^2 c_{\alpha s}^2 + 3c_{\alpha s}^4}\frac{\delta B}{B_0} + \frac{2v_\parallel^2}{v_\parallel^2 - 3c_{\alpha s}^2}\frac{\delta n}{n_0}. \tag{3.16}$$

In the $m_e \to 0$ limit, equation (3.16) reduces to

$$\delta\Delta p_e = 0. \tag{3.17}$$

The anisotropy scaling observed in the HM model leads to grossly exaggerated estimates of the electron anisotropy under the typical MHD assumption of vanishing electron inertia. Such anomalous scaling of the pressure anisotropy is not observed in other extensions to fluid MHD or kinetic MHD.

The source of the anomalous scaling of the pressure anisotropy in the HM model is the use of a single parallel heat flow, $Q_\parallel$, rather than separating

the parallel heat flow into the parallel flow of parallel heat, $q_\parallel$, and the parallel flow of perpendicular heat, $q_\perp$,

$$Q_\parallel = \int d^3v v_\parallel v^2 f = \int d^3v v_\parallel v_\parallel^2 f + \int d^3v v_\parallel v_\perp^2 f = q_\parallel + q_\perp.$$

When a single heat flow is used, the evolution of parallel and perpendicular pressure, equations (3.9) and (3.10), are both coupled to parallel gradients of the total heat flow, and the evolution of the single heat flow is driven by parallel gradients parallel and perpendicular pressure. Using separate heat flows results in the expected evolution of the pressures and heat flows, namely $dp_\parallel/dt \sim \nabla_\parallel q_\parallel$, $dp_\perp/dt \sim \nabla_\parallel q_\perp$, $dq_\parallel/dt \sim \nabla_\parallel p_\parallel$, and $dq_\perp/dt \sim \nabla_\parallel p_\perp$, as is observed in Chew, Goldberger, and Low [17], Ramos [58], Snyder, Hammet, and Dorland [62], and here in equations (4.74) - (4.77).

Though separating the two forms of parallel heat is relatively common in the literature, the distinction between the heat flows does not appear in the stress tensor, in which only the sum, $Q_\parallel = q_\parallel + q_\perp$, enters. Therefore, HM attempts a closure involving only the total heat flow, $Q_\parallel$.

Relatedly, HM does a very poor job predicting the onset of the mirror instability. Kulsrud [44] cites the mirror instability to expound on the strengths of guiding-center kinetic theory and expose the weakness of fluid theories, specifically CGL. If we perform a similar linear analysis as above except in the electrostatic limit following an approach outlined in [62], we find the HM system becomes mirror unstable when

$$0 > -\frac{2}{5}\left(\frac{T_\perp}{T_\parallel}\right)^3 + \frac{19}{15}\left(\frac{T_\perp}{T_\parallel}\right)^2 + \frac{4}{5} + \frac{B^2}{2\mu_0 p_\parallel}.$$

For comparison, CGL predicts

$$0 > \frac{T_\perp}{T_\parallel} - \frac{1}{6}\left(\frac{T_\perp}{T_\parallel}\right)^2 + \frac{B^2}{2\mu_0 p_\parallel},$$

while Ramos [58], Snyder, Hammet, and Dorland [62], kinetic theory (eg, [34] and [44]) and our theory correctly predict

$$0 > \frac{T_\perp}{T_\parallel} - \left(\frac{T_\perp}{T_\parallel}\right)^2 + \frac{B^2}{2\mu_0 p_\parallel}.$$

These expressions versus the ratio $T_\perp/T_\parallel$ for fixed plasma $\beta = 2\mu_0 p/B^2$ are plotted in figure 3.1 to provide a qualititative analysis of the difference in the models.

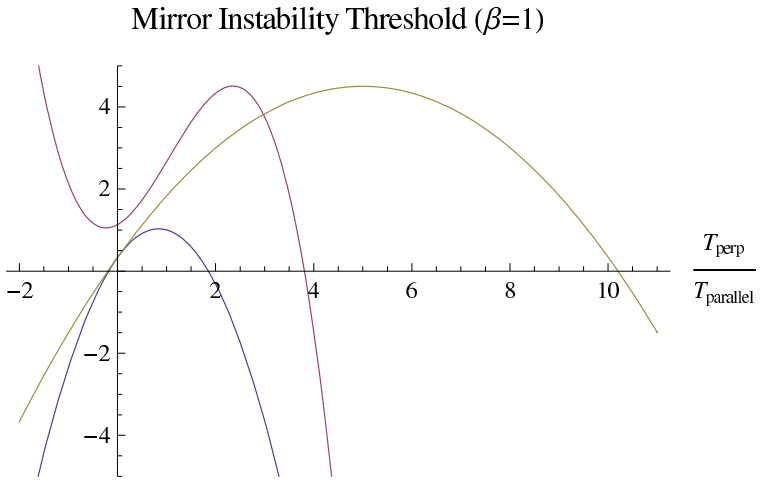

Figure 3.1: Blue = Correct Threshold, Red = HM, Gold = CGL

The source of this error is the unusual coupling of the pressures and heat flows noted above. The use of a relativistic bi-Maxwellian accurate to first order in the pressure anisotropy provides a better estimate of the mirror instability but still does not agree fully with kinetic MHD. However, a relativistic bi-Maxwellian retaining second-order pressure anisotropy terms captures

the correct mirror instability. Note, keeping accuracy to this order is reasonable since the fourth-rank moment (energy-weighted stress) will naturally have terms second-order in the anisotropy.

3.3 Thermodynamics

Examining the thermodynamics of HM leads to an unusual expression for the thermodynamic temperature. The standard thermodynamic temperature is $T_{Th} = p/n$ and is obtained via the entropy:

$$\left(\frac{\partial S_R^0}{\partial u}\right)_V^{-1} = T_{Th}.$$

For the HM system, the above expression yields a thermodynamic temperature of

$$T_{Th} = \frac{\left(p + \frac{2}{3}\Delta p\right)^2}{n\left(p + \frac{4}{3}\Delta p\right)}. \tag{3.18}$$

This form makes thermodynamic calculations awkward and can lead to confusion with the more typical definition of the thermodynamic temperature.

Also in HM, the enthalpy density, h, is defined to be $h = u + p_\parallel$. Typically, enthalpy is defined to be $h = u + p$. There is nothing inherently incorrect with this definition, but it can also lead to confusion.

These shortcomings are addressed here by modifying the distribution in HM to approximate a non-relativistic bi-Maxwellian expanded for small pressure anisotropy with only first-order terms retained, and by making a small modification to the $(0, 0)$ component of the stress tensor.

3.4 Annihilator Choice

Approximate parallel and perpendicular projection operators are used in HM as annihilators of the gyroscale portions of the exact moment equations to derive evolution equations for the parameters of the fluid system, i.e., equation (3.4). As noted in §2.4.6, the perpendicular projector can be re-cast as

$$e^{\mu\nu} = g^{\mu\nu} + U^{\mu}U^{\nu} - k^{\mu}k^{\nu}$$

Operating with $U^{\mu}U^{\nu}$ on the third rank or higher moments yields nearly redundant equations in the NR limit:

$$\begin{aligned} U_{\alpha}U_{\beta}\partial_{\gamma}M^{\gamma\alpha\beta} &\sim U_{\alpha}U_{\beta}\frac{d}{dt}M^{0\alpha\beta} \sim U_{\alpha}U_{\beta}\frac{d}{dt}T^{\alpha\beta} \sim U_{\alpha}\frac{d}{dt}T^{0\alpha} \\ &\sim U_{\alpha}\partial_{\gamma}T^{\gamma\alpha}, \end{aligned}$$

where the second equality is explained in §2.3.5. The right-hand-side (RHS) of the relationship is an evolution equation for the internal energy. The left-hand-side (LHS) agrees with the RHS only in the NR limit.

This redundancy leads to spurious instabilities in the moderate to ultra-relativistic temperature regimes of linear theory. This issue is solved by replacing the projection operators with more fundamental annihilators, such as U^{μ} and h^{μ}.

Chapter 4

Development

Having developed the machinery and provided a motivation for a more sophisticated relativistic closure, we now present such a closure. The closure begins by describing the necessary moment equations to close the system in §4.1 and 4.2. Contained within the moment equations are parameters which will be defined via a model distribution in §4.3, through which we finally arrive at a closed fluid system in §4.4. We then explore the thermodynamics of the system and some basic linear predictions in §4.5 and 4.6 respectively. Finally, we conclude with a summary of the closure in §4.7. The majority of this material was presented in TenBarge et al. [68].

4.1 Completing Closure

4.1.1 Closing Maxwell's Equations

Since plasmas are strongly coupled to the electromagnetic field, we must consider a closure involving Maxwell's equations. The coupling of the electromagnetic field to a plasma enters a fluid description through the second-moment equation, which constitutes the conservation of energy-momentum (eg Tsikarishvili et al. [70]). In relativistic form, the second-moment equation

takes the form

$$\nabla_\mu \mathcal{T}_p^{\mu\nu} - F^{\mu\nu} J_\nu = 0, \tag{4.1}$$

where $\mathcal{T}_p$ represents the the total (summed over all species) stress-energy tensor for the plasma and J_ν is the current density 4-vector. Thus, the second-moment equation is used as a constitutive relation for magnetized plasmas, providing closure to Maxwell's equations (2.14) and (2.16). It remains to compute the the current density in a magnetized plasma.

Equation (4.1), when composed with F^μ_κ, provides two components of the current density

$$e^{\mu\nu} J_\nu = -\frac{F^\mu_\kappa}{h^2} \nabla_\nu \mathcal{T}^{\kappa\nu}. \tag{4.2}$$

There are two independent components because the perpendicular quasi-projector has a two-dimensional null space. Charge conservation

$$\nabla_\nu J^\nu = 0 \tag{4.3}$$

and quasi-neutrality

$$J^\nu U_\nu = 0 \tag{4.4}$$

provide the two remaining components of the current density, where $U^\mu = (\gamma, \gamma \mathbf{V})$ is the local 4-velocity of the fluid, with $\gamma^2 = (1 - V^2)^{-1}$ the relativistic dilation factor. That equation (4.4) provides a good representation of quasi-neutrality will be shown in § 4.1.2.

We conclude that knowing the plasma stress tensor, and thus the current density, is sufficient to close Maxwell's equations.

4.1.2 Moments

Our analysis involves moments up to and including the fourth rank. The requisite moments are expressed in terms of the distribution function in §2.3.1.

The exact moments of the collisionless kinetic equation associated with the four requisite moments for our analysis represent particle conservation, momentum evolution, stress-flow evolution, and energy-weighted stress evolution:

$$\nabla_\alpha \Gamma^\alpha = 0, \tag{4.5}$$

$$\nabla_\alpha T^{\alpha\beta} = eF^{\beta\alpha}\Gamma_\alpha, \tag{4.6}$$

$$\nabla_\alpha M^{\alpha\beta\gamma} = e\left(F^{\beta\nu}T^\gamma_\nu + F^{\gamma\nu}T^\beta_\nu\right), \tag{4.7}$$

$$\nabla_\alpha R^{\alpha\beta\gamma\delta} = e\left(F^{\beta\nu}M^{\gamma\delta}_\nu + F^{\gamma\nu}M^{\beta\delta}_\nu + F^{\delta\nu}M^{\beta\gamma}_\nu\right). \tag{4.8}$$

Note in the second and higher moment equations, the left hand side involves the macroscopic scale, while the right hand side deals with the short gyroscale. Thus, the small-gyroradius limit is obtained formally by allowing the charge to become arbitrarily large, $e \to \infty$.

No restrictions on the size of higher order moments is assumed. Our analysis does not require higher moments because we only need those corresponding to the scalar coefficients appearing in the energy-momentum tensor. This tensor provides the framework for the closure of the plasma-Maxwell system.

At this point, we restrict our analysis to a plasma with a single ion species in the interest of simplicity. In order to satisfy quasi-neutrality, we require, to leading order, the electrons and ions have the same rest-frame densities, and reside in the same approximate rest frame to avoid arbitrarily large current densities; we do not restrict plasma flow, however. Equation (4.4) then follows as the leading order expression of quasi-neutrality.

4.1.3 Gyro-Ordering

We must now determine evolution equations for the four components of the flux density. First, we note that all moments can be expanded in the form

$$\Gamma^{\mu} = \Gamma^{\mu}_{(0)} + \Gamma^{\mu}_{(1)},$$

where the parenthetical subscript refers to the order of the term with respect to the gyroradius (δ). Thus, equation (4.6) provides

$$F^{\mu\nu}_{(0)}\Gamma_{(0)\mu} = 0, \tag{4.9}$$

where we distinguish the lowest order Faraday tensor, $F^{\mu\nu}_{(0)} \equiv F^{\mu\nu}\left(E_\parallel = 0\right)$, from its first-order counterpart

$$F^{\mu\nu}_{(1)} \equiv F^{\mu\nu} - F^{\mu\nu}_{(0)} \propto E_\parallel.$$

Recalling the action of the Faraday tensor on a four-vector, equation (4.9) implies

$$\Gamma^0_{(0)}\boldsymbol{E} + \boldsymbol{\Gamma}_{(0)} \times \boldsymbol{B} = 0, \tag{4.10}$$

which reproduces the familiar MHD Ohm's law, $\boldsymbol{E} + \boldsymbol{V} \times \boldsymbol{B} = 0$. As such, equation (4.9) fixes the two perpendicular components of the flow. The particle conservation law, equation (4.55), fixes another of the components.

At this point, we drop the ordering subscripts and use Γ^μ and U^μ to refer to the zeroth-order fields. Similarly, we drop the ordering subscript from the Faraday tensor where it is nonessential. We can now write the flow in the form

$$\Gamma^\mu = \gamma n_R \left(1, \boldsymbol{V}_\parallel + \boldsymbol{V}_E\right), \tag{4.11}$$

where $\boldsymbol{V}_E = \boldsymbol{E} \times \boldsymbol{B}/B^2$, $\boldsymbol{V}_\parallel = \boldsymbol{bb} \cdot \boldsymbol{V}$, and γ is evaluated at the lowest order flow velocity.

Before moving on, we note that equation (4.6) has become

$$\nabla_\nu T^{\mu\nu}_{(0)} = eF^{\mu\nu}_{(0)}\Gamma_{(1)\nu} + eF^{\mu\nu}_{(1)}\Gamma_{(0)\nu} \tag{4.12}$$

taking gyro-ordering of the moments and the Faraday tensor into account.

The remainder of this chapter is devoted to computing the stress tensor. Conventional MHD avoids this issue by assuming the stress tensor has the thermodynamic equilibrium form

$$\mathcal{T}^{\mu\nu} = pg^{\mu\nu} + hU^{\mu}U^{\nu}, \tag{4.13}$$

where p is the pressure and h the enthalpy density. This form only pertains to the highly collisional regime in which thermal relaxation occurs more rapidly than any other process of interest. Thus, our analysis can be viewed as taking place in a regime of much lower collisionallity. We ignore collisions altogether and compute the stress tensor subject to electromagnetic forces alone.

4.2 Covariant Evolution Equations

4.2.1 Magnetized Stress

We use the magnetized limit of equation (4.7) to find

$$F^{\alpha\nu}T^{\beta}_{\nu} + F^{\beta\nu}T^{\alpha}_{\nu} = 0. \tag{4.14}$$

We use indicial symmetry of the stress tensor, antisymmetry of the Faraday tensor, along with properties of the projection operators to conclude the stress tensor must have the following form:

$$\begin{aligned} T^{\alpha\beta} = {} & pg^{\alpha\beta} + hU^{\alpha}U^{\beta} + \frac{1}{3}\Delta p\left(2k^{\alpha}k^{\beta} - e^{\alpha\beta}\right) \\ & + Q_{\parallel}\left(k^{\alpha}U^{\beta} + U^{\alpha}k^{\beta}\right), \end{aligned} \tag{4.15}$$

where $p = (p_\parallel + 2p_\perp)/3$, $\Delta p = p_\parallel - p_\perp$, $Q_\parallel$, and h are Lorentz scalars corresponding to pressure, pressure anisotropy, total parallel heat flow, and enthalpy density respectively. We differentiate between the parallel flow of parallel heat, $q_\parallel$, and the parallel flow of perpendicular heat, $q_\perp$, with $Q_\parallel = q_\parallel + q_\perp$ and $\Delta Q_\parallel = \frac{2}{5}q_\parallel - \frac{3}{5}q_\perp$. It is important to note that this distinction does not enter at this order in the moment equations; the total parallel heat flow is the only distinct component that appears in the stress tensor. This stress tensor differs from that in HM primarily in notation. Here, the enthalpy presented corresponds to the standard thermodynamic definition, $h = u + p$, where $u = T_R^{00}$ is the energy density. In HM, $h = u + p_\parallel$.

The heat flow anisotropy's somewhat unusual form compared to the simple form for the pressure anisotropy is due to their differing origins. In both cases, the anisotropy is the traceless portion of the lowest rank tensor moment having their constituents as components. Upon examining the third rank moment and its trace, the symmetry properties of the components gives rise to the particular form for $Q_\parallel$ and $\Delta Q_\parallel$. The general appendix of Balescu [6] nicely outlines the symmetry properties, owing to properties of Hermite polynomials, in the non-relativistic limit.

Two evolution equations are provided by equation (4.12), once we identify an annihilator of the $\Gamma_{(1)\nu}$ term. Appropriate choices in the magnetized limit are k and U, since $k_\nu \left(U_\nu\right) F^{\kappa\nu} \sim \delta$. We find

$$k_\kappa \nabla_\nu T^{\kappa\nu} = e n_R \frac{B}{\sqrt{W}} E_\parallel \tag{4.16}$$

and

$$U_\kappa \nabla_\nu T^{\kappa\nu} = 0. \tag{4.17}$$

These equations advance the parallel momentum and total scalar pressure respectively.

4.2.2 Magnetized Stress Flow

The expression for $M^{\alpha\beta\gamma}$ given in HM does not allow for separate parallel and perpendicular heat flows. The three auxiliary parameters appearing in the stress flow tensor employed in HM permit dependence of the stress flow only on $p_\parallel$, $p_\perp$, and $Q_\parallel$. We modify the model for the stress flow to include an additional auxiliary parameter (m_4 in what follows) to permit the freedom of having two parallel heat flows.

In the magnetized limit, the fourth-rank conservation law determines the form of the stress-flow tensor

$$F^{(\alpha\kappa} M_\kappa^{\beta\gamma)} = 0, \tag{4.18}$$

where the superscript parentheses indicate indicial symmetrization over non-contracted indices:

$$\eta^{(\alpha\beta} U^{\gamma)} \equiv \eta^{\alpha\beta} U^\gamma + \eta^{\alpha\gamma} U^\beta + \eta^{\beta\gamma} U^\alpha.$$

This constraint is straightforwardly satisfied if we construct the stress-flow from tensors whose product with the Faraday tensor vanish in the magnetized

limit. The identities supplied in §2.4.7 suggest choosing U, k, and b as our constitutive tensors.

We are also constrained by the definition of the stress-flow (equation (2.27)) and particle flux (equation (2.25)). From the definitions, it can be seen that contracting two indices of the stress-flow reduces to the momentum flux

$$M_{\alpha}^{\alpha\mu} = -m^2\Gamma^{\mu} = -m^2 n_R U^{\mu}. \tag{4.19}$$

Given the above two constraints and assuming the only 4-vectors appearing in the stress-flow are U^{μ} and k^{μ}, an expression for the stress-flow is

$$M^{\alpha\beta\gamma} = m^2 n_R U^{\alpha} U^{\beta} U^{\gamma} + \sum_k m_k M_k^{\alpha\beta\gamma}, \tag{4.20}$$

where

$$M_1^{\alpha\beta\gamma} = g^{(\alpha\beta} U^{\gamma)} + 6U^{\alpha} U^{\beta} U^{\gamma}, \tag{4.21}$$

$$M_2^{\alpha\beta\gamma} = b^{(\alpha\beta} U^{\gamma)} + 4U^{\alpha} U^{\beta} U^{\gamma}, \tag{4.22}$$

$$M_3^{\alpha\beta\gamma} = g^{(\alpha\beta} k^{\gamma)} + 6U^{(\alpha} U^{\beta} k^{\gamma)}, \tag{4.23}$$

$$M_4^{\alpha\beta\gamma} = b^{(\alpha\beta} k^{\gamma)} - \frac{2}{3} g^{(\alpha\beta} k^{\gamma)}, \tag{4.24}$$

and the m_k are scalars to be determined later. The M_k are constructed to satisfy $M_{k\alpha}^{\alpha\gamma} = 0$, so that the second constraint above is satisfied.

We construct evolution equations for the magnetized stress-flow by finding annihilators for the right-hand side of equation (4.7). Two such equations are:

$$k_\alpha k_\beta \partial_\kappa M^{\kappa\alpha\beta} = 2e\frac{B}{\sqrt{W}} Q_\parallel E_\parallel, \tag{4.25}$$

$$\left(U_\alpha k_\beta + U_\beta k_\alpha\right) \partial_\kappa M^{\kappa\alpha\beta} = -2e\frac{B}{\sqrt{W}} E_\parallel \left(h + \frac{2}{3}\Delta p\right). \tag{4.26}$$

These equations can be considered to advance the parallel pressure and total parallel heat flow respectively.

We note that we cannot evolve the two parallel heat flows individually at this order. This is because evolving the separate heat flows requires a time-like (0-component) derivative of the elements of the stress-flow containing each parallel heat flow. It will become clear after evaluating the m_k that such separation is not possible at this order.

The m_k appearing in the stress flow can be taken to be auxiliary parameters of our system. Thus, we will need to express them in terms of the dynamical variables appearing in our system. As such, it is convenient to examine the instantaneous rest frame components of the stress flow in terms of the m_k, which are listed in Appendix 0.3.

4.2.3 Magnetized Energy-Weighted Stress

We construct the energy-weighted stress tensor in much the same way as the three previous tensors. We begin with the constraint provided by the fifth-rank conservation law in the magnetized limit

$$F^{(\alpha\kappa} R_{\kappa}^{\beta\gamma\delta)} = 0. \tag{4.27}$$

Our second constraint follows from the definitions of the energy-weighted stress (equation (2.28)) and the stress-energy (equation (2.26)) when contracting two indices of the energy-weighted stress

$$R_{\alpha}^{\alpha\gamma\delta} = -m^2 T^{\gamma\delta} \tag{4.28}$$

Our third constraint follows from contracting all four indices of the energy-weighted stress

$$R_{\alpha\beta}^{\alpha\beta} = m^4 \rho, \tag{4.29}$$

where $-\rho = T_{\alpha}^{\alpha} = -u + 3p$.

Unlike the third rank tensor whose indicial symmetrization is straightforward, the fourth rank tensor will have unique symmetrizations based on each tensor's construction, which are given in Appendix 0.4.

The following expression gives the simplest fourth-rank tensor that satisfies the above constraints, without introducing new independent variables

$$R^{\alpha\beta\gamma\delta} = m^2 \left[U^{(\alpha}U^{\beta}T^{\gamma\delta)} + 8pU^{\alpha}U^{\beta}U^{\gamma}U^{\delta} - Q_{\parallel}k^{(\alpha}U^{\beta}U^{\gamma}U^{\delta)}\right] + \sum_k r_k R_k^{\alpha\beta\gamma\delta}, \tag{4.30}$$

where

$$R_1^{\alpha\beta\gamma\delta} = g^{(\alpha\beta}g^{\gamma\delta)} + 6g^{(\alpha\beta}U^{\gamma}U^{\delta)} + 48U^{\alpha}U^{\beta}U^{\gamma}U^{\delta}, \tag{4.31}$$

$$R_2^{\alpha\beta\gamma\delta} = g^{(\alpha\beta}b^{\gamma\delta)} + 8b^{(\alpha\beta}U^{\gamma}U^{\delta)} + 2g^{(\alpha\beta}U^{\gamma}U^{\delta)} + 64U^{\alpha}U^{\beta}U^{\gamma}U^{\delta}, \tag{4.32}$$

$$R_3^{\alpha\beta\gamma\delta} = g^{(\alpha\beta}U^{\gamma}k^{\delta)} - 8U^{(\alpha}k^{\beta}k^{\gamma}k^{\delta)}, \tag{4.33}$$

$$R_4^{\alpha\beta\gamma\delta} = b^{(\alpha\beta}U^{\gamma}k^{\delta)} - 6U^{(\alpha}k^{\beta}k^{\gamma}k^{\delta)}, \tag{4.34}$$

$$R_5^{\alpha\beta\gamma\delta} = e^{(\alpha\beta}b^{\gamma\delta)} + 2e^{(\alpha\beta}U^{\gamma}U^{\delta)} + 2b^{(\alpha\beta}U^{\gamma}U^{\delta)} + 16U^{\alpha}U^{\beta}U^{\gamma}U^{\delta}. \tag{4.35}$$

It can be seen that the $R_{k\alpha}^{\alpha\gamma\delta} = 0$ so that $R_{\alpha}^{\alpha\gamma\delta} = -m^2T^{\gamma\delta}$ and $R_{\alpha\beta}^{\alpha\beta} = m^4\rho$. The terms multiplying m^2 in equation (4.30) account for overcounting certain elements of $T^{\alpha\beta}$ due to symmetry conditions on R.

Again, we construct evolution equations for the energy-weighted stress by identifying annihilators of the right-hand side of equation (4.8)

$$k_\alpha k_\beta k_\delta \partial_\gamma R^{\alpha\beta\gamma\delta} = 3e\frac{B}{\sqrt{W}} E_\parallel \left(m_1 + m_2\right). \tag{4.36}$$

This can be viewed as evolving the parallel component of the parallel heat flow.

As in the stress flow tensor, the r_k can be viewed as auxiliary parameters. Thus, we need to express them in terms of the rest-frame components of the energy-weighted stress. Such expressions are provided in Appendix 0.3.

We now have evolution equations for n_R, p, $p_\parallel$, $Q_\parallel$, $q_\parallel$, and the three vector components of Γ^μ. We will take these to be our set of dynamical variables. We consider the enthalpy, h, to be an auxiliary parameter in much the same way we treat the m_k and r_k as auxiliary parameters. Thus, our fluid system is nearly closed; however, we still need to evaluate the auxiliary parameters in terms of the dynamical variables. For this, we need a distribution function.

4.3 Distribution Function

4.3.1 Choosing a Distribution

Since we have auxiliary parameters not yet related to our dynamical variables, we require a distribution function to close our fluid system. Any lowest order distribution chosen must: be gyrotropic, solve the drift-kinetic equation, and reproduce the stress-energy tensor, equation (4.15). Satisfying

the first requirement is straightforward. The second is difficult to implement in a fluid treatment and typically abandons the fluid point of view in favor of kinetic MHD, making the drift-kinetic equation part of the closure [43], [59]. The third requirement restricts us to any of a class of distributions that reproduce the stress tensor.

Therefore, we choose a representative distribution from the equivalence class of distributions reproducing the stress tensor, capable of also representing the fluid equations of motion. The parameters in the distribution are proportional to the dynamical variables of the fluid system and evolve according to the fluid equations. We use such a parametrized distribution in place of the drift-kinetic equation to close our system.

4.3.2 Explicit Form

As noted in previous non-relativistic literature [58], [62], a bi-Maxwellian (or two-temperature Maxwellian) is a good choice for capturing features of kinetic theory in a fluid approach. As such, our distribution can be considered the relativistic analog of the non-relativistic bi-Maxwellian. It has the form

$$\begin{aligned} f(x,p) = f_M \Big\{ & 1 + \hat{\Delta} + (\Delta + \Delta^*)\, p_\alpha e^{\alpha\beta} p_\beta + \left(\overline{\Delta} + \overline{\Delta}^*\right) p_\alpha b^{\alpha\beta} p_\beta \\ & + p_\alpha p_\beta p_\gamma p_\delta \left(\tilde{\Delta} k^\alpha k^\beta k^\gamma k^\delta + \tilde{\Delta}^* e^{\alpha\beta} e^{\gamma\delta} + \tilde{\Delta}^{**} k^\alpha k^\beta e^{\gamma\delta}\right) \\ & + Q_\alpha b^{\alpha\beta} p_\beta \left[1 + \hat{Q} + p_\mu \left(e^{\mu\nu} + Q k^\mu k^\nu\right) p_\nu\right] \Big\}, \end{aligned} \tag{4.37}$$

where f_M is the relativistic Maxwellian discussed in §2.3.4 and given by equation (2.42). The Δ scalars describe pressure anisotropy, while the Q scalars measure heat flow. Thus, our distribution can be parametrized by our dynam-

ical variables: n_R, $p_\parallel$, $p_\perp$, $q_\parallel$, and $q_\perp$. The form of our distribution mirrors that found in HM only in the first three terms and the last term multiplying the square brackets. Note that we do not simply write the distribution in the standard non-relativistic form with the directional temperature dependence in the exponent. If we were to make such an attempt, evaluating moments of the distribution would become intractable.

Returning to evaluating the parameters of our distribution, we compare our distribution to the non-relativistic bi-Maxwellian expanded for small pressure anisotropy to determine Δ^*/Δ, $\overline{\Delta^*}/\overline{\Delta}$, $\tilde{\Delta}^*/\tilde{\Delta}$, and $\tilde{\Delta}^{**}/\tilde{\Delta}$. Doing so yields

$$\begin{aligned} f\left(x,p\right) = f_M \Big\{ & 1 + \hat{\Delta} + \Delta \left(p_\alpha e^{\alpha\beta} p_\beta - 2 p_\alpha b^{\alpha\beta} p_\beta \right) \\ & + \overline{\Delta} \left(p_\alpha e^{\alpha\beta} p_\beta + 4 p_\alpha b^{\alpha\beta} p_\beta \right) \\ & + \tilde{\Delta} p_\alpha p_\beta p_\gamma p_\delta \left(4 k^\alpha k^\beta k^\gamma k^\delta + e^{\alpha\beta} e^{\gamma\delta} - 4 k^\alpha k^\beta e^{\gamma\delta} \right) \\ & + Q_\alpha b^{\alpha\beta} p_\beta \left[1 + \hat{Q} + p_\mu \left(e^{\mu\nu} + Q k^\mu k^\nu \right) p_\nu \right] \Big\} . \end{aligned}$$

For reference, expanding a bi-Maxwellian for small pressure anisotropy yields

$$\begin{aligned} f\left(x,v\right) &= \frac{N}{p_\perp p_\parallel^{1/2}} \exp\left[-\frac{mn}{2} \left(\frac{v_\perp^2}{p_\perp} + \frac{v_\parallel^2}{p_\parallel} \right) \right] \\ &= \frac{N}{p^{3/2}} e^{-\frac{mnv^2}{p}} \left[1 - \frac{mn\Delta p}{6p^2} \left(v_\perp^2 - 2 v_\parallel^2 \right) \right. \\ &\quad + \frac{\Delta p^2}{6p^2} - \frac{mn\Delta p^2}{18 p^3} \left(v_\perp^2 + 4 v_\parallel^2 \right) \\ &\quad \left. + \frac{1}{72} \left(\frac{mn\Delta p}{p^2} \right)^2 \left(4 v_\parallel^4 + v_\perp^4 - 4 v_\parallel^2 v_\perp^2 \right) \right] , \end{aligned}$$

where N is the normalization factor, v is the particle velocity, $p_\parallel$ and $p_\perp$ refer the the parallel and perpendicular pressure, and p and Δp refer to the scalar pressure and pressure anisotropy.

In the instantaneous rest frame with coordinates oriented such that $\boldsymbol{B} = (0, 0, B)$, our distribution reduces to

$$f_R(x,p) = f_{MR}\left\{1 + \hat{\Delta} + \frac{\Delta}{m^2}\left(p_\perp^2 - 2p_\parallel^2\right) + \frac{\overline{\Delta}}{m^2}\left(p_\perp^2 + 4p_\parallel^2\right) + \frac{\tilde{\Delta}}{m^4}\left(4p_\parallel^4 + p_\perp^4 - 4p_\perp^2 p_\parallel^2\right) + \frac{Q_3 p_3}{m}\left[1 + \hat{Q} + \frac{p_\perp^2}{m^2} + Q\frac{p_\parallel^2}{m^2}\right]\right\}, \tag{4.38}$$

where $p_\parallel$ and $p_\perp$ here refer to parallel and perpendicular components of momenta.

4.3.3 Scalar Moments

We choose $\hat{\Delta}$ and $\hat{Q}$ to ensure that the rest-frame density is Maxwellian and the rest-frame flow velocity vanishes. Δ and $\overline{\Delta}$ are chosen so that $p = nT = \frac{1}{3}\left(T_R^{33} + 2T_R^{11}\right)$ and $\Delta p = T_R^{33} - T_R^{11}$, where T_R^{ij} refers to the ij^{th} components of the stress tensor in the rest frame. $\tilde{\Delta}$ is chosen by matching the non-relativistic limit ($\zeta = m/T \to \infty$) of R_R^{1133} to its bi-Maxwellian computed counterpart (eg Ramos [58]), $\frac{m}{n} p_\parallel p_\perp$. Q_3 is chosen to satisfy $T_R^{03} = Q_\parallel$, and Q is chosen by matching the non-relativistic limits of the elements of the stress flow tensor involving heat flow to their bi-Maxwellian counterparts, i.e., $M_R^{003} = 2mQ_\parallel = M_R^{333} + 2M_R^{113} = 2mq_\parallel + 2mq_\perp$.

Thus, in the rest-frame, the distribution function becomes

$$
\begin{aligned}
f_R(x,p) = f_{MR}\Bigg\{ & 1 - \frac{1}{6}\frac{\Delta p}{p}\frac{\zeta K_2}{K_3}\left(\frac{p_\perp^2}{m^2} - \frac{2p_\parallel^2}{m^2}\right) \\
& + \frac{1}{6}\frac{\Delta p^2}{p^2}\frac{K_4}{K_2} - \frac{1}{18}\frac{\Delta p^2}{p^2}\frac{\zeta K_4}{K_3}\left(\frac{p_\perp^2}{m^2} + 4\frac{p_\parallel^2}{m^2}\right) \\
& + \frac{1}{72}\frac{\Delta p^2}{p^2}\zeta^2\left(4\frac{p_\parallel^4}{m^4} + \frac{p_\perp^4}{m^4} - 4\frac{p_\parallel^2 p_\perp^2}{m^4}\right) \\
& + \frac{n_R p_\parallel}{p^2}\frac{K_2}{K_3\mathcal{K}}\left[\frac{K_3}{\zeta K_2}Q_\parallel - \left(\frac{q_\parallel}{3}\frac{p_\parallel^2}{m^2} + \frac{q_\perp}{2}\frac{p_\perp^2}{m^2}\right)\right]\Bigg\}.
\end{aligned}
\tag{4.39}
$$

where p and Δp refer to pressure and pressure anisotropy, while $p_\parallel$ and $p_\perp$ refer to parallel and perpendicular momenta. Explicitly, the scalar components of the distribution are

$$\zeta = mn_R/p, \tag{4.40}$$

$$\hat{\Delta} = \frac{1}{6}\frac{K_4}{K_2}\frac{\Delta p^2}{p^2}, \tag{4.41}$$

$$\Delta = -\frac{1}{6}\frac{K_2}{K_3}\zeta^2\frac{\Delta p}{mn_R}, \tag{4.42}$$

$$\overline{\Delta} = -\frac{1}{18}\frac{K_4}{K_3}\zeta\frac{\Delta p^2}{p^2}, \tag{4.43}$$

$$\tilde{\Delta} = \frac{\zeta^2}{72}\frac{\Delta p^2}{p^2}. \tag{4.44}$$

$$\hat{Q} = -\frac{K_3}{\zeta K_2}\frac{2Q_\parallel}{q_\perp} - 1 \tag{4.45}$$

$$Q_3 = -q_\perp \frac{\zeta^2}{2mn_R}\frac{K_2}{K_3\mathcal{K}}. \tag{4.46}$$

$$Q = \frac{2}{3}\frac{q_\parallel}{q_\perp}, \tag{4.47}$$

where $\mathcal{K} = \frac{K_3}{K_2} - \frac{K_4}{K_3}$.

4.4 Closed Fluid Equations

4.4.1 Covariant Closure Summary

We have chosen n_R, $V_\parallel$, $p_\parallel$, $p_\perp$, $q_\parallel$, and $q_\perp$ as the dynamical variables of our collisionless, small gyroradius fluid system. The covariant evolution equations for the chosen dynamical variables of our system are:

$$\nabla_\alpha \Gamma^\alpha = 0, \tag{4.48}$$

$$k_\kappa \nabla_\nu T^{\kappa\nu} = e n_R \frac{B}{h} E_\parallel, \tag{4.49}$$

$$F^\mu_\kappa \nabla_\nu \mathcal{T}^{\kappa\nu} = -h^2 e^{\mu\nu} J_\nu \tag{4.50}$$

$$U_\kappa \nabla_\nu T^{\kappa\nu} = 0, \tag{4.51}$$

$$k_\alpha k_\beta \nabla_\kappa M^{\kappa\alpha\beta} = 2e\frac{B}{h} Q_\parallel E_\parallel, \tag{4.52}$$

$$\left(U_\alpha k_\beta + U_\beta k_\alpha\right) \nabla_\kappa M^{\kappa\alpha\beta} = -2e\frac{B}{h} E_\parallel \left(u + p_\parallel\right) \tag{4.53}$$

$$k_\alpha k_\beta k_\delta \nabla_\gamma R^{\alpha\beta\gamma\delta} = 3e\frac{B}{h} E_\parallel \left(m_1 + m_2\right), \tag{4.54}$$

where the flux, Γ^α, stress, $T^{\alpha\beta}$, stress flow, $M^{\alpha\beta\gamma}$, and energy-weighted stress, $R^{\alpha\beta\gamma\delta}$, are given by equations (2.25)- (2.28) respectively, and the m_k are given in Appendix 0.3. Therefore, equations (4.48)- (4.54) constitute a closed covariant set of fluid equations.

4.4.2 3-Vector Form

It is often convenient to express fluid equations in 3-vector form, sacrificing explicit Lorentz covariance. As such, we present the 3-vector form of our closed fluid system here.

$$\frac{d}{d\tau} \log n_R + \frac{1}{\sqrt{g}} \partial_\mu \sqrt{g} U^\mu = 0, \tag{4.55}$$

$$\begin{aligned} &\gamma \left(u + p_\parallel\right) k_\mu \frac{d}{d\tau} V^\mu + \frac{d}{ds} p_\parallel - \Delta p \frac{d}{ds} \left(u + p\right) + \frac{d}{d\tau} Q_\parallel + \gamma Q_\parallel k_\mu \frac{d}{ds} V^\mu \\ &- Q_\parallel \frac{d}{d\tau} \log n_R + \left[\left(u + p_\parallel\right) k_\nu U^\mu U^\lambda + Q_\parallel k_\nu k^\mu U^\lambda\right] \Gamma^\nu_{\mu\lambda} = e n_R E_\parallel B/h, \end{aligned} \tag{4.56}$$

$$
\begin{aligned}
&-\frac{du}{d\tau}+\left(u+p_{\parallel}\right)\frac{d\log n_R}{d\tau}-\Delta p\frac{d\log h}{d\tau}-\frac{dQ_{\parallel}}{ds}+Q_{\parallel}\frac{d\log h}{ds}\\
&-2\gamma Q_{\parallel}k_{\mu}\frac{d}{d\tau}V^{\mu}-2\gamma Q_{\parallel}k_{\mu}U^{\nu}U^{\lambda}\Gamma^{\mu}_{\nu\lambda}=0,
\end{aligned}
\tag{4.57}
$$

$$
\begin{aligned}
&F^{\mu}_{\kappa}\left[\gamma\left(\mathcal{U}+\mathcal{P}_{\perp}\right)\frac{d}{d\tau}V^{\kappa}+\frac{\Delta\mathcal{P}}{h}\frac{d}{ds}h^{\kappa}+\mathcal{Q}_{\parallel}\left(\gamma\frac{d}{ds}V^{\kappa}+\frac{1}{h}\frac{d}{d\tau}h^{\kappa}\right)\right]\\
&+F^{\mu}_{\kappa}\left[\left(\mathcal{U}+\mathcal{P}_{\perp}\right)U^{\nu}U^{\lambda}+\Delta\mathcal{P}k^{\nu}k^{\lambda}+\mathcal{Q}_{\parallel}\left(k^{\nu}U^{\lambda}+k^{\lambda}U^{\nu}\right)\right]\Gamma^{\kappa}_{\nu\lambda}\\
&+F^{\mu\kappa}\partial_{\kappa}\mathcal{P}_{\perp}=-h^2\left(J^{\mu}-\frac{BJ_{\parallel}}{\gamma h}k^{\mu}\right),
\end{aligned}
\tag{4.58}
$$

$$
\begin{aligned}
&\frac{d}{d\tau}\left(m_1+m_2\right)+\left(m_1+m_2\right)\left(2\frac{d\log h}{d\tau}-3\frac{d\log n_R}{d\tau}\right)\\
&+\left(13m_3+\frac{1}{3}m_4\right)\left(\gamma k_{\mu}\frac{dV^{\mu}}{d\tau}+k_{\mu}U^{\nu}U^{\lambda}\Gamma^{\mu}_{\nu\lambda}\right)-\left(m_3+\frac{7}{3}m_4\right)\frac{d\log h}{ds}\\
&+3\frac{d}{ds}\left(m_3+\frac{1}{3}m_4\right)+\left(13m_3+\frac{1}{3}m_4\right)k_{\mu}U^{\nu}U^{\lambda}\Gamma^{\mu}_{\nu\lambda}=2eQ_{\parallel}E_{\parallel}B/h,
\end{aligned}
\tag{4.59}
$$

$$
\begin{aligned}
&\frac{d}{d\tau}\left(5m_3-\frac{1}{3}m_4\right)+\frac{d}{ds}\left(m_1+m_2\right)+\left(5m_1+3m_2\right)\gamma k_{\mu}\frac{dV^{\mu}}{d\tau}\\
&-m_2\frac{d\log h}{ds}+\left(7m_3+\frac{4}{3}m_4\right)\frac{d\log h}{d\tau}-\left(13m_3+\frac{1}{3}m_4\right)\frac{d\log n_R}{d\tau}\\
&+m^2n_R\gamma k_{\mu}\frac{dV^{\mu}}{d\tau}+\left(5m_1+3m_2+m^2n_R\right)k_{\mu}U^{\nu}U^{\lambda}\Gamma^{\mu}_{\nu\lambda}\\
&+\left(7m_3+\frac{1}{3}m_4\right)k_{\mu}k^{\nu}k^{\lambda}\Gamma^{\mu}_{\nu\lambda}=e\frac{B}{h}E_{\parallel}\left(u+p_{\parallel}\right),
\end{aligned}
\tag{4.60}
$$

$$
\begin{aligned}
&-\frac{d}{d\tau}\left(5r_3+3r_4\right)+\frac{d}{ds}\left(3r_1+6r_2\right)+\left(18r_1+30r_2+6r_5\right)\gamma k_\mu\frac{dV^\mu}{d\tau}\\
&+3\left(r_5-r_2\right)\frac{d\log h}{ds}-\left(5r_3+3r_4\right)\left(3\frac{d\log h}{d\tau}-4\frac{d\log n_R}{d\tau}\right)\\
&+3m^2p_\parallel\gamma k_\mu\frac{dV^\mu}{d\tau}+\left(18r_1+30r_2+6r_5+3m^2p_\parallel\right)k_\mu U^\nu U^\lambda\Gamma^\mu_{\nu\lambda}\\
&=3e\frac{B}{h}E_\parallel\left(m_1+m_2\right),
\end{aligned}
\tag{4.61}
$$

where the m_k and r_k are given in Appendix 0.3, $\Gamma^\mu_{\nu\lambda}$ is the relevant Christoffel symbol, $V^\mu = U^\mu/\gamma$ is the four-velocity, and calligraphic letters indicate summing over species.

In simpler Cartesian coordinates, the system may be expressed as:

$$
\frac{d}{d\tau}\log n_R+\partial_\mu U^\mu=0, \tag{4.62}
$$

$$
\begin{aligned}
&\left(u+p_\parallel\right)\gamma\mathbf{k}\cdot\frac{d\mathbf{V}}{d\tau}+\frac{dp_\parallel}{ds}-\Delta p\frac{d\log h}{ds}+\frac{dQ_\parallel}{d\tau}-2Q_\parallel\frac{d\log n_R}{d\tau}\\
&+Q_\parallel\frac{d\log h}{d\tau}=en_R\frac{B}{h}E_\parallel,
\end{aligned}
\tag{4.63}
$$

$$
\begin{aligned}
&-\frac{du}{d\tau}+\left(u+p_\parallel\right)\frac{d\log n_R}{d\tau}-\Delta p\frac{d\log h}{d\tau}-\frac{dQ_\parallel}{ds}+Q_\parallel\frac{d\log h}{ds}\\
&-2\gamma Q_\parallel\mathbf{k}\cdot\frac{d\boldsymbol{V}}{d\tau}=0,
\end{aligned}
\tag{4.64}
$$

$$
B^2J_\parallel V_\parallel\mathbf{V}_E+\left(\boldsymbol{E}G^0+\boldsymbol{B}\times\mathbf{G}\right)=h^2\mathbf{J}_\perp, \tag{4.65}
$$

$$\begin{aligned}
&\frac{d}{d\tau}\left(m_1+m_2\right)+\left(m_1+m_2\right)\left(2\frac{d\log h}{d\tau}-3\frac{d\log n_R}{d\tau}\right)\\
&+\left(13m_3+\frac{1}{3}m_4\right)\gamma\boldsymbol{k}\cdot\frac{d\boldsymbol{V}}{d\tau}-\left(m_3+\frac{7}{3}m_4\right)\frac{d\log h}{ds}\\
&+3\frac{d}{ds}\left(m_3+\frac{1}{3}m_4\right)=2e\frac{B}{h}Q_\parallel E_\parallel,
\end{aligned}\tag{4.66}$$

$$\begin{aligned}
&\frac{d}{d\tau}\left(5m_3-\frac{1}{3}m_4\right)+\frac{d}{ds}\left(m_1+m_2\right)+\left(5m_1+3m_2\right)\gamma\boldsymbol{k}\cdot\frac{d\boldsymbol{V}}{d\tau}\\
&-m_2\frac{d\log h}{ds}+\left(7m_3+\frac{4}{3}m_4\right)\frac{d\log h}{d\tau}-\left(13m_3+\frac{1}{3}m_4\right)\frac{d\log n_R}{d\tau}\\
&+m^2n_R\gamma\boldsymbol{k}\cdot\frac{d\boldsymbol{V}}{d\tau}=e\frac{B}{h}E_\parallel\left(u+p_\parallel\right),
\end{aligned}\tag{4.67}$$

$$\begin{aligned}
&-\frac{d}{d\tau}\left(5r_3+3r_4\right)+\frac{d}{ds}\left(3r_1+6r_2\right)+3\left(r_5-r_2\right)\frac{d\log h}{ds}\\
&+\left(18r_1+30r_2+6r_5\right)\gamma\mathbf{k}\cdot\frac{d\mathbf{V}}{d\tau}+3m^2p_\parallel\gamma\mathbf{k}\cdot\frac{d\mathbf{V}}{d\tau}\\
&-\left(5r_3+3r_4\right)\left(3\frac{d\log h}{d\tau}-4\frac{d\log n_R}{d\tau}\right)=3e\frac{B}{h}E_\parallel\left(m_1+m_2\right),
\end{aligned}\tag{4.68}$$

where G^0 and $\mathbf{G}$ are given by

$$\left(1-\frac{\Delta P}{h^2}\right)G^0=\partial_t P_\perp+\Delta P\partial_t\log h,\tag{4.69}$$

and

$$\begin{aligned}
\left(1-\frac{\Delta P}{h^2}\right)\mathbf{G}=\nabla P_\perp+\Delta P\nabla\log h+\left(U+P_\parallel+Q_\parallel\sqrt{\frac{B^2}{h^2}}V_\parallel\right)\gamma\frac{d\boldsymbol{V}}{d\tau}\\
+Q_\parallel\left[\sqrt{\frac{B^2}{h^2}}\frac{1}{\gamma}\frac{d\boldsymbol{b}}{d\tau}+\gamma\frac{d\boldsymbol{V}}{ds}\right].
\end{aligned}\tag{4.70}$$

4.4.3 Non-Relativistic Limit

We now present the fully non-relativistic (NR), $\zeta = \frac{m}{T} \gg 1$, $V_\parallel \sim V_\perp \sim \zeta^{-1/2}$ and $Q_\parallel \sim \zeta^{-3/2}$, form of our closed system. Since labelling the rest-frame is somewhat inappropriate in this limit, we use $n \equiv n_R$. We also use the common notation $\nabla_\parallel \equiv \boldsymbol{b} \cdot \nabla$.

In the NR limit, equations (4.62)- (4.68) become after some manipulation

$$\frac{dn}{dt} + n\nabla \cdot \boldsymbol{V} = 0, \tag{4.71}$$

$$mn\mathbf{b} \cdot \frac{d\mathbf{V}}{dt} + \nabla_\parallel p_\parallel + \left(p_\perp - p_\parallel\right) \nabla_\parallel \log B = enE_\parallel, \tag{4.72}$$

$$B^2 \mathbf{J}_\perp = \boldsymbol{B} \times \left(\mathcal{M} n \frac{d\boldsymbol{V}}{dt} + \nabla \mathcal{P}_\perp + \Delta \mathcal{P} \nabla \log B \right), \tag{4.73}$$

$$p_\parallel \frac{d}{dt} \log \left(\frac{p_\parallel B^2}{n^3} \right) + 2\nabla_\parallel q_\parallel + 2\left(q_\perp - q_\parallel\right) \nabla_\parallel \log B = 0, \tag{4.74}$$

$$p_\perp \frac{d}{dt} \log \left(\frac{p_\perp}{Bn} \right) + \nabla_\parallel q_\perp - 2q_\perp \nabla_\parallel \log B = 0, \tag{4.75}$$

$$q_\parallel \frac{d}{dt} \log \left(\frac{q_\parallel B^3}{n^4} \right) + \frac{3}{2} \frac{p_\parallel}{m} \nabla_\parallel \frac{p_\parallel}{n} = 0, \tag{4.76}$$

$$q_\perp \frac{d}{dt} \log \left(\frac{q_\perp}{n^2} \right) + \frac{p_\parallel}{m} \nabla_\parallel \frac{p_\perp}{n} - \frac{p_\perp \Delta p}{mn} \nabla_\parallel \log B = 0, \tag{4.77}$$

where calligraphic letters indicate summing over species.

The NR limit of our closure coincides with a bi-Maxwellian MHD closure in which gyroviscous components of the stress tensor are retained, as presented by Ramos [58]. Thus, the system produces dispersion relations whose numerical coefficients coincide with those obtained through kinetic theory, and the system correctly predicts the onset of the mirror and firehose instabilities.

4.5 Thermodynamics

4.5.1 Adiabatic Index

As noted above, the enthalpy density is $h = u + p = mn\frac{K_3}{K_2}$. Using the heat capacities per particle at constant pressure and volume, $c_p = \left(\frac{\partial(h/n)}{\partial T}\right)_p$ and $c_V = \left(\frac{\partial(u/n)}{\partial T}\right)_V = c_p - 1$, we can calculate the the adiabatic index, $\gamma = \frac{c_p}{c_V}$. The expression is simplest when expressed as

$$\frac{\gamma}{\gamma - 1} = c_p = -\frac{1}{\zeta^2}\frac{d}{d\zeta}\frac{K_3}{K_2} = \zeta^2 + 5\zeta\frac{K_3}{K_2} - \left(\zeta\frac{K_3}{K_2}\right)^2 \tag{4.78}$$

In the lowest order non-relativistic limit, we find γ reduces to the ideal gas value

$$\gamma = \frac{5}{3} - \frac{5}{3}\frac{T}{m} + ...,$$

and in the super-relativistic (massless) limit becomes

$$\gamma = \frac{4}{3}.$$

These computations agree with de Groot et al. [24] Chapman-Enskog relativistic closure.

4.5.2 Entropy Flow

To obtain an evolution equation for the entropy (first law of thermodynamics), we examine:

$$\begin{aligned} 0 &= U_\alpha \partial_\beta T^{\alpha\beta} \\ &= -nU^\beta \left[p\partial_\beta \left(\frac{1}{n}\right) + \partial_\beta \left(\frac{u}{n}\right)\right] - \partial_\beta \left(Q_\parallel k^\beta\right) - Q_\parallel k^\alpha U^\beta \partial_\beta U_\alpha \\ &- \frac{2}{3}\Delta p k^\alpha k^\beta \partial_\beta U_\alpha - \frac{1}{3}\Delta p U_\alpha \partial_\beta e^{\alpha\beta}. \end{aligned} \tag{4.79}$$

We now need the relativistic form of the first law, $Td\sigma = dU + \delta W$, where $\delta W = \frac{1}{n} dt \mathbf{p} : \nabla \boldsymbol{V}$ is the reversible work done by the plasma and σ is the entropy. $\frac{\delta W}{dt}$ becomes $U^\beta \partial_\beta W$ in the relativistic limit. Thus, we have $U^\beta \partial_\beta W = \frac{1}{n} p^{\alpha\beta} \partial_\beta U_\alpha$ where $p^{\alpha\beta} = p\eta^{\alpha\beta} + pU^\alpha U^\beta$ corresponds to the isotropic pressure tensor—the anisotropic portion of the gyrotropic pressure only provides dissipation. Therefore, we have

$$TU^\beta \partial_\beta \sigma = U^\beta \left[p\partial_\beta \left(\frac{1}{n}\right) + \partial_\beta \left(\frac{u}{n}\right)\right]. \tag{4.80}$$

Re-arranging equation (4.79) and using several identities from §2.4, we find

$$\partial_\beta S^\beta = -\frac{Q_\parallel}{T}\gamma^2 \mathbf{k} \cdot \frac{d\boldsymbol{V}}{dt} - \frac{Q_\parallel}{T^2}\frac{dT}{ds} + \frac{2}{3}\gamma \frac{\Delta p}{p}\frac{d\log n}{dt} - \gamma \frac{\Delta p}{p}\frac{d\log h}{dt} =: \Theta, \tag{4.81}$$

where $S^\beta = n\sigma U^\beta + \frac{Q_\parallel}{T} k^\beta$ is the entropy flow and Θ expresses the entropy production rate.

In the non-relativistic limit, we have

$$\frac{\partial S}{\partial t} + \nabla \cdot \mathbf{S} = -\frac{Q_\parallel}{T^2}\nabla_\parallel T + \frac{2}{3}\frac{\Delta p}{p}\frac{d\log n}{dt} - \frac{\Delta p}{p}\frac{d\log B}{dt}, \tag{4.82}$$

where $\mathbf{S} = n\sigma \boldsymbol{V} + \frac{Q_\parallel}{T}\mathbf{b}$ and $S = n\sigma$ is the entropy density. Note, this result is consistent with calculating the lowest order entropy production from kinetic theory [24].

4.5.3 Entropy

It remains to calculate the entropy, σ. To do so, we use the relativistic equivalent of the Shannon formula [24]

$$S^\mu = -\int \frac{d^3p}{p_0} p^\mu f \log f.$$

To perform the integral, we must expand $\log f$ for small pressure anisotropy and heat flow and retain only the lowest order contributions from each. We find

$$\begin{aligned} S^0_R &= n\sigma = -n\left[\log N + 1 - \frac{\zeta K_3}{K_2}\right] \\ &= -n\left[\log N + 1 - \frac{\zeta K_3}{K_2}\right] \end{aligned}$$

to lowest order in the anisotropy and heat flow, where $N = \frac{n}{4\pi m^3}\frac{\zeta}{K_2}$. Since the anisotropy and heat flow do not contribute to lowest order, S^0_R agrees with the relativistic entropy expressions found elsewhere, e.g., [24]. In the non-relativistic limit, S^0_R reduces to

$$S^0_R = n\sigma = n\log\frac{T^{3/2}}{n_R} + n\left[\frac{3}{2}\log(2\pi m) - 1\right]. \tag{4.83}$$

This expression for S^0_R leads to the standard definition for the thermodynamic temperature, $T_{Th} = p/n$, obtained from

$$\left(\frac{\partial S^0_R}{\partial u}\right)^{-1}_V = T_{Th}.$$

Calculating S_R^3 yields

$$S_R^3 = \frac{Q_\parallel}{T}, \tag{4.84}$$

which holds for arbitrary temperature.

4.5.4 Transport

To guarantee the second law of thermodynamics is satisfied, we examine equations (4.81) and (4.82). The simplest method to ensure the entropy production is positive definite is to make the production rate quadratic. With this in mind, we obtain condition for Δp and $Q_\parallel$ from the entropy production

$$\Delta p = \eta\gamma \left(2\frac{d\log n}{dt} - 3\frac{d\log h}{dt} \right)$$
$$Q_\parallel = -\chi \left(\frac{dT}{ds} + \gamma^2 T \mathbf{k} \cdot \frac{d\mathbf{V}}{dt} \right),$$

where η and χ correspond to the coefficients of viscosity and heat conduction respectively. These expressions agree with the similar expressions found in Weinberg with our specific form for the stress-energy tensor substituted.

In the non relativistic limit, these expressions reduce to

$$\Delta p = \eta \left(2\frac{d\log n}{dt} - 3\frac{d\log B}{dt} \right)$$

and

$$Q_\parallel = -\chi \nabla_\parallel T.$$

These agree with the conventional collision dominated viscosity and heat conduction in the magnetized limit up to a numerical factor [12]. These transport equations are also derivable and consistent with our fluid evolution equations in the short mean free path limit.

4.6 Linear Predictions

Having completed our closure, we now examine some basic predictions of the linearized relativistic system. Linearizing equations (4.62)- (4.68) about an isotropic equilibrium with no heat flow, equal electron and ion equilibrium temperatures, and non-relativistic flow speed yields a lengthy set of equations presented fully in Appendix 0.5. We present the linearized version of equation (4.66) to compare with the non-relativistic limit of the same equation as an example:

$$\begin{aligned}
&- v\zeta_s \left(f(\zeta_s) + 3\frac{K_3(\zeta_s)}{K_2(\zeta_s)} \right) \frac{\delta n}{n} \\
&+ \zeta_s \left(f(\zeta_s) + \frac{K_3(\zeta_s)}{K_2(\zeta_s)} \right) v\frac{\delta p_s}{p} + \frac{2}{3}\zeta_s \frac{K_4(\zeta_s)}{K_3(\zeta_s)} v\frac{\delta \Delta p_s}{p} \\
&- 3\left(1 - \frac{2}{5}\frac{K_4(\zeta_s)}{K_3(\zeta_s)\mathcal{K}(\zeta_s)} \right) \cos(\theta)\frac{\delta Q_{\parallel s}}{p} \\
&+ 2\frac{K_4(\zeta_s)}{K_3(\zeta_s)\mathcal{K}(\zeta_s)} \cos(\theta)\frac{\delta \Delta Q_{\parallel s}}{p} \\
&+ 2\zeta_s \frac{K_3(\zeta_s)}{K_2(\zeta_s)} \hat{\mathbf{k}}_\perp \cdot \delta\mathbf{v} = 0,
\end{aligned} \tag{4.85}$$

$$\begin{aligned}
&- 3v\zeta_s \frac{\delta n}{n} + \zeta_s v\frac{\delta p_\parallel}{p} - \frac{6}{5}\cos(\theta)\frac{Q_{\parallel s}}{p} - 2\cos(\theta)\frac{\delta Q_{\parallel s}}{p} \\
&- 2\zeta_s \hat{\mathbf{k}}_\perp \cdot \delta\mathbf{v} = 0,
\end{aligned} \tag{4.86}$$

where $v = \omega/k$, $\hat{\mathbf{k}}_\perp = \mathbf{k}_\perp/k$, $\cos(\theta) = k_\parallel/k$, $v_A^2 = B^2/\mu_0(m_i + m_e)n$, subscript s denotes species, superscript T denotes a sum over the species, and

$$f(\zeta_s) = \left[\zeta_s + \frac{K_3(\zeta_s)}{K_2(\zeta_s)} \left(1 - \zeta_s \frac{K_1(\zeta_s)}{K_2(\zeta_s)} \right) \right].$$

Using the full set of linear equations, we use Mathematica® to plot the phase velocity squared versus ζ_i (inverse temperature) in figure (1) for $v_A^2 = 10^{-6}$, $\theta = 30^o$, and $m_i/m_e = 1833$. Also plotted in figure (1) as the dashed lines are the linearized version of the non-relativistic equations, (4.71)-(4.77). From lowest to highest phase speed for large ζ, we have the slow magnetosonic, two ion acoustic, shear Alfven, fast magnetosonic, and two electron acoustic modes.

For the plotted parameters, the electron modes are the first to show significant deviation for increasing temperature at roughly $100keV$. At this temperature, the non-relativistic theory begins to predict superluminal phase velocities for the electron acoustic modes. Also of note, the phase velocity of the shear and slow magnetosonic Alfven modes behave quite differently in the ultrarelativistic regime. In this regime, the correct dispersion relation is

$$v^2 \sim \left(\frac{\zeta_i + \zeta_e}{8} \right) v_A^2,$$

where the non-relativistic theory would simply state $v^2 \sim v_A^2$.

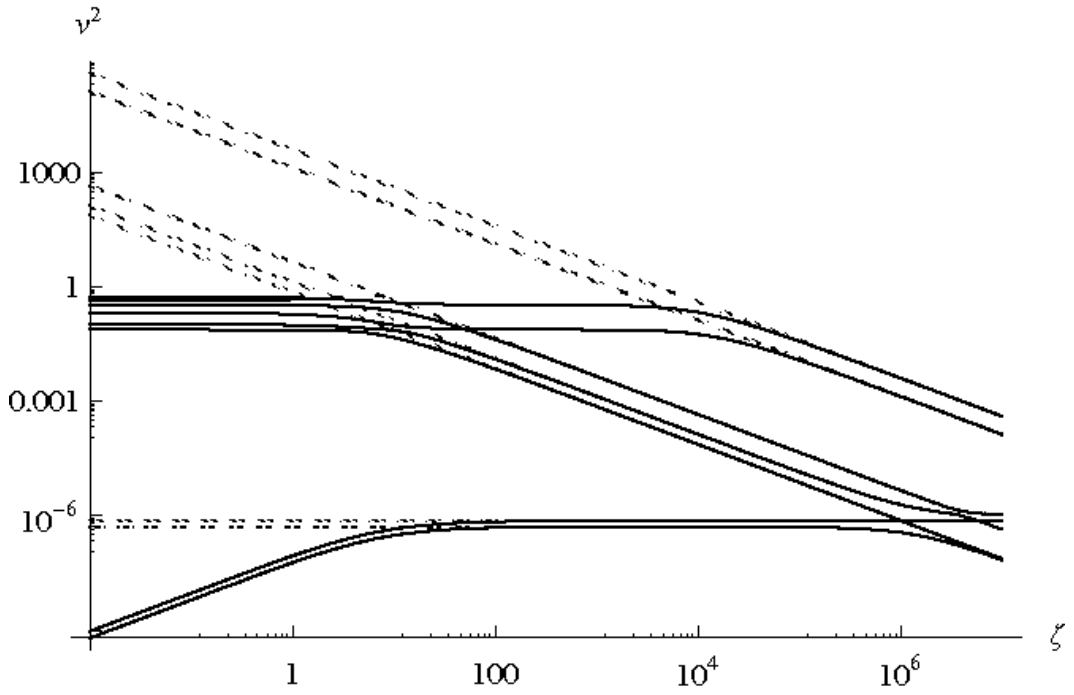

Figure 4.1: Phase velocity squared versus $\zeta_i = m_i/T$ for the general linearized evolution equations (solid) and their non-relativistic limit (dashed) are plotted. $v_A^2 = 10^{-6}$, $\theta = 30^o$, and $m_i/m_e = 1833$

4.7 Summary

Maxwell's equations are closed in a magnetized plasma when the 4-vector current can be expressed in terms of the stress tensor,

$$\mathcal{T}^{\mu\nu} = \sum_{species} T^{\mu\nu},$$

where $T^{\mu\nu}$ is the stress tensor of the individual plasma species. This closure procedure is given by equation (4.2) and later equations.

Thus, a closed fluid description of plasma dynamics relies on equations that fix the evolution of the stress tensor of each plasma species. For this reason, the stress tensor is said to provide the constitutive relation for a plasma fluid closure. We obtain our description of the stress tensor, equation (4.15), via electromagnetic constraints rather than the simpler MHD thermodynamic arguments

$$\begin{aligned} T^{\alpha\beta} = p\eta^{\alpha\beta} + hU^\alpha U^\beta + \frac{1}{3}\Delta p\left(2k^\alpha k^\beta - e^{\alpha\beta}\right) \\ + Q_\parallel\left(k^\alpha U^\beta + U^\alpha k^\beta\right), \end{aligned} \tag{4.87}$$

where $b^{\alpha\beta}$ and $e^{\alpha\beta}$ are approximate projection operators introduced in §2.4.1. The fluid 4-velocity, U^μ, and the heat flow, $Q_\parallel k^\mu = \left(q_\parallel + q_\perp\right)k^\mu$, are constrained by

$$F^\mu_\nu U^\nu = 0, \tag{4.88}$$

$$e^\mu_\nu k^\nu = 0, \tag{4.89}$$

$$U_\nu k^\nu = 0. \tag{4.90}$$

Equation (4.88) provides the first of our evolutionary constraints by reproducing the familiar $\boldsymbol{E} \times \boldsymbol{B}$ drift. We still need evolution equations for the two remaining free components of the flow, Γ^μ, which are the rest-frame density, n_R, and the parallel flow, $V_\parallel$. Also, from the stress tensor, we need to evolve $p = (p_\parallel + 2p_\perp)/3$, $\Delta p = p_\parallel - p_\perp$, h, and the two components of the rest-frame heat flow, $q_\parallel$ and $q_\perp$.

Quasineutrality, equation (4.4), requires that n_R be the same for all species, while the other quantities in the stress tensor are free to vary from species to species. Thus, we choose the following six parameters n_R, $V_\parallel$, $p_\parallel$, $p_\perp$, $q_\parallel$, and $q_\perp$ as our dynamical variables. The evolution equations for the six dynamical variables of our system in various forms are given in §4.4.

At this point in the closure, we have ten scalar auxiliary parameters which are not fixed. These are the enthalpy density, h, the four scalar parameters, m_k, of the stress flow, and the five scalar parameters, r_k, of the energy-weighted stress. We express these auxiliary parameters via a representative distribution, which is parametrized by our dynamical variables. Thus, the distribution evolves according to equations (4.48)- (4.54), and our auxiliary parameters can be expressed in terms of the dynamical variables, as presented in Appendix 0.3.

Our closure provides a more accurate physical description of relativistic, magnetized fluid plasmas than previously presented by Hazeltine and Mahajan [35]. The system allows detailed study of various astrophysical and laboratory plasmas at a more realistic level than MHD. Also, in the non-relativistic limit,

our closure reduces to a set of equations presented by Ramos [58] obtained via a bi-Maxwellian closure in which gyroviscous terms of the stress tensor are retained.

Chapter 5

Applications

Having developed an improved relativistic fluid model, we now explore some relevant applications for the model. Since relativistic plasmas are most commonly found in astrophysics, we focus our applications on such phenomena.

Shock mediated reconnection is a possible source for the high-energy non-thermal emissions observed in astrophysical systems such as pulsars and magnetars [64], gamma-ray bursts [53], and active galactic nuclei [25]. In such strongly magnetized environments, strong gyrotropic anisotropy in the pressure is expected to occur due to synchrotron emission [5] and various instabilities [22], [18]. Our newly developed covariant fluid model for magnetized plasmas, incorporating pressure anisotropy but neglecting heat flow, is used to study Petschek type reconnection in a pair plasma governed by slow-mode shocks in §5.1. The plasma parameters are found to be strongly modified by anisotropy on both sides of the shock.

We apply the full covariant fluid model, incorporating anisotropy in both temperature and heat flow, to study equatorial radial profiles of density, velocity, magnetic field, pressure, and heat flow in the hot, strongly magnetized

wind region beyond the light cylinder of pulsar magnetospheres in §5.2. We will assume radiative losses to have isotropized the wind region plasma so that $p_{\parallel} \gg p_{\perp}$. Fluid velocities and temperatures are allowed to vary from ultra- to non-relativistic regimes. This study of pulsar magnetospheres extends work by Tsikarishvili et al. [72] to a more general fluid closure including heat flow and allowing for arbitrary temperature.

5.1 Anisotropic Shocks

5.1.1 Introduction

Petschek reconnection is a form of shock mediated magnetic reconnection which proceeds rapidly and efficiently converts magnetic energy into thermal and bulk flow energy [57]. The speed of the energy conversion, inflow of the order of the Alfven speed, is achieved by assuming the dissipation region in which the magnetic field is annihilated is small. Since the magnetic field is being annihilated, the field strength crossing from the inflow to outflow regions must drop. Further, the energy lost due to reconfiguration of the field geometry causes the temperature across the shock to rise. As such, Petschek reconnection is governed by slow-mode shocks, which obey the above behavior, analogous to slow-mode compressional MHD modes. We will consider a switch-off shock, which is a special case of a slow-mode shock in which the component of the magnetic field tangent to the shock is "switched off" when crossing the shock.

Biskamp [10] argues that Petschek reconnection can not be obtained without imposing an unphysically large (anomalous) resistivity to the diffusion region. However, slow-mode shocks have been observed in the solar corona [61] and via the Cluster satellites in Earth's magnetotail [28].

Switch-off shocks in the isotropic non-relativistic limit have been explored by Biernat et al. [8]. Biernat et al. [9] extended the result to include anisotropic pressure; however, they restrict the outflowing plasma to be isotropic. Hoshino et al. [38] perform a double adiabatic style closure to include pressure anisotropy; further, they included a phenomenological heat flow term. They found including pressure anisotropy and heat flow allowed analytical calculations to better match data from Earth's magnetotail taken via the GEOTAIL spacecraft.

The problem of relativistic shock mediated magnetic reconnection was first approached by Blackman and Field [11] and Lyutikov and Uzdensky [49]. The two approaches reached similar conclusions; however, the plasma was assumed incompressible and the full energy and momentum balance was neglected in both cases. Tolstykh et al. [69] extended the results of [11] and [49] by considering non-steady-state solutions but retained the same assumptions. Lyubarsky [48] took a more sophisticated approach and used the relativistic generalization of the Rankine-Hugoniot shock jump relations to solve the switch-off shock Riemann problem. Double et al. [26] studied the effect of anisotropy on relativistic shocks; however, they assume a fixed ratio of $p_{\parallel}/p_{\perp}$ to complete their closure. Recently, two groups, Swisdak et al. [66] and Zeni-

tani and Hesse [79], have begun simulating relativistic electron-positron (pair) plasma reconnection via particle-in-cell (PIC) codes, which naturally allow for pressure anisotropy. Both groups observe strong anisotropy in the outflowing plasma giving rise to a Weibel instability which mediates the size of the diffusion region and allows fast reconnection to occur.

We construct the Rankine-Hugoniot relations for the fully relativistic pair plasma fluid system with pressure anisotropy. Plasma quantities are measured in the rest frame of the plasma and electromagnetic fields are measured in the shock frame. We consider Petschek style reconnection for a slow-mode switch-off shock in the xy-plane, as indicated in figure 5.1.1. Inflowing plasma is oriented normal to the shock (normal incidence frame), and the upstream (1) magnetic field has normal and tangential (y and x) components. The downstream (2) plasma flow has normal and tangential components, while the downstream (2) field will have only a normal component —a switch-off shock.

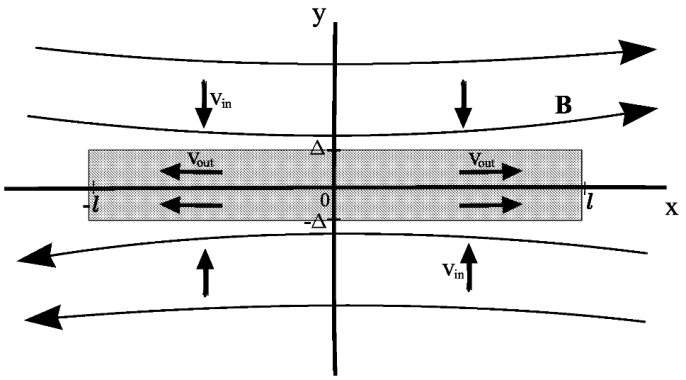

Figure 5.1: Shock mediated magnetic reconnection [48]

We do not include heat flow in this analysis because a closure involv-

ing both heat fluxes consisting purely of conservation laws is not possible. Although the Riemann problem can be solved given a set of equations in non-conservative form, knowledge of the physics in the dissipation region is required [46]. Knowledge of the dissipation region is required because the path taken by each parameter while crossing the shock can not in general be assumed to be a straight line connecting the two sides of the shock discontinuity.

5.1.2 Evolution Equations in Conservation Form

The stress-energy tensor of the plasma, equation (4.15), can be re-expressed as

$$T_p^{\mu\nu} = \left(p - \frac{1}{3}\Delta p\right)\eta^{\mu\nu} + \left(\rho W(\zeta) - \frac{1}{3}\Delta p\right)U^\mu U^\nu + \Delta p k^\mu k^\nu, \tag{5.1}$$

neglecting heat flux, where $\rho W(\zeta) = mn\frac{K_3(\zeta)}{K_2(\zeta)}$ is the enthalpy. The stress-energy tensor of the electromagnetic field, equation (2.17), can be written as

$$T_{EM}^{\mu\nu} = \frac{h^2}{2}\eta^{\mu\nu} + h^2 U^\mu U^\nu - h^\mu h^\nu.$$

We can now write conservation of flux

$$\partial_\mu n U^\mu = 0, \tag{5.2}$$

momentum

$$\partial_\mu \mathcal{T}^{\mu i} = 0, \tag{5.3}$$

and energy

$$\partial_\mu \mathcal{T}^{\mu 0} = 0, \tag{5.4}$$

where $\mathcal{T}^{\mu\nu} = T_p^{\mu\nu} + T_{EM}^{\mu\nu}$ is the total stress tensor summed over species.

At this point, we need an equation for Δp to close the system. We use $e_{\alpha\beta}\partial_\mu M^{\mu\alpha\beta} = 0$ to obtain the conservation equation from Hazeltine and Mahajan [35]

$$\partial_\mu \left(\frac{m_1 U^\mu}{h} \right) = 0, \tag{5.5}$$

where m_1 is an auxiliary parameter found in appendix 0.3. However, we neglect terms proportional to Δp^2 appearing in m_1. These terms only need to be retained when considering heat flow, which requires fourth rank moments and implicitly includes terms second order in the anisotropy.

In three vector form, equations (5.2) - (5.5) are

$$\partial_t(\gamma\rho) + \nabla \cdot (\gamma\rho \boldsymbol{v}) = 0 \tag{5.6}$$

$$\begin{aligned} &\partial_t \left[\gamma^2 \left(\rho W - \frac{1}{3}\Delta p \right) v^i + \Delta p k^0 k^i + (\boldsymbol{E} \times \boldsymbol{B})^i \right] \\ &+ \partial_j \left[\gamma^2 \left(\rho W - \frac{1}{3}\Delta p \right) v^i v^j + \left(p - \frac{1}{3}\Delta p + \frac{E^2 + B^2}{2} \right) \delta^{ij} \right. \\ &\left. + \Delta p k^i k^j - B^i B^j - E^i E^j \right] = 0 \end{aligned} \tag{5.7}$$

$$\begin{aligned} &\partial_t \left[\gamma^2 \left(\rho W - \frac{1}{3}\Delta p \right) - \left(p - \frac{1}{3}\Delta p \right) + \Delta p \left(k^0 \right)^2 + \frac{E^2 + B^2}{2} \right] \\ &+ \nabla \cdot \left[\gamma^2 \left(\rho W - \frac{1}{3}\Delta p \right) \boldsymbol{v} + \Delta p k^0 \mathbf{k} + \boldsymbol{E} \times \boldsymbol{B} \right] = 0 \end{aligned} \tag{5.8}$$

$$\partial_t \left[\frac{\gamma \left(pW + \Delta p K_4/K_3 \right)}{h} \right] + \nabla \cdot \left[\frac{\gamma \left(pW + \Delta p K_4/K_3 \right) \boldsymbol{v}}{h} \right] = 0. \tag{5.9}$$

5.1.3 Rankine-Hugoniot Relations

We now construct the Rankine-Hugoniot relations by considering a steady-state with the geometry of a slow-mode switch-off shock and integrate equations (5.6) - (5.9) along with the relevant Maxwell equations across the shock. We find

$$[E_z] = 0, \tag{5.10}$$

$$[B_n] = 0, \tag{5.11}$$

$$[\gamma \rho v_n] = 0, \tag{5.12}$$

$$\left[p - \frac{1}{3}\Delta p + \gamma^2 v_n^2 \left(\rho W - \frac{1}{3}\Delta p \right) + \Delta p \frac{h_n^2}{h^2} + \frac{B_t^2 - B_n^2}{2} \right] = 0, \tag{5.13}$$

$$\left[\gamma^2 v_n v_t \left(\rho W - \frac{1}{3}\Delta p \right) + \Delta p \frac{h_n h_t}{h^2} - B_n B_t \right] = 0, \tag{5.14}$$

$$\left[\gamma^2 v_n \left(\rho W - \frac{1}{3}\Delta p \right) + \Delta p \frac{h_n h^0}{h^2} + B_t E_z \right] = 0, \tag{5.15}$$

$$\left[\frac{\left(pW + \Delta p K_4/K_3 \right) \gamma v_n}{h} \right] = 0, \tag{5.16}$$

where bracketed terms are to be evaluated on each side of the shock.

The h-terms can be expressed in terms of v and B as

$$\begin{aligned} h_{n1} &= \gamma_1 B_n \\ h_{t1} &= \frac{B_{t1}}{\gamma_1} \\ h_1^0 &= \gamma_1 v_{n1} B_n \\ h_1 &= \sqrt{B_1^2 - v_{n1}^2 B_{t1}^2} \\ h_{n2} &= \gamma_2 B_n \left(1 - v_{t2}^2\right) \\ h_{t2} &= \gamma_2 v_{2n} v_{2t} B_n \\ h_2^0 &= \gamma_2 v_{n2} B_n \\ h_2 &= B_n \sqrt{1 - v_{t2}^2}, \end{aligned} \tag{5.17}$$

where $B_1^2 = B_n^2 + B_{t1}^2$.

We now normalize the equations and simplify to obtain our jump relations

$$B_{n1} = B_{n2} = B_n \tag{5.18}$$

$$v_{t2} = -v_{n1} \cot\theta \tag{5.19}$$

$$\frac{\rho_2}{\rho_1} = \frac{\gamma_1 v_{n1}}{\gamma_2 v_{n2}} \tag{5.20}$$

$$\frac{\gamma_1}{v_{n1}}\left[\frac{1}{\gamma_1^2}\left(\pi_1-\frac{1}{3}d\pi_1\right)+d\pi_1\frac{\sin^2\theta}{1-v_{n1}^2\cos^2\theta}+v_{n1}^2\left(W_1-\frac{1}{3}d\pi_1\right)+\frac{\sigma\cos^2\theta}{2}\right]=$$
$$\frac{\gamma_2}{v_{n2}}\left[\frac{1}{\gamma_2^2}\left(\pi_2+\frac{2}{3}d\pi_2\right)+v_{n2}^2\left(W_2+\frac{2}{3}d\pi_2\right)\right] \tag{5.21}$$

$$\frac{\gamma_1}{v_{n1}}\left[\frac{d\pi_1}{\gamma_1^2}\frac{1}{1-v_{n1}^2\cos^2\theta}-\sigma\right]\sin\theta\cos\theta=\gamma_2 v_{t2}\left(W_2+\frac{2}{3}d\pi_2\right) \tag{5.22}$$

$$\gamma_1\left(W_1-\frac{1}{3}d\pi_1+d\pi_1\frac{\sin^2\theta}{1-v_{n1}^2\cos^2\theta}+\sigma\cos^2\theta\right)=\gamma_2\left(W_2+\frac{2}{3}d\pi_2\right) \tag{5.23}$$

$$\frac{\pi_1 W_1-\frac{1}{3}d\pi_1\left(\frac{K_4}{K_3}\right)_1}{\sqrt{1-v_{n1}^2\cos^2\theta}}\sin\theta=\frac{\pi_2 W_2-\frac{1}{3}d\pi_2\left(\frac{K_4}{K_3}\right)_2}{\sqrt{1-v_{t2}^2}}, \tag{5.24}$$

where $\theta=\arctan\left(B_n/B_{t1}\right)$, $\sigma=\frac{B_1^2}{\gamma_1^2\rho_1}$, $\pi=\frac{p}{\rho}=\frac{1}{\zeta}$, and $d\pi=\frac{\Delta p}{\rho}$.

In the non-relativistic limit, this system reduces to the Rankine-Hugoniot relations for a CGL plasma. As such, the system reproduces previous results in the literature [9] and smoothly connects non-relativistic shock theory to a fully relativistic generalization.

5.1.4 Results Without Anisotropy

In the limit with no pressure anisotropy on either side of the shock, a cold plasma upstream, and a relativistically hot plasma downstream, Lyubarsky [48] found the following inflow velocity:

$$v_{n1}^2 = \frac{\sigma \sin^2\theta}{1+\sigma\cos^2\theta}. \tag{5.25}$$

To obtain analytical results for other parameters, Lyubarsky assumes $\sigma \gg 1$ and performs expansions to find:

$$v_{n1} = \tan\theta, \tag{5.26}$$

$$v_{t2} = -v_{n1}\cot\theta = -\left(1 - \frac{1}{2\sigma\cos^2\theta}\right), \tag{5.27}$$

$$v_{n2} = \frac{\sin\theta}{2\sigma\cos^3\theta}, \tag{5.28}$$

$$\pi_2 = \frac{B_1^2\cos^2\theta}{2\rho_2} = \frac{\sigma\gamma_1^2\cos^2\theta}{2}\frac{\rho_1}{\rho_2}, \tag{5.29}$$

$$\rho_2 = 2\rho_1\cos^2\theta\sqrt{\frac{\sigma}{\cos 2\theta}}. \tag{5.30}$$

We reproduce these results in the limit $\Delta p_1 = \Delta p_2 = 0$ and use the results as a baseline for comparison.

5.1.5 New Results

Combining equations (5.19), (5.22), and (5.23), the inflow velocity can be expressed as

$$v_{n1}^2 = \frac{\left(\sigma - \frac{d\pi_1}{\gamma_1^2}\frac{1}{1-v_{n1}^2\cos^2\theta}\right)\sin^2\theta}{W_1 - \frac{1}{3}d\pi_1 + d\pi_1\frac{\sin^2\theta}{1-v_{n1}^2\cos^2\theta} + \sigma\cos^2\theta}. \tag{5.31}$$

The inflow velocity is abated when the numerator vanishes, which corresponds to the onset of the firehose instability ($B_1^2 < \Delta p_1$) for the inflowing plasma. Note, equation (5.31) corresponds to the Alfven speed in the shock frame of the plasma and has no dependence on the downstream parameters.

For the same case as considered by Lyubarsky [48] except with the inclusion of pressure anisotropy in the downstream plasma (upstream cold and isotropic), one finds the following results

$$\frac{\rho_2^{\Delta p}}{\rho_2} = \frac{4}{7} \qquad \frac{v_{n2}^{\Delta p}}{v_{n2}} = \frac{7}{4}$$
$$\frac{v_{n1}^{\Delta p}}{v_{n1}} = 1 \qquad \frac{\pi_2^{\Delta p}}{\pi_2} = \frac{3}{4}$$
$$\frac{v_{t2}^{\Delta p}}{v_{t2}} = 1 \qquad \frac{d\pi_2^{\Delta p}}{\pi_2} = \frac{3}{2}$$
$$\frac{d\pi_2^{\Delta P}}{\pi_2^{\Delta P}} = 2$$

where $x^{\Delta p}$ represents results with downstream anisotropy. The downstream plasma is marked by the presence of a *strong pressure anisotropy which occurs regardless of the anisotropy of the upstream plasma.* Upstream pressure anisotropy plays a small role in the dynamics of the system until it is of the order of the magnetic energy, $\Delta p_1 \simeq B^2$.

5.1.6 Exploration of Various Parameter Regimes

Having explored simple analytical solutions to the relativistic switch-off shock with pressure anisotropy, we now turn to examining numerical results compute via Mathematica® . We choose an intermediate shock angle of 22.5^o for all of the shocks appearing in this section. All downstream parameters are plotted against the normalized upstream plasma temperature, T_1/m, so that the far left of each plot represents non-relativistic inflow temperatures.

We begin by examining three relativistic cases in which the upstream anisotropy is zero, figures 5.2 - 5.4. In each figure, red lines are results with downstream anisotropy and black are fully isotropic results, while red dashed lines are downstream temperature anisotropy. In figure 5.2, σ is chosen to be an ultra-relativistic value of 100. If we define the strength of our shock by the compression ratio, ρ_2/ρ_1, we see the anisotropic shock is weaker than its isotropic counterpart. The shock is also cooler than its isotropic counterpart but features a downstream anisotropy roughly twice its temperature. The outflowing normal velocity is enhanced but remains small compared to the tangential velocity, which is unchanged in the anisotropic case since it is proportional to the inflow velocity and determined solely by upstream parameters.

Moving on to figure 5.3, for which $\sigma = 1$, the same overall trends as the ultra-relativistic case are observed. However, the compression ratio crosses below unity for $T_1/m \gtrsim 0.45$. As in non-relativistic shocks [78], the second law of thermodynamics requires the compression ratio to increase across a shock

due to irreversible dissipation occurring in the shock. Thus, the shock in this regime is weakened to the point of becoming continuous for temperatures above approximately $0.45m$. Further, in figure 5.4 in which the magnetic field is moderately relativistic, $\sigma = 0.001$, the shock ceases to exist at a yet lower temperature and is significantly weaker than its isotropic counterpart.

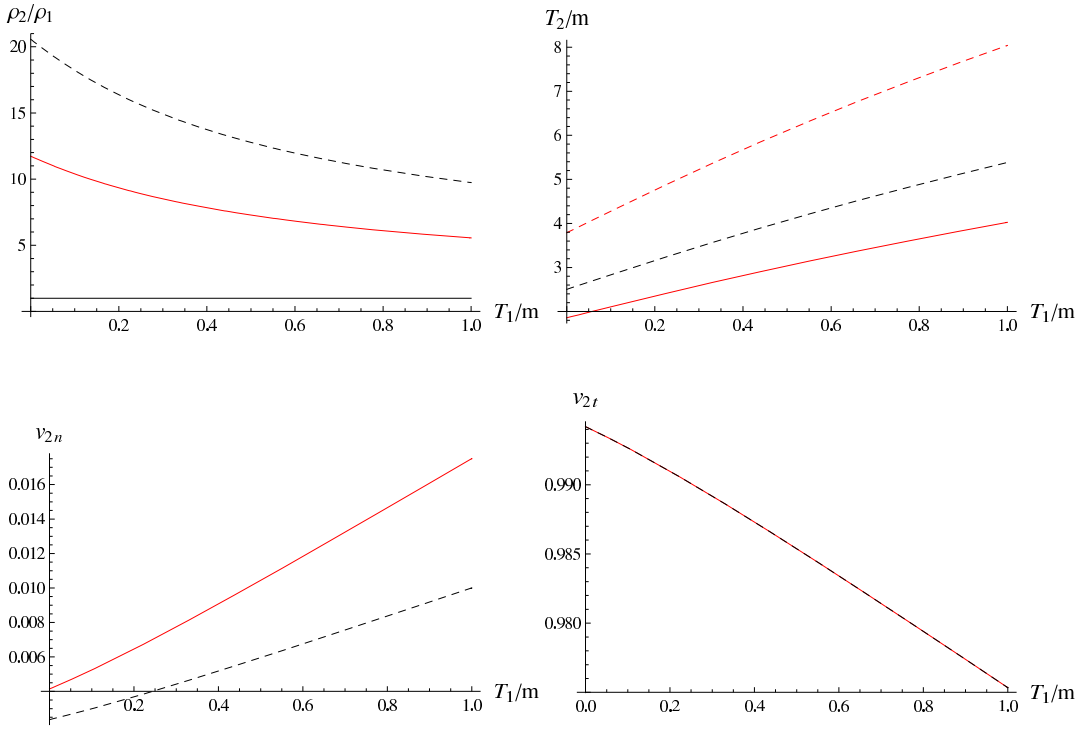

Figure 5.2: Downstream parameters of a switch-off shock with respect to upstream temperature. $\sigma = 100$, $\Delta\pi_1 = 0$, $\theta = 22.5$. Red are results with downstream anisotropy and black are fully isotropic results. Red dashed is downstream temperature anisotropy.

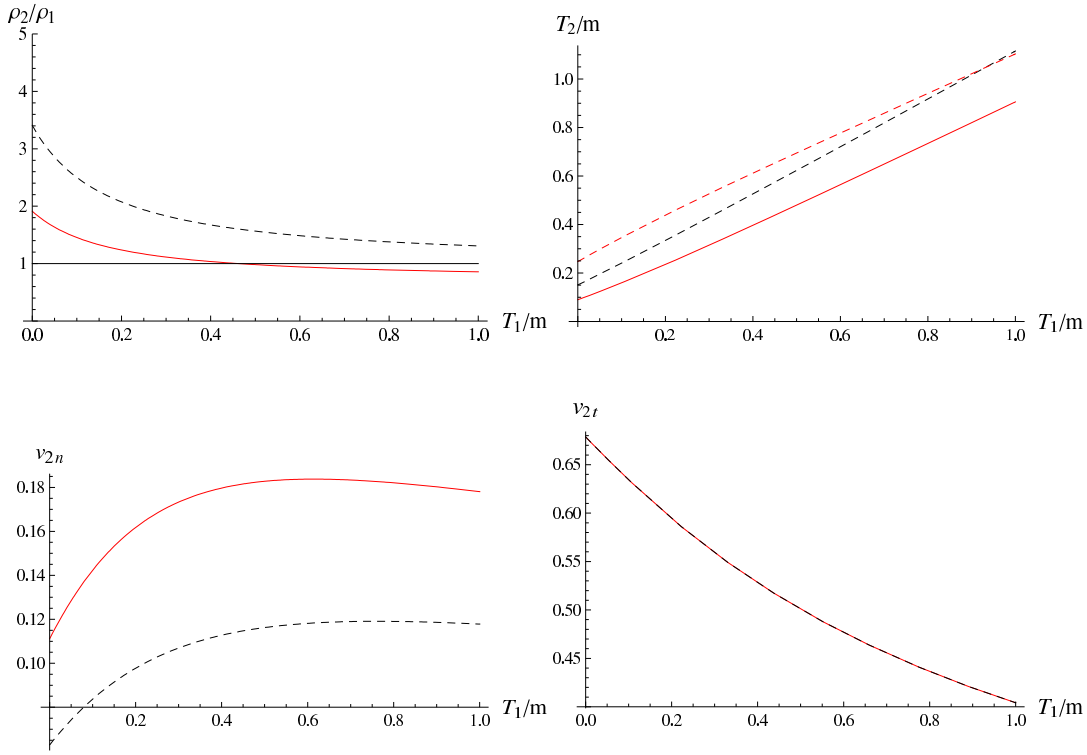

Figure 5.3: Downstream parameters of a switch-off shock with respect to upstream temperature. $\sigma = 1$, $\Delta\pi_1 = 0$, $\theta = 22.5$. Red are results with downstream anisotropy and black are fully isotropic results. Red dashed is downstream temperature anisotropy.

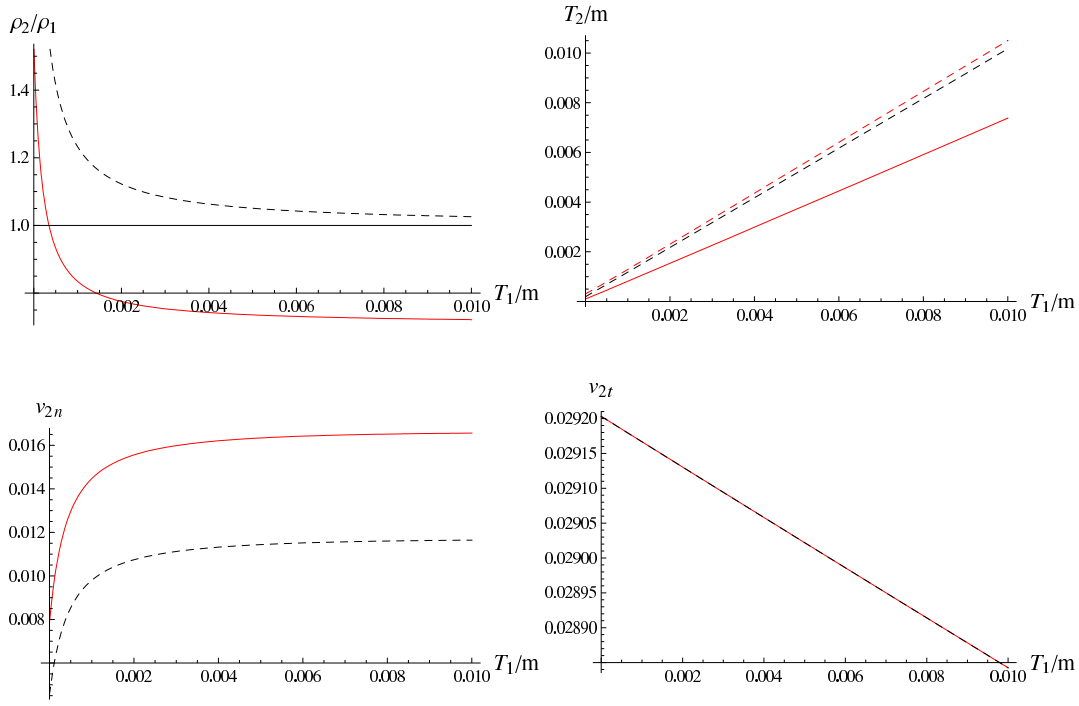

Figure 5.4: Downstream parameters of a switch-off shock with respect to upstream temperature. $\sigma = 0.001$, $\Delta\pi_1 = 0$, $\theta = 22.5$. Red are results with downstream anisotropy and black are fully isotropic results. Red dashed is downstream temperature anisotropy.

Figure 5.5 explores the effect of upstream pressure anisotropy on the switch-off shock in the relativistic regime of $\sigma = 1$. Represented by red in this figure is the case $\Delta p_1 = p_1$ ($p_{\parallel 1} = \frac{5}{2} p_{\perp 1}$), blue is the case $\Delta p_1 = -p_1$ ($p_{\parallel 1} = \frac{1}{4} p_{\perp 1}$), and black has $\Delta p_1 = 0$—all three cases permit downstream anisotropy. For non-relativistic inflow temperatures, the anisotropy of the upstream plasma plays little role in determining the downstream plasma. Also, upstream anisotropy has a negligible effect on the downstream temperature. Examining the compression ratio curves reveals positive upstream anisotropy serves to weaken the shock, while negative anisotropy strengthens and stabilizes the shock.

Figure 5.2.2 presents the case one might expect to find in a strongly magnetized pulsar magnetosphere. Relativistically strongly magnetized plasmas will rapidly radiate away their perpendicular energy (temperature) due to synchrotron radiation [5], leaving $p_{\parallel 1} \gg p_{\perp 1}$.

We take a brief aside to note the quantity $\Delta p/p$ is bounded. Explicitly,

$$\frac{\Delta p}{p} = \frac{3(p_\parallel - p_\perp)}{p_\parallel + 2p_\perp}, \tag{5.32}$$

which has two limits:

1. $p_\parallel \gg p_\perp$: in which case $\Delta p/p \to 3$.

2. $p_\parallel \ll p_\perp$: in which case $\Delta p/p \to -3/2$.

Therefore, $\Delta p/p \, \epsilon \, (-3/2, 3)$.

In figure 5.2.2, red represents the case likely to be seen in a pulsar magnetosphere, while black represents an isotropic upstream plasma. As noted above but enhanced by the stronger positive anisotropy, the shock in the pulsar case is weaker than the isotropic case and shuts off above $T_1 \simeq 0.1m$ for this parameter regime. The shut-off suggests shocks may not occur in the relativistically hot and magnetized regions of pulsar and magnetar magnetospheres.

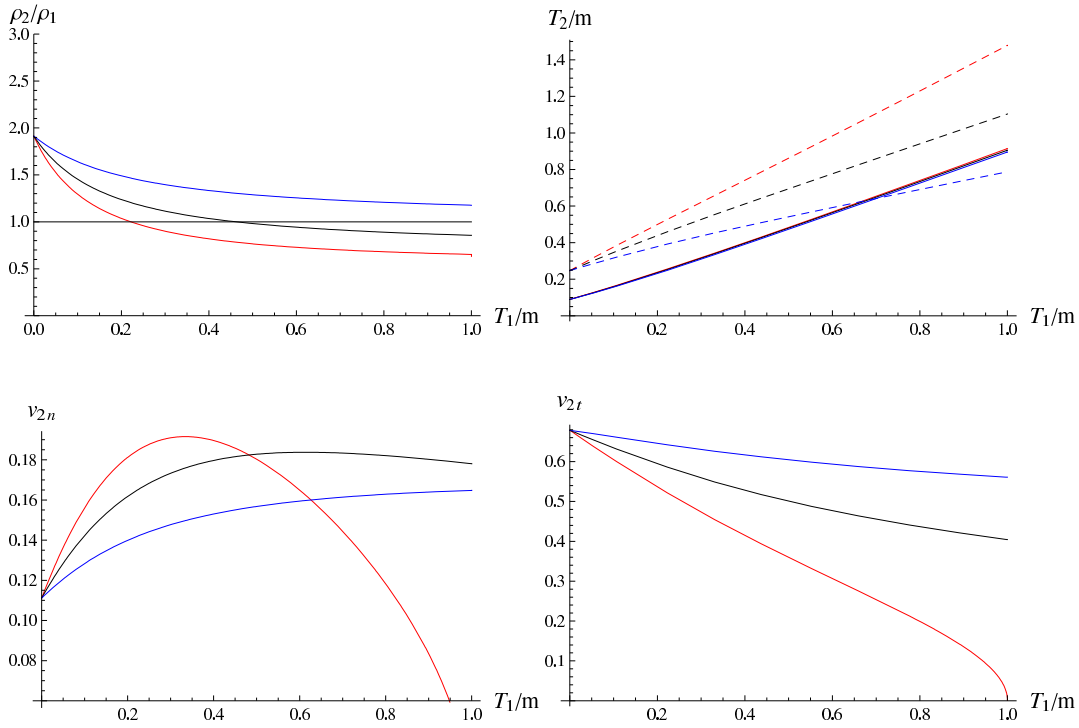

Figure 5.5: Effect of Upstream Anisotropy ($\sigma = 1$, $\theta = 22.5$). Red = $d\pi_1 = \pi_1$, Blue = $d\pi_1 = -\pi_1$, Black = $d\pi_1 = 0$, Dashed = $d\pi_2$.

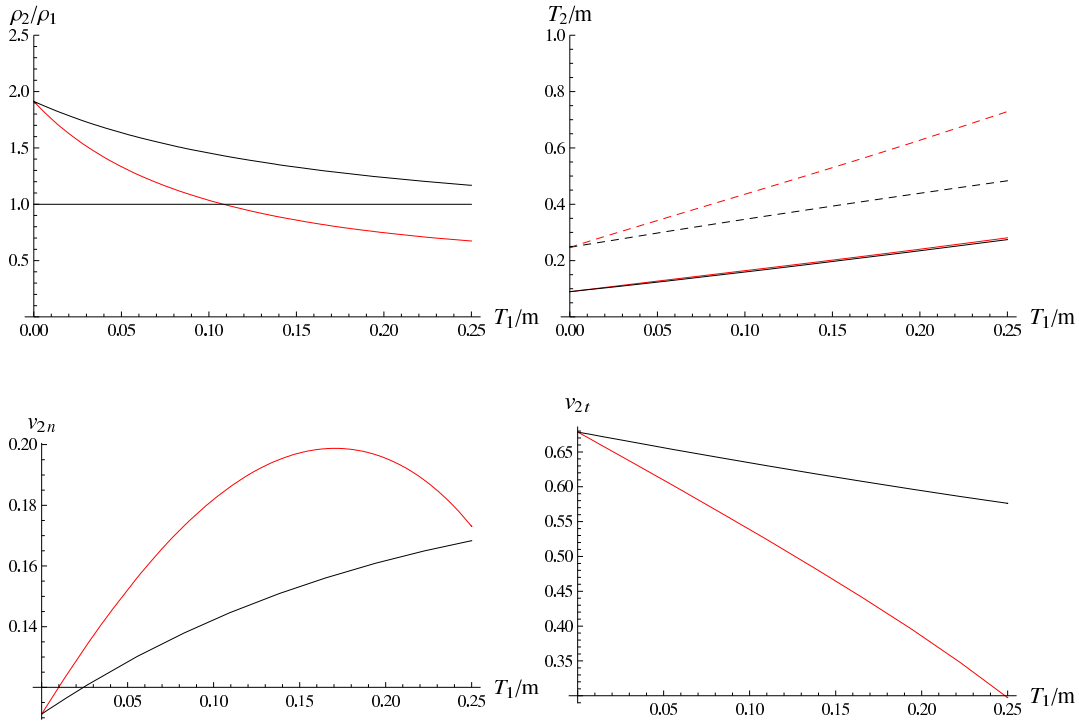

Figure 5.6: Pulsar / Magnetar Case ($\sigma = 1$, $p_{\parallel 1} \gg p_{\perp 1}$, $\theta = 22.5$). Red = $d\pi_1 = 3\pi_1$, Black = $d\pi_1 = 0$, Dashed = $d\pi_2$.

A strong anisotropy downstream of a pair plasma reconnection event has been observed in PIC simulations performed by Swisdak et al. [66] and Zenitani and Hesse [79]. In their simulations, they observed a maximum downstream anisotropy of $T_{tt}/T_{nn} \simeq 4$, where T is the stress tensor of the plasma. Also observed was an enhancement of the out-of-plane magnetic field. They argue the anisotropy drives a Weibel instability in the downstream plasma whose generated turbulence serves to limit the length of the reconnection current sheet, thereby facilitating fast reconnection. The source of the Weibel instability is the two "streams" of plasma having different temperature. In non-relativistic pair plasma simulations, Daughton and Karimabadi [23] observed the possible signature of a firehose instability in the strongly anisotropic downstream pair plasma. The role the instability played in the reconnection dynamics was not explored.

In our case, $T_{tt}/T_{nn} \simeq 1/7 + 10\gamma_2^2 v_{t2}^2/7$ for the relativistically strongly magnetized shocks with relativistic downstream temperatures considered in our analysis. For the cases considered herein, T_{tt}/T_{nn} can be of order 100. An out-of-plane magnetic field was not included in our analysis; however, the Weibel instability in the form of two warm streams is a purely kinetic instability. The only fluid analog progenitor of a Weibel instability is to impose cold beams on the plasma.

Although we can not observe a Weibel like instability in our fluid approach, another instability may play a similar role. In all parameter regimes explored, the downstream plasma exhibits a positive anisotropy on the order

of the downstream temperature. Since the firehose instability threshold is unmodified for relativistic plasmas [18], the threshold for the downstream plasma can be expressed as

$$\frac{B_2^2}{\rho_2} - \frac{\Delta p_2}{\rho_2} = \sigma \sin^2\theta \frac{\gamma_1\gamma_2 v_{n2}}{v_{n1}} - d\pi_2 < 0, \tag{5.33}$$

the strong positive anisotropy produced by the shock results in a firehose unstable plasma for relativistically strongly magnetized ($\sigma = \frac{B_1^2}{\gamma_1^2\rho_1} \gtrsim 1$) upstream plasma. This instability likely leads to turbulence in the outflowing plasma, which may play the same role as the Weibel instability for these relativistic cases.

5.1.7 Summary and Future Work

Our new relativistic fluid model produces interesting new results for relativistic slow-mode shocks compared to conventional relativistic MHD [48]. The downstream plasma always develops strong positive ($p_\parallel > p_\perp$) anisotropy, regardless of the isotropy of upstream plasma. Anisotropy in the relativistic system always weakens the shock (decreases the compression ratio) compared to the fully isotropic case. In some cases the anisotropic shock is abated due to entropy considerations, while the isotropic shock remains well behaved.

Enhancement of the perpendicular temperature will tend to provide a source for synchrotron radiation; however, our calculations indicate the parallel temperature is strongly enhanced by relativistic shocks. How an enhanced parallel temperature will manifest itself in observable radiation from an astro-

physical event is uncertain. From Wien's displacement law, the temperature of parallel component is in the hard x-ray to gamma ray spectrum, which is consistent with observations from likely astrophysical sources [4]. However, there is no reason to expect the radiation to be preferentially sourced from the parallel temperature.

We posit the effect of the downstream plasma being firehose unstable to be constraining the length of the reconnection current sheet, analogous to the effect of Weibel instabilities observed in PIC simulations. However, this hypothesis needs to be verified via PIC simulations in the relativistic regimes considered herein. Further, PIC simulations of relativistic pair plasma reconnection would be also be useful in verifying the overarching conclusions of our analysis.

Such a strongly magnetized and energetic plasma will likely strongly radiate, especially in the diffusion region where copious pair production is likely to occur due to inverse Compton scattering [49]. A further complication is resistivity in a relativistic regime. The particle-particle collision rate drops exponentially with temperature; however, particle-photon collisions and scattering from plasma turbulence and oscillations increases with temperature [50], requiring detailed knowledge of the micro-physics. Inclusion of radiation and collisions in this regime is difficult both analytically and numerically but needs to be done to better understand reconnection and shocks in relativistic regimes.

5.2 Radial Profiles in a Pulsar Magnetosphere

5.2.1 Introduction

The study of stellar winds has been extensive in the literature. The studies began with Parker's [56] discussion of thermally driven winds and emphasized the importance of the sonic critical point, at which the radial speed is equal to the local sound speed of the ejected plasma. Weber and Davis [74] extended the result to include magnetic fields and angular momentum transfer. Due to the inclusion of the magnetic field, they found three critical points: sonic, Alfvén, and supersonic. Weber and Davis found solutions numerically by requiring them to pass through all three critical points. Mestel [52] included a poloidal field strong enough to force corotation of the plasma near the stellar surface. Michel [55] studied a relativistic, fast rotating, highly magnetized, but cold ($p \ll B^2, mn$) wind in the absence of gravity. Rather than fitting to the only critical point in his approach, Mestel assumed the wind would arrange itself to exert minimal torque on the star. Goldreich and Julian [32] studied stellar winds from the perspective of Weber and Davis and Mestel but examined the non-relativistic and ultra-relativistic flow of an isothermal plasma. Kennel et al. [41] further generalized the results of Goldreich and Julian and Mestel to include a warm adiabatic plasma with relativistic injection speeds. Goldreich and Julian [31] also studied the case for a pulsar and found thermally driven winds insufficient to satisfy observations. They found a large scale electric field at the surface of the neutron star is required to eject sufficient material, and the strong magnetization of the environs is sufficient

to cause corotation of the inner plasma with the stellar surface.

Tan and Abraham [67] presented the first study of the effect of anisotropy on stellar winds. Their approach was fully non-relativistic and employed a CGL style closure. Asseo and Beufils [5] employed a relativistic inflow velocity, but used a non-relativistic CGL style closure for the temperature. They noted the intensely strong magnetic fields ($\gtrsim 10^{12}$ Gauss [4]) in pulsar and magnetar magnetospheres will have the effect of anisotropizing the plasma due to synchrotron radiation, leaving $p_\parallel \gg p_\perp$. Tsikarishvili et al. [72] (TRT) used their double polytropic relativistic closure [71] to extend the result of Asseo and Beufils and assumed ultra-relativistic temperatures. However, their closure requires the temperature to remain in the same ultra-relativistic regime indefinitely. Thus, the region of validity for their model is limited to a few light cylinder radii, where some of their assumptions ($p_\parallel \gg p_\perp$, $\frac{p_\parallel}{h^2} \sim \beta \ll 1$, and $T/m \gg 1$) begin to fail.

We follow an approach similar to TRT and assume a Goldreich and Julian [31] style magnetospheric structure (see figure 5.2.2), which has a cool plasma up to the radius at which the angular velocity ($r\Omega$) for solid body rotation is unity (the light cylinder) with a shock or other mechanism providing heating at the light cylinder. Although we employ the first of TRT's assumptions, we relax the other assumptions by numerically integrating our anisotropic model. Further, we extend the result to study the effect of parallel heat flow on the pulsar wind.

5.2.2 Evolution Equations

We assume an axisymmetric spherical system and analyze steady-state conditions on the equatorial plane in the wind region of a pulsar. Further, we assume synchrotron radiation has effectively anisotropized the plasma by dissipating the perpendicular temperature and heat flow ($p_{\parallel} \gg p_{\perp}$ and $q_{\parallel} \gg q_{\perp}$), as theorized by Sen Gupta [60] and quantified by Suvorov and Chugunov [65] for a strongly magnetized, collisionless plasma on a characteristic time scale of $t_0 = 3m^3/2e^4B^2$. We also assume the velocity and magnetic field have only radial and toroidal components, consistent with the Goldreich and Julian [31] model. Due to the high temperatures under investigation, we assume a pair plasma, and all fluid quantities are summed over plasma species. We will be working in spherical polar coordinates, whose properties are reviewed in appendix 0.1. Subscripted quantities are ordinary vector components and do not indicate covariance in the following equations.

Considering the above assumptions, Maxwell's equations and the continuity equation, equation (4.55) reduce to:

$$r^2 B_r = \Phi, \tag{5.34}$$

$$B_\phi = B_r \left(v_\phi - \Omega r\right)/v_r, \tag{5.35}$$

$$r^2 \gamma v_r \rho = f, \tag{5.36}$$

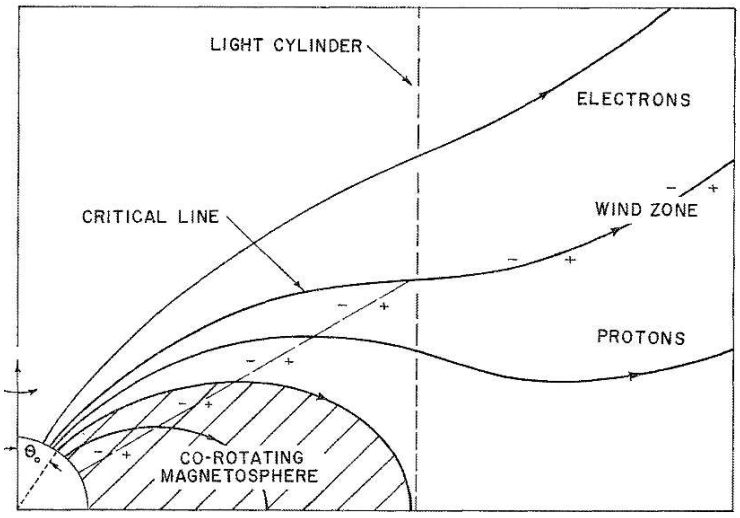

Figure 5.7: Goldreich-Julian pulsar magnetosphere [31].

where $\rho = mn$ and f, Φ, and Ω are the mass and magnetic flux per steradian, and the star's rotation frequency respectively. Equations (4.56) - (4.58) and (4.60) respectively reduce to

$$\begin{aligned}&\left(u + p_{\|}\right)\gamma^2 v_r\left[h_r\partial_r v_r + h_\phi r\partial_r\left(v_\phi/r\right)\right] + h_r\partial_r p_{\|} - h_r\partial_r\log h\\&+\gamma h v_r\left(\partial_r q_{\|} + \partial_r\log h/\rho^2\right) + \left(u + p_{\|}\right)\gamma^2\frac{v_\phi}{r}\left(2h_\phi v_r - h_r v_\phi\right) = 0,\end{aligned} \tag{5.37}$$

$$\begin{aligned}&-\gamma v_r\partial_r u + \left(u + p_{\|}\right)\gamma v_r\partial_r\log\rho - p_{\|}\gamma v_r\partial_r\log h + q_{\|}\frac{h_r}{h}\partial_r\log h\\&-\frac{h_r}{h}\partial_r q_{\|} - 2q_{\|}\gamma^2 v_r\left[h_r\partial_r v_r + h_\phi r\partial_r\left(v_\phi/r\right)\right] + 2q_{\|}\gamma^2\frac{v_\phi}{r}\left(2h_\phi v_r - h_r v_\phi\right)\\&= 0,\end{aligned} \tag{5.38}$$

$$
\begin{aligned}
&r\{\gamma^2 v_r \frac{u}{p_\parallel}\left(B_\phi \partial_r v_r - B_r \partial_r v_\phi\right) + \frac{h_r}{h^2}\left[B_\phi \partial_r h_r - B_r \partial_r h_\phi\right. \\
&\left. - \left(B_\phi v_r - B_r v_\phi\right)\partial_r h_0\right]\} - \gamma^2 v_\phi \frac{u}{p_\parallel}\left(B_r v_r + B_\phi v_\phi\right) - \frac{h_\phi}{h^2}\left(B_\phi h_\phi + B_r h_r\right) \\
&+ \frac{q_\parallel}{p_\parallel}\{\gamma \frac{v_r}{h} r\left[B_\phi \partial_r h_r - B_r r \partial_r\left(h_\phi / r\right) - \left(B_\phi v_r - B_r v_\phi\right)\partial_r h_0\right] \\
&+ \gamma \frac{h_r}{h} r\left(B_\phi \partial_r v_r - B_r r \partial_r\left(v_\phi / r\right)\right) + 2\frac{\gamma}{h}\left(B_\phi v_\phi h_\phi + B_r v_r h_\phi + B_r v_\phi h_r\right)\} \\
&= -\frac{h^2}{p_\parallel}\partial_r\left(r B_\phi\right),
\end{aligned}
\tag{5.39}
$$

$$
\begin{aligned}
&\gamma v_r \partial_r\left(5m_3 + \frac{1}{3}m_4\right) + \frac{h_r}{h}\partial_r\left(m_1 + m_2\right) - m_2 \frac{h_r}{h}\partial_r \log h \\
&+ \left(5m_1 + 3m_2\right)\gamma^2 \frac{v_r}{h}\left[h_r \partial_r v_r + h_\phi r \partial_r\left(v_\phi / r\right)\right] \\
&- \left(13m_3 + \frac{1}{3}m_4\right)\gamma v_r \partial_r \log \rho + \left(7m_3 + \frac{4}{3}m_4\right)\gamma v_r \partial_r \log h \\
&+ \rho\gamma^2 \frac{v_r}{h}\left[h_r \partial_r v_r + h_\phi r \partial_r\left(v_\phi / r\right)\right] \\
&+ \left(5m_1 + 3m_2 + \rho\right)\gamma^2 \frac{v_\phi}{hr}\left(2h_\phi v_r - h_r v_\phi\right) = 0.
\end{aligned}
\tag{5.40}
$$

Due to our isotropy assumption, we do not need equations (4.59) and (4.61), for $p_\parallel$ and $q_\parallel$ respectively, to obtain closure.

5.2.3 Numerical Results

To obtain numerical solutions, we assume $v_r \simeq 0$ and $v_\phi \simeq 1$ with pressure and heat flow singular at the light cylinder due to heating caused by instabilities or a shock, such as discussed in §5.1. For simplicity, constants are taken to be unity except for $\Omega = 10^4$ to achieve the extreme ultra-relativistic limit. We integrate our system via Mathematica® .

Figure 5.8 represents the numerical solution to equations (5.34) - (5.40). In the figure, solid red lines represent solutions with heat flow, while black dashed represent solutions without heat flux and all quantities are plotted versus light cylinder radii, $r\Omega$. For the plot of heat flux, we employ the approximation $q_{\parallel} \simeq p_{\parallel}(\boldsymbol{v} \cdot \boldsymbol{b})$ to model the non-existent heat flux. From the figure, it is clear the magnetic field, bulk flow, and density are little effected by the presence of a strong heat flux. From the velocity plots, we see the bulk plasma flow very quickly becomes primarily radial. Examining the relativistic γ factor, we see the overall flow of the plasma increases with radius, with γ growing approximately linearly with radius. The growth of γ with radius is consistent with calculations by Buckley [14] and Contopolous and Kazanas [21]. The model heat flux employed captures the correct qualitative form of the heat flow with radius, but is several orders of magnitude too small. In both cases, the heat flux drops very rapidly with radius, as does the pressure. Since the density is relatively unaffected by the presence of heat flux, the differences in the plot of $p_{\parallel}$ can effectively be viewed as changes in temperature. Expectedly, the inclusion of a large heat flux significantly heats the plasma at large radii.

Figure 5.9 plots the ratio of $p_{\parallel}$ with heat flow to that without versus radius to give a clearer picture on the effect of heat flux on temperature. We only plot pressure in this fashion since most quantities are relatively unchanged. We see the presence of heat flux causes roughly an order of magnitude increase in the temperature at large radii.

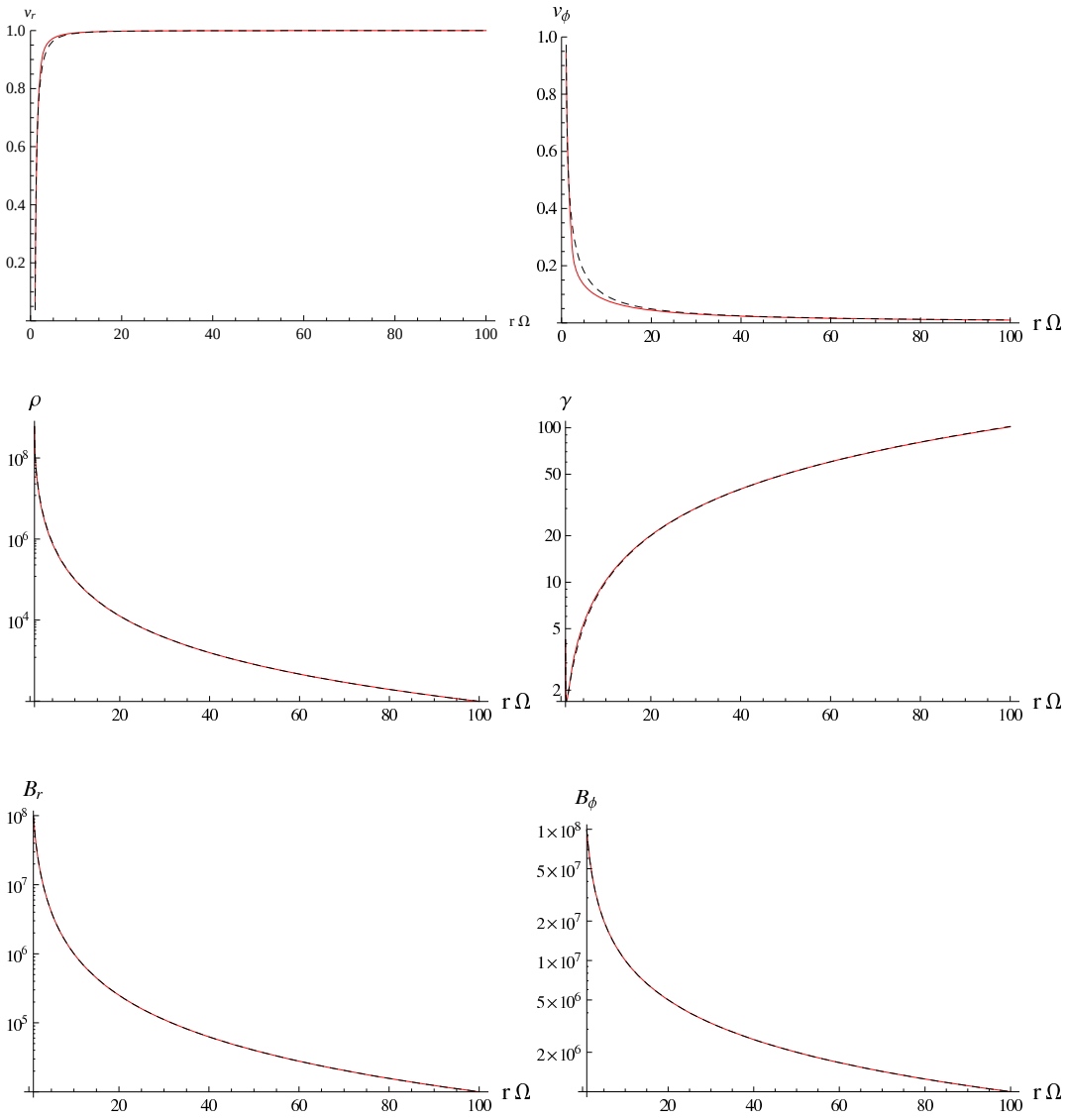
v_r
1.0
0.8
0.6
0.4
0.2
0
20
40
60
80
100
r Ω
v_ϕ
1.0
0.8
0.6
0.4
0.2
0
20
40
60
80
100
r Ω
ρ
10^8
10^6
10^4
20
40
60
80
100
r Ω
γ
100
50
20
10
5
2
20
40
60
80
100
r Ω
B_r
10^8
10^7
10^6
10^5
20
40
60
80
100
r Ω
B_ϕ
1×10^8
5×10^7
2×10^7
1×10^7
5×10^6
2×10^6
20
40
60
80
100
r Ω

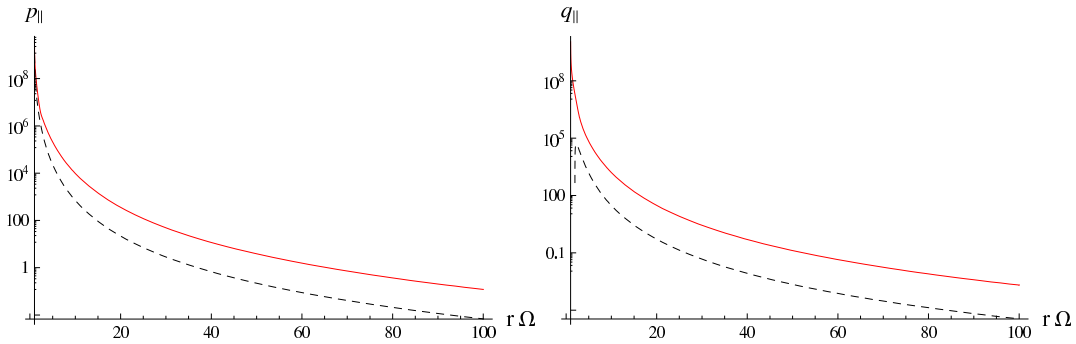

Figure 5.8: Radial profiles for pulsar magnetosphere comparing quantities without heat flow (solid red) to those with heat flow (black dashed). Only temperature and heat flow show significant differences.

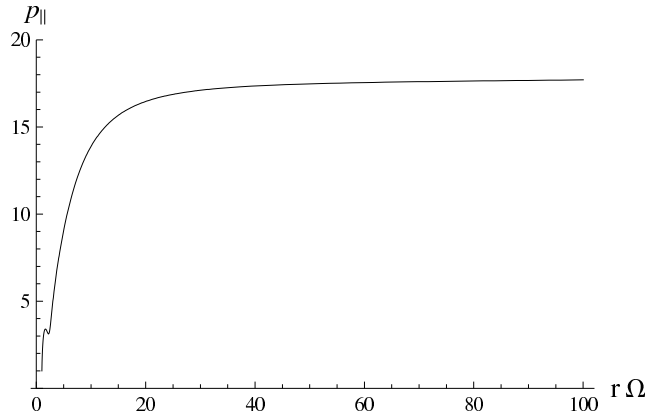

Figure 5.9: Ratio of $p_\parallel$ with to that without heat flow in a pulsar magnetosphere. A significantly enhanced temperature can be seen.

5.2.4 Comparison to TRT

TRT approach the problem in a somewhat different fashion than the above. They employ conservation equations similar to those found in §5.1.2; however, their double adiabatic approach prescribes an equation of state to close the system. Namely,

$$p_{\parallel} = \epsilon\rho \left(\rho/h\right)^{2\alpha}, \tag{5.41}$$

where ϵ is a constant and α is the adiabatic variable with which the thermodynamics are prescribed. For the ultra-relativistic assumption TRT employ, $\alpha = 0.5$.

Since TRT assumes $T/m \gg 1$ throughout the wind region and that the plasma is strongly magnetized, so that $p_{\parallel}/h^2 \ll 1$, they are able to achieve asymptotically analytical solutions to their system. They find:

$$
\begin{aligned}
v_r &= \frac{2R(x^2-1)}{2Rx^2-1}, \\
v_\phi &= \frac{x(2R-1)}{2Rx^2-1}, \\
\gamma &= \frac{2Rx^2-1}{\sqrt{(2R)^2-1)(x^2-1)}}, \\
B_r &= \frac{\Phi\Omega^2}{x^2}, \\
B_\phi &= -\frac{\Phi\Omega^2}{x}, \\
\rho &= f\Omega^2\left(\frac{4R^2-1}{4R^2}\right)^{1/2}\frac{1}{x^2(x^2-1)^{1/2}}, \\
p_\parallel &= f\Omega^2\left(\frac{4R^2-1}{4R^2}\right)\frac{1}{x^2(x^2-1)},
\end{aligned}
\tag{5.42}
$$

where $x = r\Omega$, $R = \epsilon f/\Phi$, and other constants are as defined in §5.2.2.

Despite their additional assumptions and not including heat flux, we see little difference between their results and our own. The only significant differences to note are in the toroidal velocity and the pressure. To visualize the difference, we plot in figure 5.10 the ratio of our solution to TRT. Our toroidal velocity is approximately double the TRT result beyond a few light cylinder radii, and the TRT pressure scales with an extra factor of the radius. However, the comparison would show further disagreement if we were to compare our results without heat flow to those of TRT, since our heat flowless results for the pressure are another order of magnitude smaller that those with heat flow. Thus, TRT grossly exaggerate the temperature more than a few light cylinder radii away from the light cylinder due to their ultra-relativistic assumption.

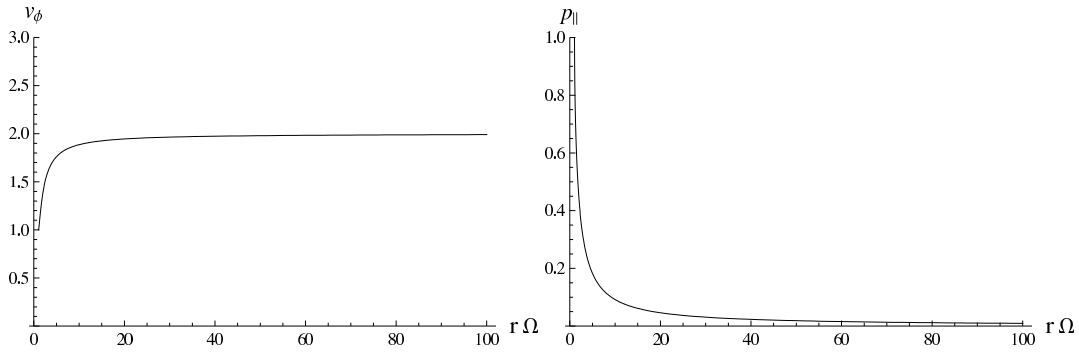

Figure 5.10: Plotted is the ratio of our solution to TRT. Most quantities are modified to a small degree; however, the toroidal velocity found by TRT is slower by a factor of ~ 2, and their pressure scales with an extra factor of the radius.

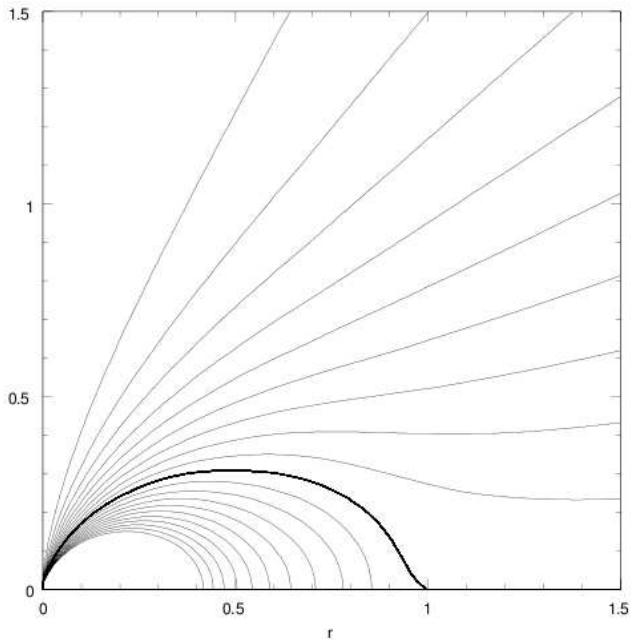

Figure 5.11: Split monopole pulsar magnetosphere solution, where r is measured in light cylinder radii [33].

5.2.5 Summary and Future Work

We calculate wind region radial profiles for pulsar magnetospheres with and without heat flow and spanning a wide range of temperature and flow velocities. We find heat flow significantly enhances the plasma temperature but has minimal effect otherwise. Further, our solution provides a significant advance beyond TRT due to a reduced set of assumptions and a more physically modeled temperature.

However, the boundary conditions we employ at the light cylinder are ad hoc and need further refinement. Also, the singular behavior at the light cylinder is suggestive of a boundary layer, which requires study. Our solution could also be extended to the termination shock, where the ejected plasma meets interstellar space. To perform such an analysis would require the ion population be included, since the plasma cools rapidly as it leaves the light cylinder.

Despite the apparent success of the application of our new closure, the Goldreich-Julian model of the magnetosphere has been superceded by iterative numerical solutions to the relativistic Grad-Shafranov equation (typically referred to as the "pulsar equation") by Contopolous et al. [20] and extensive numerical simulation of 3D force-free models (eg [63] and [40]) and MHD ([42] and [13]). These physical models, referred to as split monopoles and presented in figure 5.11, have smooth solutions when passing through the light cylinder, and thus do not assume strong heating of the plasma at the boundary. However, major gaps remain in several areas of our understanding of pulsar

magnetospheres (see, e.g., [4] and [64]), including the generation of high energy radiation and particle outflow and predicted magnetic reconnection in the equatorial plane of the wind region and in the vicinity of the light cylinder. The suspected reconnection events near the light cylinder may still give rise to a relativistically hot outflow similar to our analysis near the light cylinder as described in §5.1.

Appendix

0.1 Covariant Derivatives and Coordinate Transformations

The majority of the following properties can be found in most general relativity textbooks, such as Weinberg [75] or Wald [73].

Contravarient vectors transform between two coordinate systems according to

$$A'^{\nu} = \frac{\partial x'^{\nu}}{\partial x^{\mu}} A^{\mu}. \tag{43}$$

For example, transforming from cartesian to polar coordinates is given by

$$\begin{pmatrix} A'^{r} \\ A'^{\phi} \end{pmatrix} = \begin{pmatrix} \frac{\partial r}{\partial x} & \frac{\partial r}{\partial y} \\ \frac{\partial \phi}{\partial x} & \frac{\partial \phi}{\partial y} \end{pmatrix} \begin{pmatrix} A^{x} \\ A^{y} \end{pmatrix}. \tag{44}$$

Covariant vectors transform as

$$A'_{\nu} = \frac{\partial x^{\mu}}{\partial x'^{\nu}} A_{\mu}. \tag{45}$$

Transforming between coordinate systems extends to higher rank as expected

$$A'_{\mu\nu\cdots} = \frac{\partial x^{\alpha}}{\partial x'^{\mu}} \frac{\partial x^{\beta}}{\partial x'^{\nu}} \cdots A_{\alpha\beta\cdots}. \tag{46}$$

In Cartesian coordinates, parallel transport of a vector is simple because the vector components do not change. To generalize to non-Cartesian coordinates, we require the scalar product of two vectors remain constant under parallel transport along a curve, $\frac{d}{ds}\left(g_{\alpha\beta}A^{\alpha}B^{\beta}\right) = 0$. This requirement is determined by the metric via the Christoffel symbol,

$$\Gamma^{\nu}_{\alpha\beta} = \frac{1}{2} g^{\nu\sigma} \left[\partial_{\alpha} g_{\beta\sigma} + \partial_{\beta} g_{\alpha\sigma} - \partial_{\sigma} g_{\alpha\beta}\right]. \tag{47}$$

The Christoffel symbol is symmetric in its lower indicies $\Gamma^{\nu}_{\alpha\beta} = \Gamma^{\nu}_{\beta\alpha}$ and upon contraction yields

$$\Gamma^{\nu}_{\nu\mu} = \partial_{\mu}\sqrt{\log|g|}, \tag{48}$$

where $g = \det g_{\mu\nu}$.

Ordinary partial derivatives of tensors above rank 0 do not transform as tensors. Having developed the concept of parallel transport, we can now describe a proper tensor, covariant, derivative. The covariant derivative of a scalar is an ordinary gradient, $\nabla_{\mu}A = \partial_{\mu}A$. The covariant derivative of a contravariant vector is

$$\nabla_{\alpha}A^{\nu} = \partial_{\alpha}A^{\nu} + \Gamma^{\nu}_{\gamma\alpha}A^{\gamma}, \tag{49}$$

and the covariant derivative of a covariant vector is

$$\nabla_{\alpha}A_{\nu} = \partial_{\alpha}A_{\nu} - \Gamma^{\gamma}_{\alpha\nu}A_{\gamma}. \tag{50}$$

Moving to second rank, the covariant derivative of a contravariant tensor is

$$\nabla_{\alpha}A^{\mu\nu} = \partial_{\alpha}A^{\mu\nu} + \Gamma^{\mu}_{\gamma\alpha}A^{\gamma\nu} + \Gamma^{\nu}_{\gamma\alpha}A^{\gamma\mu}, \tag{51}$$

of a covariant tensor is

$$\nabla_{\alpha}A_{\mu\nu} = \partial_{\alpha}A_{\mu\nu} - \Gamma^{\gamma}_{\mu\alpha}A_{\gamma\nu} - \Gamma^{\gamma}_{\nu\alpha}A_{\gamma\mu}, \tag{52}$$

and of a mixed tensor

$$\nabla_{\alpha}A^{\mu}_{\nu} = \partial_{\alpha}A^{\mu}_{\nu} - \Gamma^{\gamma}_{\nu\alpha}A^{\mu}_{\gamma} + \Gamma^{\mu}_{\gamma\alpha}A^{\gamma}_{\nu}. \tag{53}$$

The extension to higher rank is straightforward.

From these properties, it is clear the covariant derivative of any metric must vanish. Thus, metric tensors commute with the covariant derivative. However, metric tensors do not in general commute with partial derivatives. Only in the case of cartesian coordiantes do metric tensors commute with partial derivatives.

Owing to property the contraction property of the Christoffel symbols (48), the covariant divergence of a four-vector is simply:

$$\nabla_\mu A^\mu = \frac{1}{\sqrt{|g|}} \partial_\mu \left(\sqrt{|g|} A^\mu \right), \tag{54}$$

while the covariant divergence of a tensor is:

$$\nabla_\mu A^{\mu\nu} = \frac{1}{\sqrt{|g|}} \partial_\mu \left(\sqrt{|g|} A^{\mu\nu} \right) + \Gamma^\nu_{\mu\gamma} A^{\mu\gamma}. \tag{55}$$

For the case of an antisymmetric tensor, the second term in equation (55) must vanish.

Two coordinate bases are used in the main body of this work and their properties are summarized below:

1. Cartesian coordinates: For Cartesian coordinates, the metric takes the simple form $g^{\mu\nu} = diag\{-1, 1, 1, 1\}$, which we denote by $\eta^{\mu\nu}$ and is typically referred to as the Minkowski metric. Clearly, the Christoffel symbols must vanish in this case. Thus, covariant and partial derivatives behave the same.

2. Spherical polar coordinates: For spherical polar coordinates, the metric can be calculated using equation (46) and takes the form $g^{\mu\nu} = diag\{-1, 1, 1/r^2, 1/r^2 \sin^2\theta\}$, where θ is measured with respect to the z-axis. This metric has the following non-zero Christoffel symbols:

$$\begin{aligned} \Gamma^1_{22} &= -r \\ \Gamma^1_{33} &= -r\sin^2\theta \\ \Gamma^2_{12} = \Gamma^2_{21} &= 1/r \\ \Gamma^2_{33} &= -\cos\theta\sin\theta \\ \Gamma^3_{13} = \Gamma^3_{31} &= 1/r \\ \Gamma^3_{23} = \Gamma^3_{32} &= \cot\theta. \end{aligned} \tag{56}$$

Four-vectors have the following contra- and covariant forms respectively:

$$\begin{aligned} V^\mu &= (V_t, V_r, V_\theta/r, V_\phi/r\sin\theta) \\ V_\mu &= (-V_t, V_r, V_\theta r, V_\phi r\sin\theta)\,, \end{aligned} \tag{57}$$

where (V_r, V_θ, V_ϕ) are the ordinary three-vector spherical components.

0.2 Properties of MacDonald Functions

The following properties and more of MacDonald functions can be found in most handbooks of mathematical functions, such as Abramowitz [1].

MacDonald functions are modified Bessel functions of the second kind. Derivatives of the n^{th} MacDonald function give

$$\begin{aligned} \frac{\partial}{\partial z}(z^n K_n(z)) &= -z^n K_{n-1}(z) \\ \frac{\partial}{\partial z}(z^{-n} K_n(z)) &= -z^{-n} K_{n+1}(z). \end{aligned} \tag{58}$$

The derivative relations give rise to the recurrence relation

$$K_{n+1}(z) - K_{n-1}(z) = \frac{2n}{z} K_n(z). \tag{59}$$

Since all of the MacDonald functions appearing in our theory are functions of the temperature, their limiting forms play an important role:

$$K_n(z) \simeq \frac{\Gamma(n)}{2} \left(\frac{2}{z}\right)^n \tag{60}$$

for $z \to 0$ (ultrarelativistic temperatures) and

$$K_n(z) \simeq \sqrt{\frac{\pi}{2z}} e^{-z} \left[1 + \frac{4n^2 - 1}{8z} + \frac{(4n^2 - 1)(4n^2 - 9)}{128 z^2} + \mathcal{O}(z^{-4})\right] \tag{61}$$

for $z \to \infty$ (nonrelativistic temperature).

0.3 Auxiliary Parameters

Here, we list the non-vanishing rest-frame moments of the third and fourth rank in terms of the auxiliary parameters m_k and r_k and express the auxiliary parameters of our system in terms of the dynamical variables. We orient our rest-frame such that $\boldsymbol{B} = (0, 0, B)$.

The non-vanishing components of the third rank moments are

$$M_R^{000} = m^2 n_R + 3m_1 + m_2,$$

$$M_R^{003} = 5m_3 - \frac{1}{3} m_4,$$

$$M_R^{011} = M_R^{022} = m_1,$$

$$M_R^{033} = m_1 + m_2,$$

$$M_R^{113} = M_R^{223} = m_3 - \frac{2}{3}m_4,$$

$$M_R^{333} = 3m_3 + m_4.$$

And for the fourth rank, we have

$$R_R^{0000} = m^2\left(u + 3p\right) + 15r_1 + 10r_2 + 4r_5,$$

$$R_R^{0011} = R_R^{0022} = m^2 p_\perp + 5r_1 + r_2 + r_5,$$

$$R_R^{0033} = m^2 p_\parallel + 5r_1 + 8r_2 + 2r_5,$$

$$R_R^{0003} = m^2 Q_\parallel - 3r_3 - 3r_4,$$

$$R_R^{0113} = R_R^{0223} = r_3,$$

$$R_R^{0333} = -5r_3 - 3r_4,$$

$$R_R^{1111} = R_R^{2222} = 3R_R^{1122} = 3r_1,$$

$$R_R^{1133} = R_R^{2233} = r_1 + r_2 + r_5,$$

$$R_R^{3333} = 3r_1 + 6r_2.$$

The auxiliary parameters of our system are determined by evaluating the rest frame moments above via our distribution function, equation (4.39)

$$m_1 = m\left[p\frac{K_3}{K_2} - \frac{1}{3}\Delta p\frac{K_4}{K_3} + \frac{\Delta p^2}{p}\left(\frac{1}{6}\frac{K_4K_3}{K_2^2} - \frac{4}{9}\frac{K_4^2}{K_3K_2} + \frac{5}{18}\frac{K_5}{K_2}\right)\right],$$

$$m_2 = m\Delta p\left[\frac{K_4}{K_3} - \frac{1}{3}\frac{\Delta p}{p}\left(\frac{K_4^2}{K_3K_2} - \frac{K_5}{K_2}\right)\right],$$

$$m_3 = \frac{mQ_\parallel}{\zeta}\left[1 - \frac{2}{3}\frac{K_4}{\mathcal{K}K_3}\frac{1+2Q}{2+3Q}\right],$$

$$m_4 = \frac{mQ_\parallel}{\zeta}\frac{K_4}{\mathcal{K}K_3}\frac{2\,(1-Q)}{2+3Q}.$$

$$r_1 = \frac{m}{n_R}\left[p^2\frac{K_3}{K_2} - \frac{2}{3}p\Delta p\frac{K_4}{K_3} + \Delta p^2\left(\frac{1}{6}\frac{K_4K_3}{K_2^2} - \frac{5}{9}\frac{K_4^2}{K_3K_2} + \frac{1}{2}\frac{K_5}{K_2}\right)\right],$$

$$r_2 = \frac{1}{2}\frac{m}{n_R}\left[2p\Delta p\frac{K_4}{K_3} + \Delta p^2\left(-\frac{2}{3}\frac{K_4^2}{K_3K_2} + \frac{K_5}{K_2}\right)\right],$$

$$r_3 = \frac{m^2}{\zeta}\frac{K_4}{K_3\mathcal{K}}Q_\parallel\left(\mathcal{K}_2 - \frac{2}{2+3Q}\frac{K_5}{K_4}\right),$$

$$r_4 = -\frac{2}{3}\frac{m^2}{\zeta}\frac{K_4}{K_3\mathcal{K}}Q_\parallel\left(4\mathcal{K}_2 - \frac{5+3Q}{2+3Q}\frac{K_5}{K_4}\right),$$

$$r_5 = -\frac{1}{2}\frac{m}{n_R}\Delta p^2\frac{K_5}{K_2},$$

where

$$\mathcal{K}_2(\zeta_s) = \frac{K_3(\zeta_s)}{K_2(\zeta_s)} - \frac{K_5(\zeta_s)}{K_4(\zeta_s)}.$$

We can also now express the enthalpy density in terms of our dynamical variables by look at $T_R^{00} = h - p$

$$h = mn_R\frac{K_3}{K_2}.$$

0.4 Fourth Rank Symmetrization

The construction of $R^{\alpha\beta\gamma\delta}$ will involve tensors of the three following forms, aside from fully asymmetric and fully symmetric

1. Symmetric times asymmetric, i.e., $\eta^{\alpha\beta}U^{\gamma}k^{\delta}$. This form will have 12 terms in the symmetrization

$$\begin{aligned} A_1^{(\alpha\beta\gamma\delta)} &= A^{\alpha\beta\gamma\delta} + A^{\alpha\beta\delta\gamma} + A^{\alpha\delta\gamma\beta} + A^{\alpha\delta\beta\gamma} \\ &+ A^{\alpha\gamma\beta\delta} + A^{\alpha\gamma\delta\beta} + A^{\beta\delta\alpha\gamma} + A^{\beta\delta\gamma\alpha} \\ &+ A^{\beta\gamma\alpha\delta} + A^{\beta\gamma\delta\alpha} + A^{\delta\gamma\alpha\beta} + A^{\delta\gamma\beta\alpha}. \end{aligned}$$

2. Symmetric times symmetric, i.e., $\eta^{\alpha\beta}U^{\gamma}U^{\delta}$. This form will have 6 terms

$$\begin{aligned} A_2^{(\alpha\beta\gamma\delta)} &= A^{\alpha\beta\gamma\delta} + A^{\alpha\gamma\beta\delta} + A^{\alpha\delta\beta\gamma} + A^{\beta\gamma\alpha\delta} \\ &+ A^{\beta\delta\alpha\gamma} + A^{\delta\gamma\alpha\beta}. \end{aligned}$$

   For the special case of a fourth rank composed of the two identical symmetric second rank tensors, i.e., $\eta^{\alpha\beta}\eta^{\gamma\delta}$, only the first three terms contribute to symmetrization.

3. Third rank symmetric times a four-vector, i.e., $k^{\alpha}U^{\beta}U^{\gamma}U^{\delta}$. This form has four terms

$$A_3^{(\alpha\beta\gamma\delta)} = A^{\alpha\beta\gamma\delta} + A^{\beta\alpha\gamma\delta} + A^{\gamma\alpha\beta\delta} + A^{\delta\alpha\beta\gamma}.$$

0.5 Linearized Evolution Equations

Here, we present the full set of linearized equations (4.2) and (4.48)-(4.54) about an isotropic equilibrium with no heat flow, equal electron and ion equilibrium temperatures, and non-relativistic flow speed:

$$v\frac{\delta n}{n} - \cos(\theta)\delta v_{\parallel} - \hat{\mathbf{k}}_{\perp}\cdot\delta\mathbf{v} = 0, \tag{62}$$

$$\begin{aligned}&\zeta_s\frac{K_3(\zeta_s)}{K_2(\zeta_s)}v\delta v_{\parallel} - \cos(\theta)\frac{\delta p_s}{p} - \frac{2}{3}\cos(\theta)\frac{\delta\Delta p_s}{p}\\ &+ v\frac{\delta Q_{\parallel s}}{p} = \frac{iq_s n}{kp}E_{\parallel},\end{aligned} \tag{63}$$

$$\begin{aligned}&\zeta_s f(\zeta_s)v\frac{\delta n}{n} + (1-\zeta_s f(\zeta_s))\,v\frac{\delta p_s}{p} + \cos(\theta)\frac{\delta Q_{\parallel s}}{p}\\ &= 0,\end{aligned} \tag{64}$$

$$\begin{aligned}&- v\zeta_s\left(f(\zeta_s) + 3\frac{K_3(\zeta_s)}{K_2(\zeta_s)}\right)\frac{\delta n}{n}\\ &+ \zeta_s\left(f(\zeta_s) + \frac{K_3(\zeta_s)}{K_2(\zeta_s)}\right)v\frac{\delta p_s}{p} + \frac{2}{3}\zeta_s\frac{K_4(\zeta_s)}{K_3(\zeta_s)}v\frac{\delta\Delta p_s}{p}\\ &- 3\left(1 - \frac{2}{5}\frac{K_4(\zeta_s)}{K_3(\zeta_s)\mathcal{K}(\zeta_s)}\right)\cos(\theta)\frac{\delta Q_{\parallel s}}{p}\\ &+ 2\frac{K_4(\zeta_s)}{K_3(\zeta_s)\mathcal{K}(\zeta_s)}\cos(\theta)\frac{\delta\Delta Q_{\parallel s}}{p}\\ &+ 2\zeta_s\frac{K_3(\zeta_s)}{K_2(\zeta_s)}\hat{\mathbf{k}}_{\perp}\cdot\delta\mathbf{v} = 0,\end{aligned} \tag{65}$$

$$
\begin{aligned}
&\zeta_s\left(\zeta_s+5\frac{K_3(\zeta_s)}{K_2(\zeta_s)}\right)v\delta v_\parallel+\zeta_s f(\zeta_s)\cos(\theta)\frac{\delta n}{n}\\
&-\zeta_s\left(f(\zeta_s)+\frac{K_3(\zeta_s)}{K_2(\zeta_s)}\right)\cos(\theta)\frac{\delta p_s}{p}\\
&-\frac{2}{3}\zeta_s\frac{K_4(\zeta_s)}{K_3(\zeta_s)}\cos(\theta)\frac{\delta\Delta p_s}{p}\\
&+\left(5-2\frac{K_4(\zeta_s)}{K_3(\zeta_s)\mathcal{K}(\zeta_s)}\right)v\frac{\delta Q_{\parallel s}}{p}\\
&=\frac{iq_sn}{kp}\zeta_s\frac{K_3(\zeta_s)}{K_2(\zeta_s)}E_\parallel,
\end{aligned}
\tag{66}
$$

$$
\begin{aligned}
&\left(6\frac{K_3(\zeta_s)}{K_2(\zeta_s)}+\zeta_s\right)v\delta v_\parallel+\left(f(\zeta_s)+\frac{K_3(\zeta_s)}{K_2(\zeta_s)}\right)\cos(\theta)\frac{\delta n}{n}\\
&-\left(f(\zeta_s)+2\frac{K_3(\zeta_s)}{K_2(\zeta_s)}\right)\cos(\theta)\frac{\delta p_s}{p}-\frac{4}{3}\frac{K_4(\zeta_s)}{K_3(\zeta_s)}\cos(\theta)\frac{\delta\Delta p_s}{p}\\
&+\frac{v}{K_3(\zeta_s)\mathcal{K}(\zeta_s)}\left(K_4(\zeta_s)\mathcal{K}_2(\zeta_s)-\frac{2}{5}K_5(\zeta_s)\right)\frac{\delta Q_{\parallel s}}{p}\\
&-\frac{2}{3}\frac{vK_5(\zeta_s)}{K_3(\zeta_s)\mathcal{K}(\zeta_s)}\frac{\delta\Delta Q_{\parallel s}}{p}=\frac{iq_sn}{kp}\frac{K_3(\zeta_s)}{K_2(\zeta_s)}E_\parallel,
\end{aligned}
\tag{67}
$$

$$
\begin{aligned}
&\left[\left(\zeta_i\frac{K_3(\zeta_i)}{K_2(\zeta_i)}+\zeta_e\frac{K_3(\zeta_e)}{K_2(\zeta_e)}\right)v^2-(\zeta_i+\zeta_e)v_A^2\cos(\theta)^2\right]\delta\mathbf{v}_\perp\\
&-(\zeta_i+\zeta_e)v_A^2\hat{\mathbf{k}}_\perp\left(\hat{\mathbf{k}}_\perp\cdot\delta\mathbf{v}\right)-v\hat{\mathbf{k}}_\perp\frac{\delta p^T}{p}\\
&+\frac{1}{3}\frac{v}{n}\hat{\mathbf{k}}_\perp\frac{\delta\Delta p^T}{p}=0.
\end{aligned}
\tag{68}
$$

Bibliography

[1] M. Abramowitz, *Handbook of Mathematical Functions*, ed. M. Abramowitz and I. A. Stegun (Dover Publications, 1972).

[2] M. A. Aloy, E. Müller, J. M. Ibanez, J. M. Marti, and A. MacFayden, Ap. J. **531**, L119 (2000).

[3] A. M. Anile, *Relativistic Fluids and Magneto-Fluids: With Applications in Astrophysics and Plasma Physics* (Cambridge Univ. Press, 1989).

[4] J. Arons, *Neutron Stars and Pulsars, 40 years after the discovery*, ed. W. Becker, arXiv:0708.1050 (2008).

[5] E. Asseo and D. Beufils, Astrophys. and Space Sci. **89**, 133 (1983).

[6] R. Balescu, *Transport Processes in Plasmas, Vol. 1* (North-Holland, 1988).

[7] V. I. Berezhiani and S. M. Mahajan, Phys. Rev. E **52**, 1968 (1995).

[8] H. K.Biernat, M. F. Heyn, and V. S. Semenov, J. Geophys. Res. **92**, 3392 (1987).

[9] H. K. Biernat, S. Mühlbachler, V. S. Semenov, N. V. Erkaev, D. F. Vogl, and V. V. Ivanova, Adv. Space Res. **29**, 1069 (2002).

[10] D. Biskamp, Phys. Fluids **29**, 1520 (1986).

[11] E. G. Blackman and G. B. Field, Phys. Rev. Letters **72**, 494 (1994).

[12] S. I. Braginskii, *Transport Processes in a Plasma, Vol. 1*, edited by M. A. Lentovich (Consultants Bureau, New York, 1965).

[13] N. Bucciantini, T. A. Thompson, J. Arons, E. Quataert, L. Del Zanna, MNRAS **368**, 1717 (2006).

[14] R. Buckley, Nature **266**, 37 (1977).

[15] M. Camenzind, Astro. & Astrophys. **156**, 137 (1986).

[16] S. Chapman and T.G. Cowling, *The Mathematical Theory of Non-Uniform Gases* (Cambridge University Press, 1953).

[17] G. F. Chew, M. L. Goldberger, and F. E. Low, Proc. R. Soc. London A, **236**, 112 (1956).

[18] M. Chou and L.-N. Hau, Ap. J. **611**, 1200 (2004).

[19] M. Cissoko, Ann. Inst. Henri Poincaré **XII** (1), 1 (1975).

[20] I. Contopolous, D. Kazanas, and C. Fendt, Ap. J. **511**, 351 (1999).

[21] I. Contopolous and D. Kazanas, Ap. J. **566**, 336 (2002).

[22] W. Daughton, G. Lapenta, and P. Ricci, Phys. Rev. Lett. **93**, 105004 (2004).

[23] W. Daughton and H. Karimabadi, Phys. Plasmas **14**, 072303 (2007).

[24] S. R. de Groot, W. A. van Leeuwen, and Ch. G. van Weert, *Relativistic Kinetic Theory* (North-Holland Publishing Company, 1980).

[25] T. Di Matteo, MNRAS **299**, L15 (1998).

[26] G. P. Double, M. G. Baring, F. C. Jones, and D. C. Ellison, Ap. J. **600**, 485 (2004).

[27] C. Eckart, Phys. Rev. **58**, 919 (1940).

[28] S. Eriksson, M. Øieroset, D. N. Baker, C. Mouikis, A. Vaivads, M. W. Dunlop, H. Réme, R. E. Ergun, and A. Balogh, J. Geophys. Res. **109**, A10212 (2004).

[29] A. Ferrari, Ann. Rev. Ast. & Astrophys. **36**, 539 (1998).

[30] M. E. Gedalin, J. G. Lominadze, and E. G. Tsikarishvili, Astrophys. and Space Sci. **175**, 291 (1991).

[31] P. Goldreich and W. H. Julian, Ap. J. **157**, 869 (1969).

[32] P. Goldreich and W. H. Julian, Ap. J. **160**, 971 (1970).

[33] A. Gruzinov, Phys. Rev. Lett. **94**, 021101 (2005).

[34] A. Hasegawa, Phys. Fluids **12**, 2642 (1969).

[35] R. D. Hazeltine and S. M. Mahajan, Ap. J. **567**, 1262 (2002a).

[36] R. D. Hazeltine and S. M. Mahajan, Phys. Plasmas **9**, 1882 (2002b).

[37] R. D. Hazeltine and S. M. Mahajan, Phys. Plasmas **9**, 3341 (2002c).

[38] M. Hoshino, Y. Saito, T. Mukai, A. Nishida, S. Kokubun, and T. Yamamoto, Adv. Space Res. **20**, 973 (1997).

[39] J. D. Jackson *Classical Electrodynamics, Third Edition* (John Wiley & Sons, 1998).

[40] C. Kalapotharakos and I. Contopolous, arXiv:0811.2863v1 (2008).

[41] C. F. Kennel, F. S. Fujimura, and I. Okamoto, Geophys. Ap. Fluid Dyn. **26**, 147 (1983).

[42] S. S. Komissarov, MNRAS **367**, 19 (2006).

[43] M. D. Kruskal and C. R. Oberman, Phys. Fluids **1**, 275 (1958).

[44] R. M. Kulsrud, *Handbook of Plasma Physics*, ed. M. N. Rosenbluth and R. Z. Sagdeev (North Holland New York, 1983).

[45] L. D. Landau and E. M. Lifshitz, *Fluid Mechanics* (Pergamon Press, London, 1959).

[46] P. G. LeFloch, Institute for Math. and Its App., Minneapolis, Preprint **593** (1989).

[47] A. Lichnerowicz, *Relativistic Magnetohydrodynamics* (W. A. Benjamin, 1967).

[48] Y. E. Lyubarsky, MNRAS **358**, 113 (2005).

[49] M. Lyutikov and D. Uzdensky, Ap. J. **589**, 893 (2003).

[50] M. Lyutikov, MNRAS **346**, 540 (2003).

[51] A. I. MacFayden, S. E. Woolsey, and A. Hager, Ap. J. **550**, 410 (2001).

[52] L. Mestel, MNRAS **138**, 359 (1968).

[53] P. Mészáros, Rep. Prog. Phys. **69**, 2259 (2006).

[54] F. C. Michel, Ap. J. **158**, 727 (1969).

[55] F. C. Michel, Rev. Mod. Phys. **54**, 1 (1982).

[56] E. N. Parker, *Interplanetary Dynamical Processes*, (Interscience, New York, 1963).

[57] H. E. Petschek, *Physics of Solar Flares*, ed. W. N. Hess, (NASA Publication No. SP-50, p. 425 1964).

[58] J. J. Ramos, Phys. Plasmas **10**, 3606 (2003).

[59] M. N. Rosenbluth and N. Rostoker, Phys. Fluids **2**, 23 (1958).

[60] N. D. Sen Gupta, Phys. Letters **32A**, 103 (1970).

[61] K. Shibata, Adv. Space Res. **17**, 9 (1996).

[62] P. B. Snyder, G. W. Hammett, and W. Dorland, Phys. Plasmas **4**, 11 (1997).

[63] A. Spitkovsky, Ap. J. **648**, L51 (2006).

[64] A. Spitkovsky, *40 Years of Pulsars-Millisecond Pulsars, Magnetars, and More*, ed. C. G. Bassa, Z. Wang, A. Cumming, and V. M. Kaspi (American Institute of Physics, 2008).

[65] E. V. Suvorov and Y. V. Chugunov, Astrophys. and Space Sci. **23**, 189 (1973).

[66] M. Swisdak, Yi-Hsin Liu, and J. F. Drake, Ap. J. **680**, 999 (2008).

[67] M. Tan and B. Abraham, Ap. J. **3**, 71 (1972).

[68] J. M. TenBarge, R. D. Hazeltine, and S. M. Mahajan, Phys. Plasmas **15**, 062112 (2008).

[69] Y. V. Tolstykh, V. S. Semenov, H. K. Biernat, M. F. Heyn, and T. Penz, Adv. Space Res. **40**, 1538 (2007).

[70] E. G. Tsikarishvili, J. G. Lominadze, A. D. Rogava, and J. I. Javakhishvili, Phys. Rev. A **46**, 1078 (1992).

[71] E. G. Tsikarishvili, J. G. Lominadze, and J. I. Javakhishvili, Phys. Plasmas **1**, 150 (1993).

[72] E. G. Tsikarishvili, A. D. Rogava, and D. G. Tsiklauri, Ap. J. **439**, 822 (1995).

[73] R. M. Wald, *General Relativity* (Univ. Chicago Press, 1984).

[74] E. I. Weber and L. Davis, Ap. J **148**, 217 (1967).

[75] S. Weinberg *Graviation and Cosmology* (John Wiley & Sons, 1972).

[76] Wolfram Research, Inc., *Mathematica Edition: Version 6.0* (Champaign, Illinois, 2007).

[77] Y. B. Zel'dovich and I. Novikov, *Relativistic Astrophysics* (Univ. Chicago Press, 1983).

[78] Y. B. Zel'dovich and Y. P. Raizer, *Physics of Shock Waves and High-Temperature Hydrodynamic Phenomena*, ed. W. D. Hayes and R. F. Probstein (Dover Publications, 2002).

[79] S. Zenitani and M. Hesse, Phys. Plasmas **15**, 022101 (2008).

Vita

Jason Michael TenBarge was born April 3, 1981 in Evansville, Indiana on, the only son of Steven A. TenBarge and Karen L. TenBarge. He attended Indiana University at Bloomington and graduated *magna cum laude*, receiving Bachelor of Science degrees in Astrophysics and Mathematics in 2003. He applied and was accepted to the physics graduate studies program at the University of Texas at Austin, where he began graduate studies in the fall of 2003.

Permanent address: 3911 Becker Avenue
Austin, Texas 78751

This dissertation was typeset with LaTeX[†] by the author.

[†]LaTeX is a document preparation system developed by Leslie Lamport as a special version of Donald Knuth's TeX Program.